LUND UNIVERSITY

Modelling and Simulation of Gearset Behavior

Effects of Manufacturing Errors and Electrification

Hjelm, Rikard

2023

Document Version:
Publisher's PDF, also known as Version of record

Modelling and Simulation of Gearset Behavior

Effects of Manufacturing Errors and Electrification

RIKARD HJELM
DIVISION OF MECHANICS, MATERIALS AND COMPONENT DESIGN | LUND UNIVERSITY

Tryckt av Media-Tryck, Lund 2023 Svanenmärkt trycksak, 3041 0903

Faculty of Engineering
Department of Mechanical Engineering Sciences
Division of Mechanics, Materials and Component Design

ISBN 978-91-8039-607-3

Modelling and Simulation of Gearset Behavior

Effects of Manufacturing Errors and Electrification

Modelling and Simulation of Gearset Behavior

Effects of Manufacturing Errors and Electrification

Rikard Hjelm

LUND
UNIVERSITY

Thesis for the degree of Doctor
Thesis advisor: Prof. Jens Wahlström
Faculty opponent: Prof. Jorge Seabra

To be presented, with the permission of the Faculty of Engineering, LTH of Lund University, for public criticism at KC:G, Kemicentrum, LTH on Friday the 31st of March 2023 at 9:00.

Organization	Document name
LUND UNIVERSITY Department of Mechanical Engineering Sciences Box 118 SE–221 00 LUND Sweden	**DOCTORAL THESIS** Date of disputation 2023-03-31 Sponsoring organization VINNOVA
Author(s) Rikard Hjelm	

Title and subtitle

Modelling and Simulation of Gearset Behavior Effects of Manufacturing Errors and Electrification

Abstract

Due to electrification, new demands are imposed on gears regarding e.g., quality, noise, lubrication, and gear ratio. Therefore, a better understanding of gearset meshing and operation is needed. Experiments are valuable tools, but also tend to be cumbersome and time consuming. Moreover, contact pressure cannot be measured satisfactorily.

Thus, a simulation tool is needed. In this thesis, an LTCA simulation tool is developed, which simulates meshing of gears with manufacturing errors (ME). Contact is found from common normal directions together with a compliance condition, instead of using a predetermined load distribution. The LTCA accounts for non-Hertzian pressure, contact outside the nominal line of action (LOA), and tip contact. Contact pressure of gearsets with different combinations of ME tolerances is simulated, i.e., relating deviations in geometry caused by manufacturing to performance of the gearset.

The transmission of motion should also be smooth. This is quantified by the transmission error (TE). TE is simulated together with contact pressure. Since they tend to counter-vary, optimization is performed. Design curves are presented to show how to choose tolerances to simultaneously optimize TE and contact pressure.

It is concluded that ME adversely impact gearsets. Too tight tolerances, however, increase the risk of unjustified scrapping, which increases production time and cost, material waste, and environmental impact. To avoid this, it is suggested to use tip contact threshold torque as a single metric to assess ME, i.e., basing assessment on performance instead of only geometry. The feasibility of the method is shown in a case study, where some scrapping is shown to be unjustified.

To account for lubrication, a thermal elasto-hydrodynamic lubrication (TEHL) method is developed. It finds lubricant pressure and temperature by solving the Reynolds equation and the heat equation, and considers varying viscosity and density, as well as cavitation. Load distribution found from the LTCA is used as input to include ME. Results show that ME also cause an increase in temperature and a decrease in film thickness.

Apart from the single gear pairs, a study of a two-stage gear reduction used in an electric vehicle is presented. Two stages open further possibilities for optimization. This is done by finding the optimum dog leg angle by means of the lowest reaction forces, which in turn allows for smaller bearings. The decreased enclosed volume of the gearset also results in a lower housing mass. Both propulsion and regenerative braking are accounted for.

Key words

electrification, gears, LTCA, tip contact, pitch error, profile slope error, transmission error, tolerance, scrapping, lubrication, TEHL, optimization

Classification system and/or index terms (if any)

Supplementary bibliographical information	Language
	English
ISSN and key title	ISBN
	978-91-8039-607-3 (print) 978-91-8039-608-0 (pdf)
Recipient's notes	Number of pages: 235 / Price
	Security classification

Modelling and Simulation of Gearset Behavior

Effects of Manufacturing Errors and Electrification

Rikard Hjelm

LUND
UNIVERSITY

A doctoral thesis at a university in Sweden takes either the form of a single, cohesive research study (monograph) or a summary of research papers (compilation thesis), which the licentiate student has written alone or together with one or several other author(s).

In the latter case the thesis consists of two parts. An introductory text puts the research work into context and summarizes the main points of the papers. Then, the research publications themselves are reproduced, together with a description of the individual contributions of the authors. The research papers may either have been already published or are manuscripts at various stages (in press, submitted, or in draft).

Funding information: The thesis work was financially supported by VINNOVA.

Faculty of Engineering, LTH, Department of Mechanical Engineering Sciences

ISBN: 978-91-8039-607-3 (print)
ISBN: 978-91-8039-608-0 (pdf)

Printed in Sweden by Media-Tryck, Lund University, Lund 2023

Media-Tryck is a Nordic Swan Ecolabel certified provider of printed material. Read more about our environmental work at www.mediatryck.lu.se

Printed matter 3041 0903

MADE IN SWEDEN

Dedicated to whomever
who has nothing better to do
than to read about gears

Contents

List of publications

This thesis is based on the following publications, referred to by their Roman numerals.

I **A Method for Calculating Contact Pressure and Tip Contact in Spur Gear Sets with Manufacturing Errors**
R. Hjelm, L.Vedmar
Proceedings of International Gear Conference, 2018, 2(1), pp. 488-497

II **Influence of manufacturing error tolerances on contact pressure in gears**
R. Hjelm, H. Hansson, C. Andersson, A. Ahadi, J. Wahlström
Proceedings of the Institution of Mechanical Engineers Part C: Journal o Mechanical Engineering, 2021, 235(20), pp. 5173-5185

III **Gear tolerancing for simultaneous optimization of transmission error and contact pressure**
R. Hjelm, A. Ahadi, J. Wahlström
Results in Engineering, 2021, 9 March 2021

IV **Reducing scrapping of gears by assessment of tip contact threshold torque**
R. Hjelm, A. Ahadi, J. Wahlström
Proceedings of the Institution of Mechanical Engineers Part C: Journal of Engineering Tribology, 2021, 236(8), pp. 1613-1622

V **Influence of Manufacturing Error Tolerances on Thermal EHL Behavior of Gears**
R. Hjelm, J. Wahlström
MDPI Lubricants, 2022, 10(11), 323

VI **Optimum dog-leg angle for mass and bearing force optimization of multi-stage gear reduction**
M. Svahn, **R. Hjelm**
Proceedings of the Institution of Mechanical Engineers Part D: Journal of Automobile Engineering, 2021, 236(13), pp. 2795-2805

Publications not included in this thesis:

An Experimental Study of Forced Vibration Influence on Disc Brake Drag Torque in Heavy Commercial Road Vehicles

P. Fyhr, **R. Hjelm**, J. Wahlström
Tribology in Industry, 2022, 44(1), pp. 123–131

Airborne Wear Particles from Dry Clutches

R. Hjelm, J. Wahlström, D. Sabani, I. Yenibayrak, P. Runsten, Y. Lyu
MDPI Atmosphere, 2022, 13(10), 1700

Acknowledgements

This work was carried out at the Division of Machine Elements, now Division of Mechanics, Materials, and Component Design, under supervision of, in turn, Associate Professor Lars Vedmar, Associate Professor Anette Andersson, Professor Carin Andersson, Professor Aylin Ahadi, and finally Professor Jens Walström. I want to thank you all for contributing to this work and making me a better researcher, each of you in your own way.

I want to thank my co-authors Lars Vedmar, Hans Hansson, Carin Andersson, Aylin Ahadi, Jens Wahlström, and Mattias Svahn, as well as my co-authors for other publications, Pontus Fyhr, Driton Sabani, Isa Yenibayrak, Paula Runsten, and Yezhe Lyu.

I also want to thank Dan W Petersen, Chairman of Skånska Ingenjörsklubben, SIK, for his commitment and interest in gearing and tribology. Dan sadly passed away during the autumn of 2022, but he is fondly remembered and his contributions to the engineering community in southern Sweden are greatly acknowledged.

I want to thank my partners in the project TED - Driveline components for electrified powertrains, namely Rise IVF, Swerim, KTH, Uppsala University, Husqvarna, Höganäs, Bodycote, Uddeholm, Scania, SwePart, GKN ePowertrain, Ovako, Curtiss-Wright, Volvo, and Volvo Penta.

I also want to thank my partners in the project Effigears, namely Tribonex, KTH, OTEC Präzisionsfinish, and OptoSurf.

I wish to express my gratitude to those I have worked with under different circumstances during these years, with special reference to Hans Hansson at SwePart, Ellen Bergseth at KTH, Eva Troell at Rise, Linus Everlid at Tribonex, and our administrator Rose-Marie Hermansson. Thank you all.

I want to thank my past and present colleagues for all the fun we have had both at and off work. And of course, thank you to my personal friends, all of whom have motivated me during these years.

Last but definitely not least, mom, dad, Malin, Sven, and Micke - I can't thank you enough.

Highlights

This following bullet points highlight the novelty and major findings of the thesis.

- A novel Loaded Tooth Contact Analysis (LTCA) tool is presented. Simulations using the tool show the importance of treating contact outside the nominal line of action, including tip contact.
- The methodology of using design curves for simultaneous optimization of transmission error and contact pressure is proposed, and shown to be easy to use. It serves as a guide to choose manufacturing error tolerances with respect to gearset behavior rather than geometry.
- The concept of tip contact threshold torque is introduced. It is suggested as a means to assess the severity of manufacturing errors, and to compare different types of error and modification.
- Combining simulations and statistical predictions is shown to reduce computational burden without loss of accuracy.
- A novel Thermal Elasto-Hydrodynamic Lubrication (TEHL) tool is presented. Manufacturing errors are shown to have a large impact on TEHL behavior, predominantly through alteration of load distribution between simultaneous contacts.
- By optimizing the dog-leg angle of a two-stage reduction, both bearing forces and housing mass can be considerably decreased, independently of other optimizations.

Summary

Gears are old machine elements, invented at least a few thousand years ago, but they still face new challenges. Due to electrification, new demands are imposed on gearsets regarding quality, NVH (noise, vibration, harshness) behavior, lubrication performance, gear ratio, and so on. To fulfill these new requirements, a better understanding of gear meshing and gearset operation is needed. While experiments are versatile and valuable tools for assessing gearset operation, they also have some drawbacks: they tend to be cumbersome and time consuming, and they cannot isolate the influence of certain parameters. Moreover, pressure in the contact cannot be measured in a satisfactory way.

To solve these problems, a simulation tool is needed. In this thesis, a simulation tool of the type LTCA, or Loaded Tooth Contact Analysis, is developed in Paper I. The LTCA simulates the meshing of spur gears subjected to pitch error and profile slope error. Contact is found by searching for common normal directions of the flanks together with a compliance condition, instead of using a predetermined load distribution. The LTCA accounts for non-Hertzian pressure, contact outside the nominal line of action (LOA), and tip contact. This model is then used in Paper II to simulate contact pressure of gearsets with different combinations of manufacturing error tolerances, i.e., relating deviations in geometry, caused by manufacturing, to performance of the running gearset.

Apart from keeping contact pressure below a certain level, the transmission of motion should be smooth. This is quantified by the transmission error (TE), defined as the difference between the nominal and actual position along the LOA. In Paper III, TE is simulated together with contact pressure. Since they tend to counter-vary, optimization can be performed. Design curves are presented to show how to choose tolerances to simultaneously optimize transmission error and contact pressure.

From Papers I-III it can be concluded that too large manufacturing errors adversely impact gearsets. Too tight tolerances, however, increase the risk of scrapping of gears that would work properly, which increases production time and cost, material waste, environmental impact, and so on, counteracting the Global Sustainability Goals. To avoid this problem, Paper IV suggests the novel method of using the tip contact threshold torque as a single metric to assess the severity of manufacturing errors, i.e., basing the assessment on performance instead of only geometry. The feasibility of the method is shown in a case study of manufactured gears, where some scrapping is shown to be unjustified.

As gearsets in real applications are lubricated, lubrication needs to be included in the simulations. In Paper V, a thermal elasto-hydrodynamic lubrication (TEHL) method

is developed. This method calculates lubricant pressure and temperature by solving the Reynolds equation and the heat equation. It considers varying viscosity and density, as well as cavitation of the lubricant. Load distribution found from the LTCA is used as input to include manufacturing errors. Results show that apart from increased pressure, manufacturing errors may also cause an increase in temperature and a decrease in film thickness.

Apart from the single gear pairs in Papers I-V, Paper VI presents a study of a two-stage gear reduction used in an electric vehicle. Two stages means that there are three shafts, which opens further possibilities for optimization. This is done by finding the optimum dog leg angle, or diversion angle, by means of the lowest reaction forces, which in turn allows for smaller bearings without a loss of rating life. The decreased enclosed volume of the gearset also results in a lower housing mass. Both propulsion and regenerative braking are accounted for.

Together, several aspects of gears for electrified drivelines as treated. Future work includes adding surface roughness in the TEHL method, to account for asperity contact and mixed lubrication in a physically reasonable and coherent way. The overall goal is to have a full treatment of the contact integrated in a larger system, including bearings, shafts, and housing.

Populärvetenskaplig sammanfattning på svenska

Övergången till elbilar ställer nya krav på kugghjul. Man vill ha en tystare växellåda och kugghjul med bättre precision, samtidigt som kraven på hållbarhet och miljöpåverkan ökar. Samtidigt har man större frihet i växellådans design. Den här avhandlingen visar hur man löser dessa problem samtidigt.

Kugghjul har funnits i åtminstone ett par tusen år, men de möter ständigt nya krav. Kugghjulen i en elbil måste vara tystare eftersom växellådan inte längre överröstas av en förbränningsmotor. Elmotorns höga varvtal ställer ökade krav på kugghjulens kvalitet, men även på smörjning och hela växelns uppbyggnad. Den här avhandlingen studerar dessa nya krav.

För att få ökad förståelse för vad som händer med kugghjulen under drift kan man utföra experiment. Detta är ett viktigt område, men det har samtidigt en del problem. Experiment är ofta dyra och tidskrävande, och kan sällan isolera enskilda faktorer. Dessutom kan man inte direkt mäta kontakttryck, som är en viktig parameter för kuggväxeln. Dessa problem kan lösas genom att i stället simulera växelns beteende med en modell i ett datorprogram.

I den här avhandlingen har en simuleringsmodell av en kuggväxel byggts upp. Modellen inkluderar flera viktiga fenomen, som toppkontakt där det ena kugghjulets skarpa topp kommer i kontakt med det andra kugghjulet. Detta är ett stort problem, eftersom det skadar ytorna vilket leder till försämrad funktion och slutligen till haveri av växellådan. Modellen tar även hänsyn till tillverkningsfel, dvs. geometriska fel som ofrånkomligen uppstår vid tillverkningen. Om felen leder till ökat tryck, till exempel genom att orsaka toppkontakt, är de särskilt allvarliga.

Simuleringarna ger både tryck och s k transmissionsfel, som relateras till oljud. Eftersom minskat tryck kan resultera i ökat oljud och vice versa finns här en potential att optimera växeln så att både tryck och oljud hålls på tillräckligt låga nivåer. Samtidigt kan även för stora krav ställa till problem, eftersom man då riskerar att skrota kugghjul som hade fungerat tillräckligt bra i drift. I avhandlingen presenteras en metod för att undvika detta genom att bedöma tillverkningsfel efter när toppkontakt inträffar i stället för baserat på geometri. En fallstudie visar att metoden har god potential och industriell nytta.

För att minska friktion och öka verkningsgrad smörjer man kuggväxlar med någon olja. Att inkludera oljan i simuleringarna är viktigt för att förstå hur växeln beter sig. Det är ett komplext problem där trycket i oljan orsakar deformation av ytorna, vilket ändrar oljefilmens tjocklek. Detta påverkar i sin tur trycket, vilket innebär att trycket påverkar sig självt. Trycket påverkar även oljans temperatur, och temperaturen

har stor inverkan på oljans egenskaper som densitet och viskositet – en varm olja är mer lättflytande. Sammantaget är egenskaperna starkt kopplade till varandra, och problemet ytterst olinjärt.

Förutom kontakten påverkas hela växelns uppbyggnad av övergången till eldrift. Elmotorn går mycket snabbare än en förbränningsmotor, men bilens hjul är lika stora och den ska köras lika snabbt. Därför måste utväxlingen bli mycket större, och typiskt delas upp i fler steg. Med flera steg och därmed flera par kugghjul och axlar har man större frihet i växelns design. Den här avhandlingen visar också hur design kan väljas för att få så låg vikt som möjligt, och för att lagren ska hålla längre. Därmed kan växeln förbättras på både stor och liten skala, och din elbil blir lättare, tystare, får bättre räckvidd och mindre miljöpåverkan.

Modelling and Simulation of Gearset Behavior

Effects of Manufacturing Errors and Electrification

Chapter 1

Introduction

1.1 Old machine elements face new demands

Gears are old machine elements, predating the common era. According to Lewis [1], they were invented in ancient Greece a few hundred years BC.

Although the basic principle of gearing is old, mathematical descriptions of gear flanks came later. Huygens introduced the concept of evolute and involute in 1673 [2], and the major breakthrough was made by Euler in the mid eighteenth century [3] when he suggested the involute of a circle, the so called base circle, as geometry of the gear flank. In this thesis, the term 'gears' always refers to involute gears.

Involute gears have been studied extensively for over a century by pioneers such as Maag and Fölmer [4]. Among the classical works is also that of Lewis [5], who considered bending of gear teeth by studying an equivalent cantilever beam. Since then, much work has focused on root and contact stress in gears to find out how much load the gearset can transmit.

Experimental work

Much experimental work has been made on root stress, typically by fitting strain gauges on the gear teeth. An early example of this method is an experiment conducted in 1962 by Utagawa and Harada [6], followed by Houser and Seireg [7] in 1970 and Ichimaru and Hirano [8] in 1974. The basic idea of measuring strain with gauges for gears having known manufacturing errors seems to be fairly static throughout the years, but with the aim of achieving better measuring accuracy and better correspondence with computations. This is achieved by e.g. Handschuh et al. [9].

Root stress is a suitable subject for experimental measurements as the strain gauges do not interfere with the gear meshing. This is also true for other properties of a running gearset, such as transmission error (early work by Houser and Blankenship [10]; more recently by Benatar et al. [11]), vibration (Ratanasumawong et al. [12], Grzeszkowski et al. [13]), efficiency (pioneering work by Hyde et al. [14]; early work by Kasuba and Radzimovsky [15]; recent work by Andersson et al. [16], Li et al. [17]), and mesh stiffness by means of digital image correlation, DIC (Raghuwanshi and Parey [18]).

Contact pressure cannot be measured

This is however not the case for contact stress. Few experimental studies of contact stress in gearsets have been published; among the few is a study using the stress-optical method of caustics performed by Spitas et al. [19]. Results were compared to isochromatic fringe patterns obtained by photoelasticity. Another method is to use ultrasound, as presented by Quinn et al. [20] who report good agreement with Hertzian contact theory. Contrarily, Pau et al. [21] report a disagreement between the two approaches.

However, none of the methods measure contact pressure directly. Rather, the results are translated to contact pressure via some assumption. But a strain gauge at the root of the gear says more about the equivalent load of a pressure distribution than about the pressure distribution itself, in accordance with Saint-Venant's principle [22, 23].

Another method has to be used: Simulations

Still, assessment of contact pressure in gearsets is of great importance. Since it cannot be measured in a reasonable way, researchers have turned to analytical and numerical methods to calculate contact pressure and simulate meshing and gearset behavior, which is used here as a collective term for gearset properties such as contact pressure, transmission error, lubricant temperature, et cetera.

Demands are then imposed on gearset behavior, such as contact pressure and transmission error. Ultimately, the demands stem from end users, such as demands on low noise from buyers of electric vehicles. However, specifications for manufacture are made much earlier, and the decision of whether a gear should be kept or scrapped after manufacturing and control measuring is made long before the part is in use. Therefore, a link must be established between gear geometry and gearset behavior. The aim of this thesis is to add an increment to this link.

Manufacturing errors

There are several ways to manufacture gears, for example by generating methods such as hobbing [24], shaving [25], honing [26], broaching [27], skiving [28], and polishing [29]. These methods are typically combined with treatments such as coating [30],

shot peening [31], and case hardening [32]. Alternatively, copying methods such as sintering of powder metal [33] can be used. All of these methods result in some degree of deviation from the desired gear geometry. The relation between different manufacturing methods and the geometrical deviations on the produced gears has been investigated by Svahn [34] and Gravel [35].

To formalise this deviation, a few different manufacturing errors are introduced. Lin and He [36] show graphically how geometrical deviations can be divided into pitch error, profile error, and helix error. In turn, profile and helix errors are divided into slope and form error. This is formalised by standards, such as the ISO standard [37] used throughout this thesis.

Due to electrification, with its increased demands on gears, understanding gear meshing becomes even more important.

Dry contact pressure

The reason that contact pressure in gearsets is of interest to study is the relation between pressure and different damage or failure mechanisms, such as pitting [38], wear [39], and scuffing [40]. Many authors have studied contact pressure in gearsets. The following gives an overview, with special focus on contact pressure in gearsets with manufacturing errors.

Extensive work using the finite element method (FEM) on spur gears with manufacturing errors has been presented by Li [41, 42]. A major conclusion from the studies is that load distribution, i.e., the load sharing ratio between simultaneous tooth pairs in mesh, is greatly altered by manufacturing errors. With increased load comes increased contact pressure as a result of manufacturing errors.

Zhang et al. [43] performed a FEM simulation of helical gears with manufacturing errors, including pitch error and a profile error. A comparison between contact force for gearsets with and without pitch error shows a great increase in presence of pitch errors.

FEM was also used by Wei et al. [44] who studied different manufacturing errors of classes 5 and 7. While acknowledging that the matter needs further investigation, their results indicate that combined effect of manufacturing errors appears, for some cases as a superposition. Classes 5 and 7 are also used by Luo et al. [45] in their study of load distribution. Apart from drawing conclusions of combined effect and superposition similar to those made by Wei et al. [44], Luo et al. [45] also found that manufacturing errors (helix deviations) have a greater impact on load distribution than on root stress.

The change in geometry due to manufacturing errors is reflected in the effective stiffness distribution as shown by Wang et al. [46]. This translates to altered load distri-

bution and contact pressure.

Guilbault et al. developed a method [47] that was then used to study manufacturing errors [48]. Their findings also showed that contact pressure was more affected by manufacturing errors than root stress was, as well as an effect of combined errors, not only on the same gear, but also on mating teeth.

Here it can be concluded that there is a large impact on load distribution and contact pressure from manufacturing errors. To accurately simulate meshing and contact pressure, the simulation approach should include certain features or capabilities, as described and discussed below.

In Hertzian contact theory, only the equivalent radius of curvature of each surface in contact is used, i.e., a single value per surface. It is then impossible to accurately include contact where the radius of curvature changes rapidly, such as near the tip. Non-Hertzian contact pressure is treated by e.g. Bruzzone et al. [49].

By using non-Hertzian contact pressure, asymmetric pressure can be found, and tip contact [50] can be modeled. This is done by Ye and Tsai [51] who found greatly increased contact pressure due to tip contact. Consequences of tip contact include pitting, as discussed by Errichello et al. [52].

Tip contact occurs when the tip relief [53] is too small to compensate for the elastic deformations due to the torque applied to the gearset. This generally takes place outside the nominal line of action; see Munro et al. [54, 55] or Jedliński [56].

From this it is concluded that the simulation approach should be able to simulate tip contact using non-Hertzian contact theory and off line of action contact. To achieve this, a Loaded Tooth Contact Analysis [57], or LTCA, needs to be performed. The LTCA takes into account the deformation of gears and possibly other components such as shafts, as opposed to the Tooth Contact Analysis (TCA) which uses nominal gear geometry.

Transmission error

An LTCA can provide more results besides contact pressure. Since deformation is found at all contact points, the variation of deformation along the LOA can be captured. This variation, as a distance along the LOA, reflects deviation from the perfect transmission of motion, and is therefore denoted by transmission error [58], typically abbreviated TE. Sometimes, division is made into static transmission error [59] (STE) and dynamic transmission error [60] (DTE). While static transmission error is a commonly used term, it is more correctly denoted by quasi-static, a terminology adapted by e.g. Velex and Ajmi [61]. When a single measurement is desired, the peak-to-peak transmission error (PPTE; PPSTE, PPDTE) is used [62]. Apart from deformation,

other deviations from perfect involute geometry also contribute to the TE; thus, it is related to tooth modifications [63].

Since manufacturing errors are deviations from the intended geometry, TE can be linked to manufacturing errors as well. This has been done in some of the previously mentioned studies, such as Lin and He [36] who report an increase in STE due to manufacturing errors. Li [41] also concludes that increased manufacturing errors increase transmission error values, but also change their form.

Guo and Fang [64] and Hajnayeb and Sun [65] performed statistical analyses of randomly distributed manufacturing errors and their impact on transmission error. They used error grades according to ISO standard [37]. The fact that both vibration amplitude increases and that chaotic vibrations can take place due to manufacturing errors is shown by Bonori and Pellicano [66].

Transmission error is often described by amplitude and frequency spectra. This is done by Yuan et al. [67], who show how manufacturing errors cause sidebands in the vibration frequency spectrum. Similar results are presented by Fernández-del-Rincón et al. [68].

Talbot et al. [69] and Inalpolat et al. [70] also report alteration of the TE spectra, including additional peaks due to pitch errors. They report good agreement between simulated and measured data. Contrary to contact pressure, transmission error can be measured in a straightforward way, using laser vibrometers [71], optical encoders [72], or acceleration sensors [73]. The latter method was used by Hedlund and Lehtovaara [74] for gears with manufacturing errors. They concluded that the gear ratio is sensitive to manufacturing errors. This reflects yet another way to view TE, namely as a deviation from the nominal gear ratio.

Altogether, manufacturing errors are shown to impact transmission error as well, even though this field seems to have gotten less attention the relation between manufacturing errors and contact pressure. However, TE is of special interest as it can be linked to gearbox noise [72, 75] which becomes increasingly important as an electric motor does not drown out gearbox noise as an internal combustion engine does. Furthermore, due to the higher rotational speed of the electric motor, the noise gets more high pitched, which is tends to be perceived as more annoying than low pitched noise. This opens up for application of psychoacoustics to gearbox noise, as done by Stadtfeld [76].

Another rising field in noise reduction of electric vehicle gearboxes is the use of powder metal, which can be used to reduce NVH [77, 78, 79]. The lower equivalent modulus of elasticity contributes to a smoother and more silent meshing.

The link between noise and transmission error is interesting, since an inconvenience experienced by the end user, such as drivers and passengers of electric vehicles, can be related to gear geometry, and ultimately manufacturing errors and their tolerances. Thus, if the link is fully explored, tolerances can be chosen such that a certain acceptable noise level can be reached. Optimization of TE with respect to noise in a truck timing multistage gearset was made by Carbonelli et al. [80].

Since both contact pressure and transmission error can be related to manufacturing error tolerances, there is a possibility to choose manufacturing error tolerances to optimize the gearset with respect to both contact pressure and transmission error simultaneously.

Tolerancing and scrapping

Choosing tolerances is a complicated task which in itself is an optimization problem. A course tolerance, corresponding to a low quality gear, typically results in poor performance of the gearset. Pacana and Pacana [81] conclude that "It is necessary to be extremely careful when manufacturing gears of the most accurate profile possible, as it may significantly prolong its durability". Improving quality, however, comes at the expense of an increase in production cost, time, environmental impact, and so on. Furthermore, gears are scrapped as soon as one or more error measurements fall outside the allowed tolerance. If these tolerances are too tightly chosen, there is a risk of scrapping a gear that would work well in practice. It their study of end-of-life management in the automotive industry, Karagoz et al. [82] concluded that material waste reduction is in need of greater consideration.

There are ways to mitigate unjustified scrapping, such as by reparation [83] and remanufacturing [84, 85]. It is however desirable to avoid the problem altogether if this can be done already at the tolerancing stage.

Due to the complexity of this problem, tolerancing is traditionally carried out on a trial-and-error basis [86], but this approach makes it difficult to find an optimal solution. To make the best possible choice, a more rigorous approach is needed. Matters are complicated further due to the sensitive nature of the relation between tolerances and gearset performance. Bonori and Pellicano [66] state that "The stochastic approach shows that slightly different profile errors, within the same tolerance class, can lead to differences in terms of amplitude of oscillation that are not negligible".

Tolerancing has been treated as a general subject [87] as well as applied specifically to gears [88, 89, 90]. Lin et al. [91] found that manufacturing costs can be reduced by optimization of tolerances. An extensive overview of cost analysis of tolerances is provided by Hallman et al. [92].

While tolerancing should be reasonable from a manufacturing point of view, Chen and Li [93] suggest a change of focus to design rather than manufacturing, i.e., more consideration of allowable deviations from the perfect geometry than the result of manufacturing.

Bruyere et al. [94] performed an extensive study on tolerances using statistical analysis, including the relation between manufacturing errors and transmission error. They stated that "In the case of tolerance analysis of gears, we are not sure that the worse transmission error corresponds to the worse possible configurations of tolerances". This is an important conclusion, because it shows that the relation between manufacturing error tolerances and gearset performance is not as straightforward as one would expect. They also stress that choosing tolerances based on worst-case manufacturing outcome can lead to unnecessarily tight tolerances and consequently high production cost.

To summarize, there is a need for a method that connects manufacturing error tolerances to gearset behavior. With such a method, tolerances can be chosen based on properties of the running gearset, such as contact pressure and transmission error, rather than just geometry. By both avoiding unjustified scrapping due to too tight tolerances, and premature failure due to too course tolerances, waste of material, cost, energy, and time can be kept to a minimum.

Lubricated contact pressure

Thus far it has been shown that there are ways to calculate contact pressure in gearsets. In most cases, this pressure is close to Hertzian, for which there are closed form expressions. These expressions, however, are based on contact between two solids under dry conditions and do not account for the lubricant. In practice, gearsets are however lubricated. In some applications, grease lubrication [95] is used, but due to the higher likelihood of starvation [96] it is quite different from oil lubrication. Unless stated otherwise, lubrication always refers to oil lubrication in this thesis.

Some problems can be solved using this dry contact assumption, and in those cases it is convenient to omit the lubricant. In other problems, where the lubricant is of interest, another method is needed. Such methods are described and discussed below.

An equation that governs pressure in a thin lubricant film was derived by Reynolds [97] and holds his name, the Reynolds equation. It is derived by applying the equations of hydrodynamics to lubrication conditions, but can also be derived from equilibrium of an oil element. Almqvist and Larsson [98, 99] compared results obtained by using the Reynolds equation to those found from the more general Navier–Stokes approach. They found good agreement between the two approaches. The Reynolds approach can be concluded to have two advantages in the study of thin lubricant films,

namely avoidance of a singularity that appears in the Navier–Stokes formulation, and easier handling due to reduced complexity. This latter advantage, however, comes at the expense of accuracy according to Peterson et al. [100]. Still, it is assumed that the Reynolds equation is sufficient to model major phenomena such as pressure and film height.

The Reynolds equation relates pressure, viscosity, density, and film height of the lubricant. It also includes the velocities of the mating surfaces, and it is these velocities that allows a pressure to build up. For very low pressure, deformation of the surfaces is negligible, and one speaks of the hydrodynamic lubrication (HL) problem. In most applications, pressure is high and deformation cannot be neglected. When elastic deformation is included, the problem is denoted by elasto-hydrodynamic (EHL). This problem becomes nested, as pressure depends on film height, which is altered by deformation, which in turn is caused by pressure. This means that pressure depends on itself. The relation between pressure and elastic deformation is often chosen as that of Johnson [101]. While it is also possible to model plasticity, as done by Bobach et al. [102], the surfaces should not carry such a high load that they deform plastically (other than in case of asperity contact).

The EHL problem has been treated by many authors and from many viewpoints. A general approach is to study EHL of point contacts [103] or line contacts [104]. Cylinder-to-cylinder contact [105, 106, 107] and cylinder-to-plane contact [108] studies allows for a description that can be applied to different machine elements, such as cam and follower in a valve, roller and race in a bearing, or between flanks in a gearset. Thereby, geometry specific to gearsets is omitted, such as the radius of curvature changing along the contact at a certain contact position. Instead, they can focus on other aspects such as surface roughness [105], temperature [106], or starved lubrication [107]. Furthermore, they are suitable for comparison with experiments, such as ball-on-disc [109] or twin disc [110].

Instead, other authors treat gear geometry such as crowning [111] and tip relief [112, 113]. While the former used a full EHL treatment, the latter two used a partial formulation based on formulas. This eases computational burden, but typically lowers accuracy and makes it more difficult to explain phenomena as discussed by Echávarri Otero et al. [114]. It can be concluded that an accurate model should have a full EHL treatment, while also covering gear geometry.

A key parameter in the EHL formulation is the viscosity, which increases with pressure. An early model was proposed by Barus [115]. This relation is exponential, and results in gigantic values for the pressure values typically encountered in gearsets. This can be dealt with in different ways. Jacobson [116] introduced the solidification theory, in which the lubricant behaves like a solid when the viscosity becomes

high enough. Li and Kahraman [117] used av viscosity formulation based on three different pressure regions based on Goglia et al. [118]. Another viscosity model is presented by Roelands [119], which has been widely used.

While viscosity increases with pressure, it decreases with temperature. The immense viscosity predicted by formulas in highly pressurized contacts are thus counteracted by a temperature increase. The Roelands formula can be modified [120] to include temperature, as used by e.g. Liu et al. [121], or the Rodermund formula [122] can be used instead [107]. Density varies considerably less, and is typically modeled by the Dowson–Higginson relation [123].

Here it can be concluded that temperature also is a key parameter in the EHL problem, so much so that the term thermal elasto-hydrodynamic lubrication, or TEHL, is often used. TEHL analyses are performed by several authors [124, 125, 126, 127, 128, 129, 130]. These studies show very different results. Whereas Peng et al. [129] report temperature rise in the contact of only a few degrees, Yang et al. [130] show flash temperature of several hundred degrees.

Apart from the impact on the lubricant itself, temperature is of interest for other reasons. Arana et al. [131] investigated thermal expansion of gears in lubricated gearsets. They concluded that the expansion corresponds to pitch error and profile slope error, which approached their maximum allowed values dictated by their tolerances. Moreover, the expansion caused a decrease in backlash as well as premature contact, i.e., contact outside the LOA. Thermal treatments including heat transfer in the gears, not only the lubricant, are presented by Ziegltrum et al. [132] and Li and Kahraman [40]. From this, it can be concluded that a thermal treatment is needed for accurate results.

It is possible to include non-Newtonian properties of the lubricant, see Liu et al. [121]. However, they show that this has only a small effect on pressure and film height. Quiñonez showed that Newtonian and non-Newtonian descriptions produce very similar results under steady-state conditions, whereas more difference was observed under dynamic conditions. While dynamic treatments are important in many engineering applications, they are claimed [130] to have little influence on lubrication performance, even though opposing claims have been made [133]. Here it is assumed that non-Newtonian effects and dynamics can be neglected without much loss of accuracy unless those effects are of primary interest, and as a first model.

As previously discussed, pressure can be non-symmetric as opposed to the symmetric Hertzian pressure. This is a result of the surfaces being non-symmetric in the contact. For a hydrodynamically lubricated contact, however, the pressure is non-symmetric even for a symmetric geometry; instead, the surface velocities break the symmetry. At the outlet, the column formed by the surfaces diverges. As the lubricant cannot fill all the space, it cavitates. Just like the involute, the idea of cavitation was speculated by

Euler [134] but later formalised by others, including early work by Floberg [135] and later work by van Emden [136] and Gao et al. [137]. A description of cavitation must be included for the model to be physically reasonable.

Manufacturing errors, as previously discussed, were shown to have a large impact on gearset behavior under dry conditions. Furthermore, assembly errors strongly influence gearsets under lubricated conditions [138]. It is therefore reasonable to assume that manufacturing errors affect TEHL behavior. Despite this, not many studies have investigated this matter. Liu et al. [127] made a parametric study in which they varied the pressure angle, which corresponds to a profile slope error. This was concluded to have a significant effect on lubrication properties.

The impact of profile slope error was also treated by Clarke et al. [139], whose results "suggest that deviations in the profile affect oil film formation to an extent that may not be appreciated". This seems like a sensible conclusion, as few studies treat the impact of manufacturing errors on TEHL behavior, but those who do report a large impact. Zhou et al. [140] compare measurements and calculation of the friction coefficient, and attribute the discrepancy to pitch errors being excluded from the computation but present, as they always are to some degree, in the tested gears. Instead, studies of the impact of manufacturing errors on EHL behavior tends to focus on surface roughness [141, 142], i.e., the manufacturing error called form deviation [143]. This is a smaller scale manufacturing error than pitch error and profile slope error.

Thus, it remains to fill the research gap of the relation between manufacturing errors and TEHL behavior of gearsets.

In conclusion, manufacturing errors seem to have been given little attention despite their large impact. Ideally, they should be included in a TEHL model that also takes into account varying temperature, viscosity, and density.

Two and more stages

Thus far, only the contact between a pinion and a gear has been considered. This assumption, i.e., neglecting all surrounding machine elements, is an effective way of isolating the influence of one or a few parameters. In real applications, however, a single gear pair is not isolated from all surroundings. Instead, they influence and are influenced by shafts, bearings, housing, and so on, cf. Tudose et al. [144]. Moreover, when for example large gear ratios are needed, a single gear pair is seldom a good choice. Instead, multistage or planetary gearsets are favoured.

Large gear ratios are becoming increasingly important due to electrification, with electric motor rotational speed of around 10 000 to 20 000 rpm [145]. Since wheel size and

speed regulations are not changed, gear ratio of the transmission has to be changed instead. Together with demands on lower noise, potential to decrease mass of already heavy vehicles, and fewer limitations from previous internal combustion engine (ICE) vehicle designs, this opens up a whole new field of possible optimizations [146, 147].

Such an optimization was made by Kim et al. [62], who optimized a gearset with respect to NVH, mass, and efficiency. They concluded that when one of these parameters was omitted, the optimized gearset displayed considerably decreased performance with respect to that parameter. Optimization of volume and/or mass of the gearset is of interest, as it decreases inertia and mass, both of the gearset and, e.g., housing, but also since reduced volume allows for more battery storage. Mass optimizations were performed by, e.g., Wang et al. [148] and Moya-Rodríguez et al. [149]. The latter studied asymmetric teeth, which is an appealing design for electric vehicles who also use regenerative braking.

The studies mentioned above have focused single stage gearsets. When instead the gearset is divided into two or more stages, it is also possible to find the optimum gear ratio of each stage [150, 151]. Pi et al. [152] also found optimum gear ratios, and used this to minimize the cross section area of the gearset. Volume decrease is also reported by Sanghvi et al. [153]. To make the gearset more compact, minimum length is also considered by some authors [154, 155, 156]. Volume minimization for more stages was performed by Golabi et al. [157].

Two-stage gearsets subjected to manufacturing errors were treated by Ma et al. [158]. Pitch error and profile slope error were shown to have large impact on STE and DTE. Furthermore, based on extensive literature search, they claim that few studies include manufacturing errors, while those that do tend to neglect other important aspects.

An alternative to multistage gearsets is to use planetary gearsets. This was done fairly early by Bodas and Kahraman [159], and more recently by e.g. Xun et al. [160]. Both these studies include the effect of manufacturing errors. This case has gotten much attention, likely since manufacturing errors change the load distribution not only between simultaneous contacts of certain gear pairs, but also the total load between the planets, such that adding more planets may result in an increase in maximum planet load in presence of manufacturing errors, contrary to the desired decrease.

Conclusions

It is seen from the literature review above that electrification of vehicles gives rise to many gearset challenges that need to be addressed. In the vast overview of tribological phenomena in electric vehicles presented by Farfan-Cabrera [161], transmissions are considered as one of the most critical tribological components. It is the aim of this thesis to address these challenges.

1.2 Research questions

The conclusions and research gaps found in the previous section are summarized here as the following research questions (RQ).

RQ1: How could gear contacts be modeled, in a physically reasonable way, to account for modifications and manufacturing errors?

RQ2: How do manufacturing errors and their tolerances influence gearset behavior?

RQ3: How could new challenges, imposed by electrification, be addressed at the gearbox design phase?

It is the goal of each paper appended in this thesis to answer at least one of these questions, and the goal of the thesis to answer all of them. However, it should be noted that 'answer' in this context hardly means exhausting the field - rather, it provides some answers and insights, and shines light on a few new questions arising.

1.3 Scope and limitations

This thesis answers the research questions stated above using theoretical and numerical methods. Theoretical frameworks are set up and implemented as computer programs, and simulations and case studies are performed. Simulations focus on mechanical and tribological aspects of gearing.

Experiments, where applicable, are not performed in this thesis, but remains as (ongoing) future work.

1.4 Research overview

This section gives an overview of the research included in this thesis, its relation to other fields of research, and the outline of the thesis.

A great trend today is electrification of the vehicle fleet, which sparks many new challenges within science and engineering in fields such as energy, infrastructure, battery technology, electronics, environment, and many more [145, 162, 163]. The field of interest in this thesis is gears, which can be studied both from a component perspective,

or from a system perspective. The component perspective in this thesis is applied to contact analysis.

As discussed in Section 1.1, contacts can be studied under both dry and lubricated conditions. Dry contact modeling, in form of an LTCA, is published in Paper I-IV, and presented in Chapter 2. Lubricated contact modeling is published in Paper V and presented in Chapter 3. Finally, system perspective is published in Paper VI, and presented in Chapter 4.

Figure 1.1 shows a schematic overview of the research included in this thesis, including the link between dry (LTCA) and lubricated (TEHL) contact analysis.

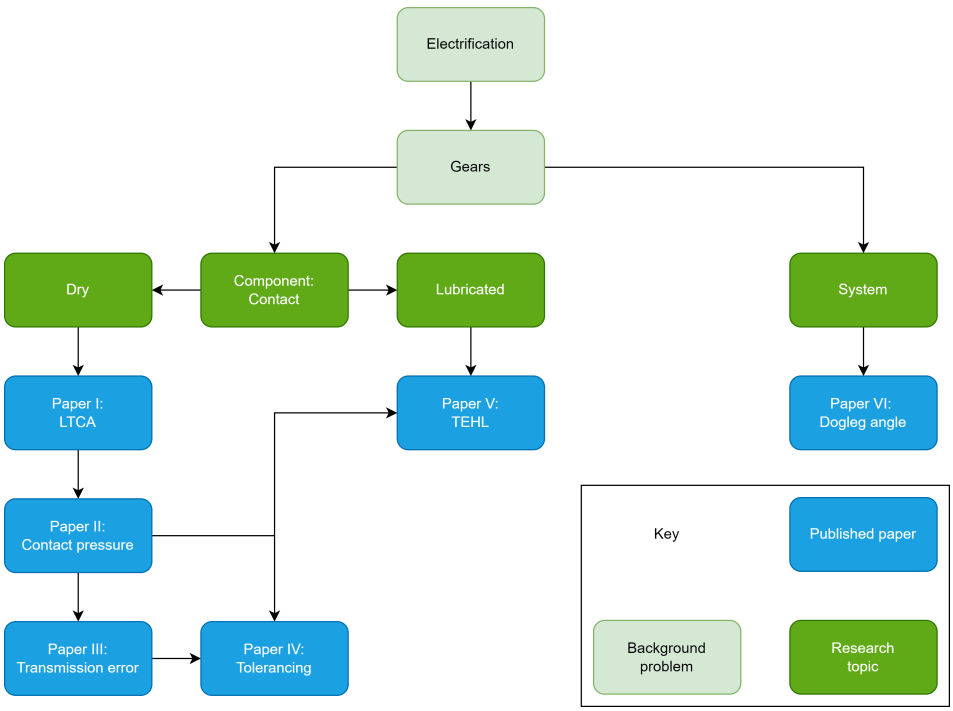

Figure 1.1: Schematic overview of the problem background and the research output included in this thesis.

An overview similar to that of Figure 1.1, but with ongoing and potential future work, can be seen in Chapter 6.

Chapter 2

Dry contacts - LTCA

This chapter describes the Loaded Tooth Contact Analysis (LTCA), i.e., the model and simulation tool of dry contacts. It was concluded in the literature review of the introduction that the model should include non-Hertzian pressure distribution, contact outside the nominal line of action, and tip contact. The description of the gears should include intentional modifications, such as tip relief, as well as unintentional manufacturing errors and their tolerances.

2.1 The LTCA model

This section gives some more theoretical background to the LTCA model that is not covered by the literature review in the Introduction section.

2.1.1 Load distribution

An important aspect when studying gear meshing is the load distribution, sometimes known as load sharing. In the single engagement zone, only one tooth pair is in mesh and consequently carries all the load. Thus, the load in the single engagement zone is known. In the dual engagement zone, however, the load distribution remains an unknown. For this reason, many authors make an assumption *a priori*. A common assumption is that the tooth pairs each carry half the load during dual engagement, see e.g. Kumar et al. [164]. Others, such as Bobach et al. [102] use a trapezoidal function in the dual engagement zone.

Assumptions like the ones mentioned above serve the purpose of reducing computa-

tional time. Once the load is known along the entire line of action, the corresponding contact pressure can be calculated using, e.g., Hertzian contact theory. However, the assumptions come with major drawbacks:

- They are not always physically consistent. From a pressure distribution comes a deformation in each simultaneous contact. These deformations are not independent, but should instead fulfil a compliance condition.
- They do not account for geometrical deviations such as intentional modifications or manufacturing errors. By assuming that tooth pairs carry the same load irrespective of manufacturing errors, most of the adverse effect of manufacturing errors is neglected.

Instead, in the LTCA, contact is found from searching for common contact normal together with a compliance condition.

Furthermore, most studies as well as standards (such as ISO 6336 [165]) neglect the influence of friction on tooth load. Reimann et al. [166] showed in detail how load distribution is altered by inclusion of friction. The reason is that the friction force also contributes to the torque since it has a lever around the axis of rotation. Since the sliding direction is reversed at the pitch point, so is the friction force and thus the torque contribution. This is seen as a sudden jump in load, or contact force, at the pitch point, as demonstrated by Marques et al. [167]. For this reason, friction is included in the LTCA.

2.1.2 Hybrid model

The problem of deformation in gears is ill-conditioned, as the contact deformation is very small compared to the size of the gear tooth and possibly the whole gear. To accurately describe both contact and bending deformation using e.g. finite elements (FE), an extremely fine FE mesh would be needed, resulting in immense computational time. Alternatively, an adaptable mesh could be utilized, but re-meshing is also computationally demanding, especially since contact positions are not known beforehand. The problem of ill-conditioning is further discussed by, e.g., Bodas and Kahraman [159].

A way to solve the problem is to use a hybrid model, combining the versatility of finite elements with the accuracy and low computation time of analytical methods. Simultaneously, good agreement with experiments are reported [58]. Hybrid models are discussed by Langlois et al. [168], who concluded that hybrid models "can be run in

time scales orders of magnitude quicker than FE tooth contact analyses, while retaining similar accuracy". Early hybrid models were developed by Atluri and Murakawa [169] for general problems in solid mechanics. A hybrid model of gear compliance was developed by Vedmar [170]. This model is implemented in the LTCA.

2.2 Theory

The LTCA simulation tool and the method for simulating dry contacts is published in Paper I. The description of the theoretical framework is however rather condensed. In this section, this is elaborated on and the gaps are filled.

2.2.1 Reference profile

The reference profile is an imaginary line or plane that is complementary to the (rack cutter) tool that manufactures the gear, as well as to the rack that is conjugated to the gear. Different segments on the reference profile thus correspond to different segments on the gear as shown in Figure 2.1.

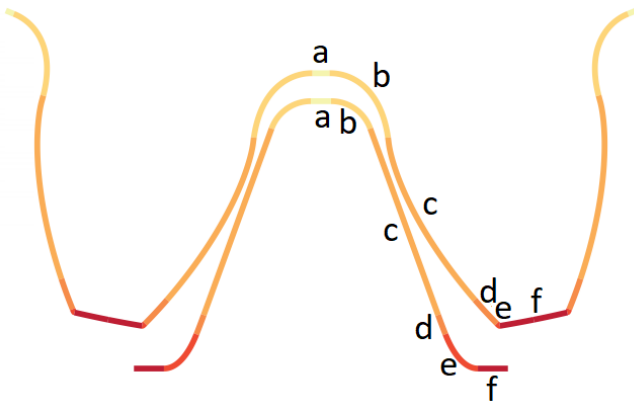

Figure 2.1: Tool (bottom) and conjugated gear (top). The letters correspond to the different regions of the gear; a: bottom circle, b: fillet, c: involute, d: tip relief, e: tip rounding, and f: top circle. Reproduced with permission from Paper II.

The geometry of the reference profile can be seen in Figure 2.2.

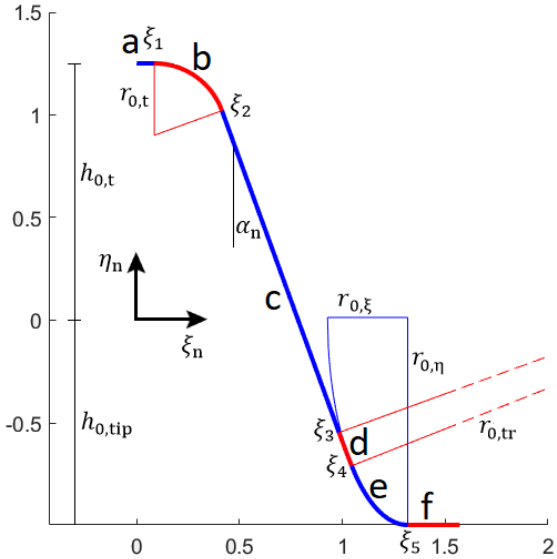

Figure 2.2: Reference profile geometry. The lettered regions are the same as those in Figure 2.1. Reproduced with permission from Paper I.

α_n is the pressure angle in the normal plane. $r_{0,t}$ is the fillet radius and $r_{0,tr}$ is the tip relief radius. The coordinate ξ_n is used as a parameter, since it has unique values at all points. Thus, $\eta_n = \eta_n(\xi_n)$ which is given by

$$\eta_n = \begin{cases} h_{0,t}, & 0 \le \xi_n \le \xi_1 : \text{a} \\ \eta_{f,c} + \sqrt{r_{0,t}^2 - (\xi_n - \xi_{f,c})^2}, & \xi_1 \le \xi_n \le \xi_2 : \text{b} \\ (\xi_0 - \xi_n)/\tan\alpha_n, & \xi_2 \le \xi_n \le \xi_3 : \text{c} \\ \eta_{tr,c} - \sqrt{r_{0,tr}^2 - (\xi_n - \xi_{tr,c})^2}, & \xi_3 \le \xi_n \le \xi_4 : \text{d} \\ \eta_{r,c} - \sqrt{r_{0,\eta}^2 - \frac{r_{0,\eta}^2}{r_{0,\xi}^2}(\xi_n - \xi_{r,c})^2}, & \xi_4 \le \xi_n \le \xi_5 : \text{e} \\ -h_{0,tip}, & \xi_5 \le \xi_n \le \frac{\pi}{2} : \text{f} \end{cases} \tag{2.1}$$

The reference profile thus generates bottom circle (a), fillet (b), involute (c), tip relief (d), tip rounding (e), and top circle (f). The tip relief is circular on the reference profile whereas the tip rounding is elliptical with half-axes $r_{0,\xi}$ and $r_{0,\eta}$, linking tip relief and top circle with continuous coordinates and first derivative. The tip relief circle center is given by the coordinates $(\xi_{tr,c}, \eta_{tr,c})$ which are far outside the figure.

The coordinates of the points on the reference profile are given by the following equations.

$$\xi_0 = \pi/4 \tag{2.2}$$

$$\eta_{\mathrm{fc}} = h_{0,\mathrm{t}} - r_{0,\mathrm{t}} \tag{2.3}$$

$$\eta_2 = \eta_{\mathrm{fc}} + r_{0,\mathrm{t}} \sin\alpha_{\mathrm{n}} \tag{2.4}$$

$$\xi_2 = \xi_0 - \eta_2 \tan\alpha_{\mathrm{n}} \tag{2.5}$$

$$\xi_1 = \xi_2 - r_{0,\mathrm{t}} \cos\alpha_{\mathrm{n}} \tag{2.6}$$

$$\xi_{\mathrm{fc}} = \xi_1 \tag{2.7}$$

$$\xi_3 = \xi_0 + h_{0,\mathrm{tr}} \tan\alpha_{\mathrm{n}} \tag{2.8}$$

$$\xi_{\mathrm{tr,c}} = \xi_3 - r_{0,\mathrm{tr}} \cos\alpha_{\mathrm{n}} \tag{2.9}$$

$$\eta_{\mathrm{tr,c}} = -h_{0,\mathrm{tr}} - r_{0,\mathrm{tr}} \sin\alpha_{\mathrm{n}} \tag{2.10}$$

The coordinate $\eta_{\mathrm{n}} = \eta_{\mathrm{n}}(\xi_{\mathrm{n}})$ in the different regions is then given by

$$0 \le \xi_{\mathrm{n}} \le \xi_1 : \eta_{\mathrm{n}} = h_{0,\mathrm{t}} \tag{2.11}$$

$$\xi_1 \le \xi_{\mathrm{n}} \le \xi_2 : \eta_{\mathrm{n}} = \eta_{\mathrm{f,c}} + \sqrt{r_{0,\mathrm{t}}^2 - (\xi_{\mathrm{n}} - \xi_{\mathrm{f,c}})^2} \tag{2.12}$$

$$\xi_2 \le \xi_{\mathrm{n}} \le \xi_3 : \eta_{\mathrm{n}} = (\xi_0 - \xi_{\mathrm{n}})/\tan\alpha_{\mathrm{n}} \tag{2.13}$$

$$\xi_3 \le \xi_{\mathrm{n}} \le \xi_4 : \eta_{\mathrm{n}} = \eta_{\mathrm{tr,c}} - \sqrt{r_{0,\mathrm{tr}}^2 - (\xi_{\mathrm{n}} - \xi_{\mathrm{tr,c}})^2} \tag{2.14}$$

$$\xi_4 \leq \xi_\mathrm{n} \leq \xi_5 : \eta_\mathrm{n} = \eta_\mathrm{r,c} - \sqrt{r_{0,\eta}^2 - \frac{r_{0,\eta}^2}{r_{0,\xi}^2}(\xi_\mathrm{n} - \xi_\mathrm{r,c})^2} \tag{2.15}$$

$$\xi_5 \leq \xi_\mathrm{n} \leq \frac{\pi}{2} : \eta_\mathrm{n} = -h_{0,\mathrm{tip}} \tag{2.16}$$

The corresponding first derivative $\frac{\mathrm{d}\eta_\mathrm{n}}{\mathrm{d}\xi_\mathrm{n}}$ is given by the following expressions, where sign denotes the signum function, $\mathrm{sign}(x) = x/|x|$ for some real number x.

$$0 \leq \xi_\mathrm{n} \leq \xi_1 : \frac{\mathrm{d}\eta_\mathrm{n}}{\mathrm{d}\xi_\mathrm{n}} = 0 \tag{2.17}$$

$$\xi_1 \leq \xi_\mathrm{n} \leq \xi_2 : \frac{\mathrm{d}\eta_\mathrm{n}}{\mathrm{d}\xi_\mathrm{n}} = -\mathrm{sign}(\xi_\mathrm{n}) \frac{\xi_\mathrm{n} - \xi_\mathrm{f,c}}{\sqrt{r_{0,\mathrm{t}}^2 - (\xi_\mathrm{n} - \xi_\mathrm{f,c})^2}} \tag{2.18}$$

$$\xi_2 \leq \xi_\mathrm{n} \leq \xi_3 : \frac{\mathrm{d}\eta_\mathrm{n}}{\mathrm{d}\xi_\mathrm{n}} = -\mathrm{sign}(\xi_\mathrm{n}) \cot \alpha_\mathrm{n} \tag{2.19}$$

$$\xi_3 \leq \xi_\mathrm{n} \leq \xi_4 : \frac{\mathrm{d}\eta_\mathrm{n}}{\mathrm{d}\xi_\mathrm{n}} = \mathrm{sign}(\xi_\mathrm{n}) \frac{\xi_\mathrm{n} - \xi_\mathrm{tr,c}}{\sqrt{r_{0,\mathrm{tr}}^2 - (\xi_\mathrm{n} - \xi_\mathrm{tr,c})^2}} \tag{2.20}$$

$$\xi_4 \leq \xi_\mathrm{n} \leq \xi_5 : \frac{\mathrm{d}\eta_\mathrm{n}}{\mathrm{d}\xi_\mathrm{n}} = \mathrm{sign}(\xi_\mathrm{n}) \frac{\xi_\mathrm{n} - \xi_\mathrm{r,c}}{\sqrt{r_{0,\eta}^2 - \frac{r_{0,\eta}^2}{r_{0,\xi}^2}(\xi_\mathrm{n} - \xi_\mathrm{r,c})^2}} \frac{r_{0,\eta}^2}{r_{0,\xi}^2} \tag{2.21}$$

$$\xi_5 \leq \xi_\mathrm{n} \leq \frac{\pi}{2} : \frac{\mathrm{d}\eta_\mathrm{n}}{\mathrm{d}\xi_\mathrm{n}} = 0 \tag{2.22}$$

The second derivative $\frac{\mathrm{d}^2\eta_\mathrm{n}}{\mathrm{d}\xi_\mathrm{n}^2}$ is given by

$$0 \leq \xi_\mathrm{n} \leq \xi_1 : \frac{\mathrm{d}^2\eta_\mathrm{n}}{\mathrm{d}\xi_\mathrm{n}^2} = 0 \tag{2.23}$$

$$\xi_1 \leq \xi_\mathrm{n} \leq \xi_2 : \frac{\mathrm{d}^2\eta_\mathrm{n}}{\mathrm{d}\xi_\mathrm{n}^2} = -\mathrm{sign}(\xi_\mathrm{n}) \frac{r_{0,\mathrm{t}}^2}{\left(r_{0,\mathrm{t}}^2 - (\xi_\mathrm{n} - \xi_\mathrm{f,c})^2\right)^{3/2}} \tag{2.24}$$

$$\xi_2 \leq \xi_\mathrm{n} \leq \xi_3 : \frac{\mathrm{d}^2\eta_\mathrm{n}}{\mathrm{d}\xi_\mathrm{n}^2} = 0 \tag{2.25}$$

$$\xi_3 \leq \xi_\mathrm{n} \leq \xi_4 : \frac{\mathrm{d}^2\eta_\mathrm{n}}{\mathrm{d}\xi_\mathrm{n}^2} = \mathrm{sign}(\xi_\mathrm{n}) \frac{r_{0,\mathrm{tr}}^2}{\left(r_{0,\mathrm{tr}}^2 - (\xi_\mathrm{n} - \xi_{\mathrm{tr,c}})^2\right)^{3/2}} \tag{2.26}$$

$$\xi_4 \leq \xi_\mathrm{n} \leq \xi_5 : \frac{\mathrm{d}^2\eta_\mathrm{n}}{\mathrm{d}\xi_\mathrm{n}^2} = \mathrm{sign}(\xi_\mathrm{n}) \frac{1}{\left(r_{0,\eta}^2 - \frac{r_{0,\eta}^2}{r_{0,\xi}^2}(\xi_\mathrm{n} - \xi_{\mathrm{r,c}})^2\right)^{3/2}} \frac{r_{0,\eta}^4}{r_{0,\xi}^2} \tag{2.27}$$

$$\xi_5 \leq \xi_\mathrm{n} \leq \frac{\pi}{2} : \frac{\mathrm{d}^2\eta_\mathrm{n}}{\mathrm{d}\xi_\mathrm{n}^2} = 0 \tag{2.28}$$

Coordinates on the tip relief part of the flanks are given by the coordinates (ξ', η') according to

$$\begin{cases} \xi' = \xi_i - \delta_{0,\mathrm{tr}} \cos\psi_i \\ \eta' = \eta_i - \delta_{0,\mathrm{tr}} \sin\psi_i \end{cases} \tag{2.29}$$

where index i here denotes involute, and $\delta_{0,\mathrm{tr}}$ is the (dimensionless) amount of tip relief.

Rotate an angle $\frac{\pi}{z}$, i.e., half a pitch, to center the coordinate system around the gap instead of the tooth:

$$\begin{pmatrix} \xi \\ \eta \end{pmatrix} = \begin{pmatrix} \cos\frac{\pi}{z} & -\sin\frac{\pi}{z} \\ \sin\frac{\pi}{z} & \cos\frac{\pi}{z} \end{pmatrix} \begin{pmatrix} \xi' \\ \eta' \end{pmatrix} \tag{2.30}$$

This can be seen in Figure 2.3.

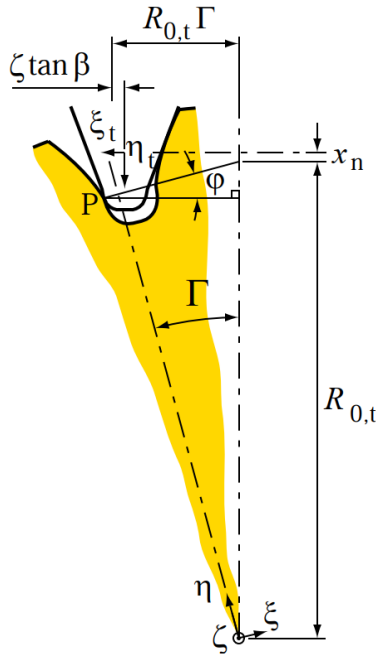

Figure 2.3: Geometry during gear manufacturing. The tool (top, transparent) cuts the gear (bottom, colored) at point *P*.

From this, the coordinates are given by

$$\begin{cases} \xi = R_{0,t} \sin\Gamma - \frac{\eta_n - x}{\sin\varphi} \cos(\Gamma - \varphi) \\ \eta = R_{0,t} \cos\Gamma - \frac{\eta_n - x}{\sin\varphi} \sin(\Gamma - \varphi) \end{cases} \tag{2.31}$$

where

$$\Gamma = \frac{1}{R_{0,t}} \left[-\frac{\xi_n}{\cos\beta} + (\eta_n - x)\cot\varphi + \zeta \tan\beta \right] \tag{2.32}$$

For spur gears, the helix angle is zero, thus

$$\beta = 0 \implies \Gamma = \frac{1}{R_{0,t}} \left[-\xi_n + (\eta_n - x)\cot\varphi \right] \tag{2.33}$$

where

$$\cot\varphi = -\frac{\partial\eta_{\mathrm{n}}}{\partial\xi_{\mathrm{n}}}\cos\beta = -\frac{\partial\eta_{\mathrm{n}}}{\partial\xi_{\mathrm{n}}} \implies \varphi = \operatorname{arccot}\left(-\frac{\partial\eta_{\mathrm{n}}}{\partial\xi_{\mathrm{n}}}\right) \tag{2.34}$$

Since

$$\eta_{\mathrm{n}} = \eta_{\mathrm{tr,c}} - \sqrt{r_{0,\mathrm{tr}}^2 - (\xi_{\mathrm{n}} - \xi_{\mathrm{tr,c}})^2} \tag{2.35}$$

it follows that

$$\frac{\mathrm{d}\eta_{\mathrm{n}}}{\mathrm{d}\xi_{\mathrm{n}}} = \operatorname{sign}(\xi_{\mathrm{n}})\frac{\xi_{\mathrm{n}} - \xi_{\mathrm{tr,c}}}{\sqrt{r_{0,\mathrm{tr}}^2 - (\xi_{\mathrm{n}} - \xi_{\mathrm{tr,c}})^2}} \tag{2.36}$$

Unknowns are now $r_{0,\mathrm{tr}}$ and ξ_{n}, which are found using a Newton-Raphson scheme. To do this, define the functions

$$\begin{cases} f_1 = f_1(\xi_{\mathrm{n}}, r_{0,\mathrm{tr}}) \\ f_2 = f_2(\xi_{\mathrm{n}}, r_{0,\mathrm{tr}}) \end{cases} \tag{2.37}$$

where

$$\begin{aligned} f_1 = {} & R_{0,\mathrm{t}}\sin\Gamma - \frac{\eta_{\mathrm{n}} - x}{\sin\varphi}\cos(\Gamma - \varphi) - (\xi_i - \delta_{0,\mathrm{tr}}\cos\psi_i)\cos\frac{\pi}{z} \\ & + (\eta_i - \delta_{0,\mathrm{tr}}\sin\psi_i)\sin\frac{\pi}{z} \end{aligned} \tag{2.38}$$

and

$$\begin{aligned} f_2 = {} & R_{0,\mathrm{t}}\cos\Gamma + \frac{\eta_{\mathrm{n}} - x}{\sin\varphi}\sin(\Gamma - \varphi) - (\eta_i - \delta_{0,\mathrm{tr}}\sin\psi_i)\cos\frac{\pi}{z} \\ & - (\xi_i - \delta_{0,\mathrm{tr}}\cos\psi_i)\sin\frac{\pi}{z} \end{aligned} \tag{2.39}$$

In matrix format, Newton-Raphson is written as

$$\mathbf{f}(\mathbf{x} + \Delta\mathbf{x}) = \mathbf{f}(\mathbf{x}) + D\mathbf{f}(\mathbf{x})\Delta\mathbf{x} = \mathbf{0} \tag{2.40}$$

where

$$\Delta \mathbf{x} = -\left(D\mathbf{f}(\mathbf{x})\right)^{-1} \mathbf{f}(\mathbf{x}) \tag{2.41}$$

Thus,

$$\mathbf{x}_{k+1} = \mathbf{x}_k - \left(D\mathbf{f}(\mathbf{x}_k)\right)^{-1} \mathbf{f}(\mathbf{x}_k) \tag{2.42}$$

where index k here denotes iteration, and the functional matrix is given by

$$D\mathbf{f}(\mathbf{x}) = \begin{pmatrix} \frac{\partial f_1}{\partial \xi_\mathrm{n}} & \frac{\partial f_1}{\partial r_{0,\mathrm{tr}}} \\ \frac{\partial f_2}{\partial \xi_\mathrm{n}} & \frac{\partial f_2}{\partial r_{0,\mathrm{tr}}} \end{pmatrix} \tag{2.43}$$

Its inverse is given by

$$\left(D\mathbf{f}(\mathbf{x})\right)^{-1} = \frac{1}{\frac{\partial f_1}{\partial \xi_\mathrm{n}}\frac{\partial f_2}{\partial r_{0,\mathrm{tr}}} - \frac{\partial f_1}{\partial r_{0,\mathrm{tr}}}\frac{\partial f_2}{\partial \xi_\mathrm{n}}} \begin{pmatrix} \frac{\partial f_2}{\partial r_{0,\mathrm{tr}}} & -\frac{\partial f_1}{\partial r_{0,\mathrm{tr}}} \\ -\frac{\partial f_2}{\partial r_{0,\mathrm{tr}}} & \frac{\partial f_1}{\partial \xi_\mathrm{n}} \end{pmatrix} \tag{2.44}$$

Thus,

$$\begin{cases} \Delta \xi_\mathrm{n} = \frac{-1}{\frac{\partial f_1}{\partial \xi_\mathrm{n}}\frac{\partial f_2}{\partial r_{0,\mathrm{tr}}} - \frac{\partial f_1}{\partial r_{0,\mathrm{tr}}}\frac{\partial f_2}{\partial \xi_\mathrm{n}}} \left(\frac{\partial f_2}{\partial r_{0,\mathrm{tr}}} f_1 - \frac{\partial f_1}{\partial r_{0,\mathrm{tr}}} f_2 \right) \\ \Delta r_{0,\mathrm{tr}} = \frac{-1}{\frac{\partial f_1}{\partial \xi_\mathrm{n}}\frac{\partial f_2}{\partial r_{0,\mathrm{tr}}} - \frac{\partial f_1}{\partial r_{0,\mathrm{tr}}}\frac{\partial f_2}{\partial \xi_\mathrm{n}}} \left(\frac{\partial f_2}{\partial \xi_\mathrm{n}} f_1 - \frac{\partial f_1}{\partial \xi_\mathrm{n}} f_2 \right) \end{cases} \tag{2.45}$$

The respective derivatives are given by the following expressions.

$$\begin{aligned} \frac{\partial f_1}{\partial \xi_\mathrm{n}} = {} & R_{0,\mathrm{t}} \cos\Gamma \frac{\partial \Gamma}{\partial \xi_\mathrm{n}} - \frac{\partial \eta_\mathrm{n}}{\partial \xi_\mathrm{n}} \frac{\cos(\Gamma - \varphi)}{\sin\varphi} \\ & + (\eta_\mathrm{n} - x) \frac{\cos\varphi}{\sin^2\varphi} \frac{\partial \varphi}{\partial \xi_\mathrm{n}} \cos(\Gamma - \varphi) \\ & + \frac{\eta_\mathrm{n} - x}{\sin\varphi} \sin(\Gamma - \varphi) \left(\frac{\partial \Gamma}{\partial \xi_\mathrm{n}} - \frac{\partial \varphi}{\partial \xi_\mathrm{n}} \right) \end{aligned} \tag{2.46}$$

$$\begin{aligned}\frac{\partial f_1}{\partial r_{0,\mathrm{tr}}} &= R_{0,\mathrm{t}}\cos\Gamma\frac{\partial\Gamma}{\partial r_{0,\mathrm{tr}}} - \frac{\partial\eta_\mathrm{n}}{\partial r_{0,\mathrm{tr}}}\frac{\cos(\Gamma-\varphi)}{\sin\varphi}\\ &\quad + (\eta_\mathrm{n}-x)\frac{\cos\varphi}{\sin^2\varphi}\frac{\partial\varphi}{\partial r_{0,\mathrm{tr}}}\cos(\Gamma-\varphi)\\ &\quad + \frac{\eta_\mathrm{n}-x}{\sin\varphi}\sin(\Gamma-\varphi)\left(\frac{\partial\Gamma}{\partial r_{0,\mathrm{tr}}} - \frac{\partial\varphi}{\partial r_{0,\mathrm{tr}}}\right)\end{aligned} \tag{2.47}$$

$$\begin{aligned}\frac{\partial f_2}{\partial \xi_\mathrm{n}} &= -R_{0,\mathrm{t}}\sin\Gamma\frac{\partial\Gamma}{\partial\xi_\mathrm{n}} + \frac{\partial\eta_\mathrm{n}}{\partial\xi_\mathrm{n}}\frac{\sin(\Gamma-\varphi)}{\sin\varphi}\\ &\quad - (\eta_\mathrm{n}-x)\frac{\cos\varphi}{\sin^2\varphi}\frac{\partial\varphi}{\partial\xi_\mathrm{n}}\sin(\Gamma-\varphi)\\ &\quad + \frac{\eta_\mathrm{n}-x}{\sin\varphi}\cos(\Gamma-\varphi)\left(\frac{\partial\Gamma}{\partial\xi_\mathrm{n}} - \frac{\partial\varphi}{\partial\xi_\mathrm{n}}\right)\end{aligned} \tag{2.48}$$

$$\begin{aligned}\frac{\partial f_2}{\partial r_{0,\mathrm{tr}}} &= -R_{0,\mathrm{t}}\sin\Gamma\frac{\partial\Gamma}{\partial r_{0,\mathrm{tr}}} + \frac{\partial\eta_\mathrm{n}}{\partial r_{0,\mathrm{tr}}}\frac{\sin(\Gamma-\varphi)}{\sin\varphi}\\ &\quad - (\eta_\mathrm{n}-x)\frac{\cos\varphi}{\sin^2\varphi}\frac{\partial\varphi}{\partial r_{0,\mathrm{tr}}}\sin(\Gamma-\varphi)\\ &\quad + \frac{\eta_\mathrm{n}-x}{\sin\varphi}\cos(\Gamma-\varphi)\left(\frac{\partial\Gamma}{\partial r_{0,\mathrm{tr}}} - \frac{\partial\varphi}{\partial r_{0,\mathrm{tr}}}\right)\end{aligned} \tag{2.49}$$

In turn, these expressions contain the following derivatives.

$$\Gamma = \frac{1}{R_{0,\mathrm{t}}}\left[-\xi_\mathrm{n} + (\eta_\mathrm{n}-x)\cot\varphi\right] = \frac{1}{R_{0,\mathrm{t}}}\left[-\xi_\mathrm{n} - (\eta_\mathrm{n}-x)\frac{\partial\eta_\mathrm{n}}{\partial\xi_\mathrm{n}}\right] \implies \tag{2.50}$$

$$\frac{\partial\Gamma}{\partial\xi_\mathrm{n}} = \frac{1}{R_{0,\mathrm{t}}}\left[-1 - \left(\frac{\partial\eta_\mathrm{n}}{\partial\xi_\mathrm{n}}\right)^2 - (\eta_\mathrm{n}-x)\frac{\partial^2\eta_\mathrm{n}}{\partial\xi_\mathrm{n}^2}\right] \tag{2.51}$$

$$\frac{\partial\Gamma}{\partial r_{0,\mathrm{tr}}} = \frac{1}{R_{0,\mathrm{t}}}\left[-\frac{\partial\eta_\mathrm{n}}{\partial r_{0,\mathrm{tr}}}\frac{\partial\eta_\mathrm{n}}{\partial\xi_\mathrm{n}} - (\eta_\mathrm{n}-x)\frac{\partial^2\eta_\mathrm{n}}{\partial\xi_\mathrm{n}\partial r_{0,\mathrm{tr}}}\right] \tag{2.52}$$

$$\eta_\mathrm{n} = -h_{0,\mathrm{tr}} + r_{0,\mathrm{tr}}\sin\alpha_\mathrm{n} - \sqrt{r_{0,\mathrm{tr}}^2 - (\xi_\mathrm{n} - \xi_3 - r_{0,\mathrm{tr}}\cos\alpha_\mathrm{n})^2} \implies \tag{2.53}$$

$$\frac{\partial \eta_{\mathrm{n}}}{\partial \xi_{\mathrm{n}}} = \frac{\xi_{\mathrm{n}} - \xi_3 - r_{0,\mathrm{tr}} \cos \alpha_{\mathrm{n}}}{\sqrt{r_{0,\mathrm{tr}}^2 - (\xi_{\mathrm{n}} - \xi_3 - r_{0,\mathrm{tr}} \cos \alpha_{\mathrm{n}})^2}} \tag{2.54}$$

$$\frac{\partial \eta_{\mathrm{n}}}{\partial r_{0,\mathrm{tr}}} = \sin \alpha_{\mathrm{n}} - \frac{r_{0,\mathrm{tr}} + (\xi_{\mathrm{n}} - \xi_3 - r_{0,\mathrm{tr}} \cos \alpha_{\mathrm{n}}) \cos \alpha_{\mathrm{n}})}{\sqrt{r_{0,\mathrm{tr}}^2 - (\xi_{\mathrm{n}} - \xi_3 - r_{0,\mathrm{tr}} \cos \alpha_{\mathrm{n}})^2}} \tag{2.55}$$

Finally,

$$\varphi = \operatorname{arccot} x \implies \frac{\mathrm{d}\varphi}{\mathrm{d}x} = -\frac{1}{1 + x^2} \tag{2.56}$$

$$\frac{\mathrm{d}\varphi}{\mathrm{d}u} = \frac{\mathrm{d}\varphi}{\mathrm{d}x} \frac{\mathrm{d}x}{\mathrm{d}u} \tag{2.57}$$

$$\frac{\mathrm{d}\varphi}{\mathrm{d}u} = -\frac{1}{1 + x^2} \frac{\mathrm{d}x}{\mathrm{d}u} \tag{2.58}$$

$$x = -\frac{\partial \eta_{\mathrm{n}}}{\partial \xi_{\mathrm{n}}}, \quad u = \xi_{\mathrm{n}} \implies \tag{2.59}$$

$$\frac{\partial \varphi}{\partial \xi_{\mathrm{n}}} = \frac{1}{1 + \left(\frac{\partial \eta_{\mathrm{n}}}{\partial \xi_{\mathrm{n}}}\right)^2} \frac{\partial^2 \eta_{\mathrm{n}}}{\partial \xi_{\mathrm{n}}^2}; \quad \frac{\partial^2 \eta_{\mathrm{n}}}{\partial \xi_{\mathrm{n}}^2} = \frac{r_{0,\mathrm{tr}}^2}{\left(r_{0,\mathrm{tr}}^2 - (\xi_{\mathrm{n}} - \xi_3 - r_{0,\mathrm{tr}} \cos \alpha_{\mathrm{n}})^2\right)^{3/2}} \tag{2.60}$$

$$\frac{\partial \varphi}{\partial r_{0,\mathrm{tr}}} = \frac{1}{1 + \left(\frac{\partial \eta_{\mathrm{n}}}{\partial \xi_{\mathrm{n}}}\right)^2} \frac{\partial^2 \eta_{\mathrm{n}}}{\partial \xi_{\mathrm{n}} \partial r_{0,\mathrm{tr}}}; \quad \frac{\partial^2 \eta_{\mathrm{n}}}{\partial \xi_{\mathrm{n}} \partial r_{0,\mathrm{tr}}} = \frac{f' g - {}' f g'}{g^2} \tag{2.61}$$

where

$$\begin{cases} f = \xi_{\mathrm{n}} - \xi_3 - r_{0,\mathrm{tr}} \cos \alpha_{\mathrm{n}} \\ f' = -\cos \alpha_{\mathrm{n}} \\ g = \sqrt{r_{0,\mathrm{tr}}^2 - (\xi_{\mathrm{n}} - \xi_3 - r_{0,\mathrm{tr}} \cos \alpha_{\mathrm{n}})^2} \\ g' = \frac{r_{0,\mathrm{tr}} + (\xi_{\mathrm{n}} - \xi_3 - r_{0,\mathrm{tr}} \cos \alpha_{\mathrm{n}}) \cos \alpha_{\mathrm{n}})}{\sqrt{r_{0,\mathrm{tr}}^2 - (\xi_{\mathrm{n}} - \xi_3 - r_{0,\mathrm{tr}} \cos \alpha_{\mathrm{n}})^2}} \end{cases} \tag{2.62}$$

$r_{0,\mathrm{tr}}$ and ξ_{n} are now known.

Here, a tip rounding is introduced. The reason is that contact is sought for based on the normal direction of the contact surface, which makes it impossible to use a sharp corner which has an infinite number of normals. Also in practice, the radius of curvature of the corner is not exactly zero, but rather has a small value.

For the tip rounding, introduce the simplified notation $a = r_{0,\xi}$, $b = r_{0,\eta}$, $x = \xi_4$, $x_c = \xi_{\mathrm{tr,c}}$, $x_e = \xi_{\mathrm{r,c}}$, $y = \eta_4$, $y_c = \eta_{\mathrm{tr,c}}$, $y_e = \eta_{\mathrm{r,c}}$, $r = r_{0,\mathrm{tr}}$.

Where tip relief and tip rounding regions meet, they have a common position:

$$\begin{cases} y = y_c - \sqrt{r^2 - (x - x_c)^2} \\ y = y_e - \sqrt{b^2 - \frac{b^2}{a^2}(x - x_e)^2} \end{cases} \tag{2.63}$$

as well as a common slope:

$$\begin{cases} \frac{\mathrm{d}y}{\mathrm{d}x} = \frac{x - x_c}{\sqrt{r^2 - (x - x_c)^2}} \\ \frac{\mathrm{d}y}{\mathrm{d}x} = \frac{b^2}{a^2} \frac{x - x_e}{\sqrt{b^2 - \frac{b^2}{a^2}(x - x_e)^2}} \end{cases} \tag{2.64}$$

The common slope gives

$$\frac{b^2}{a^2}(x - x_e)^2 = a^2 \frac{(x - x_c)^2}{\left(\frac{a^2}{b^2} - 1\right)(x - x_c)^2 + r^2} \tag{2.65}$$

which, inserted into the common position, gives the function

$$f(x) = y_c - \sqrt{r^2 - (x - x_c)^2} - y_e + \sqrt{b^2 - \frac{(x - x_c)^2}{\left(\frac{a^2}{b^2} - 1\right)(x - x_c)^2 + r^2}} \tag{2.66}$$

The equation $f(x) = 0$ is solved by a Newton-Raphson scheme:

$$x_{n+1} = x_n - \frac{f(x_n)}{f'(x_n)} \tag{2.67}$$

where

$$f'(x) = \frac{x - x_c}{\sqrt{r^2 - (x - x_c)^2}} - \frac{a^2(x - x_c)^2 r^2}{\sqrt{b^2 K^4 - a^2(x - x_c)^2 K^3}} \tag{2.68}$$

with

$$K = \left(\frac{a^2}{b^2} - 1\right)(x - x_c)^2 + r^2 \tag{2.69}$$

2.2.2 Coordinates with simulated errors

Introduce a rotation $\Delta\alpha_\mathrm{n}$ of the reference profile around the reference pitch point. The modified coordinates become

$$\begin{cases} \xi_\mathrm{m} = (\xi_\mathrm{n} - \frac{\pi}{4} + x_\mathrm{n}\tan\alpha_\mathrm{n})\cos\Delta\alpha_\mathrm{n} - (\eta_\mathrm{n} - x_\mathrm{n})\sin\Delta\alpha_\mathrm{n} + \frac{\pi}{4} - x_\mathrm{n}\tan\alpha_\mathrm{n} \\ \eta_\mathrm{m} = (\xi_\mathrm{n} - \frac{\pi}{4} + x_\mathrm{n}\tan\alpha_\mathrm{n})\sin\Delta\alpha_\mathrm{n} + (\eta_\mathrm{n} - x_\mathrm{n})\cos\Delta\alpha_\mathrm{n} + x_\mathrm{n} \end{cases} \tag{2.70}$$

In the transverse plane for the tool with introduced errors, the coordinates are given by

$$\begin{cases} \xi_\mathrm{t} = \frac{\xi_\mathrm{m}}{\cos\beta} \\ \eta_\mathrm{t} = \eta_\mathrm{m} \end{cases} \tag{2.71}$$

In the point of contact, the slope gives that

$$\cot\varphi = -\frac{\mathrm{d}\eta_\mathrm{t}}{\mathrm{d}\eta_\mathrm{t}} = -\frac{\mathrm{d}\eta_\mathrm{m}}{\mathrm{d}\eta_\mathrm{m}}\cos\beta = -\frac{\frac{\mathrm{d}\eta_\mathrm{m}}{\mathrm{d}\xi_\mathrm{n}}}{\frac{\mathrm{d}\xi_\mathrm{m}}{\mathrm{d}\xi_\mathrm{n}}}\cos\beta \tag{2.72}$$

where

$$\frac{\mathrm{d}\xi_\mathrm{m}}{\mathrm{d}\xi_\mathrm{n}} = \cos\Delta\alpha - \frac{\mathrm{d}\eta_\mathrm{n}}{\mathrm{d}\xi_\mathrm{n}}\sin\Delta\alpha \tag{2.73}$$

and

$$\frac{\mathrm{d}\eta_{\mathrm{m}}}{\mathrm{d}\xi_{\mathrm{n}}} = \sin\Delta\alpha + \frac{\mathrm{d}\eta_{\mathrm{n}}}{\mathrm{d}\xi_{\mathrm{n}}}\cos\Delta\alpha \tag{2.74}$$

which gives

$$\cot\varphi = -\frac{\sin\Delta\alpha + \frac{\mathrm{d}\eta_{\mathrm{n}}}{\mathrm{d}\xi_{\mathrm{n}}}\cos\Delta\alpha}{\cos\Delta\alpha - \frac{\mathrm{d}\eta_{\mathrm{n}}}{\mathrm{d}\xi_{\mathrm{n}}}\sin\Delta\alpha}\cos\beta \tag{2.75}$$

Simultaneously,

$$\cot\varphi = \frac{R_{0,\mathrm{t}}\Gamma - \zeta_{\mathrm{s}}\tan\beta + \xi_{\mathrm{t}}}{\eta_{\mathrm{t}} - x} \tag{2.76}$$

Thus

$$\Gamma = \frac{1}{R_{0,\mathrm{t}}}\left[-\frac{\xi_{\mathrm{m}}}{\cos\beta} + (\eta_{\mathrm{m}} - x)\cot\varphi + \zeta_{\mathrm{s}}\tan\beta\right] \tag{2.77}$$

The coordinates for P become

$$\xi_{\mathrm{s}} = R_{0,\mathrm{t}}\sin\Gamma - \frac{\eta_{\mathrm{m}} - x}{\sin\varphi}\cos(\Gamma - \varphi) \tag{2.78}$$

$$\eta_{\mathrm{s}} = R_{0,\mathrm{t}}\cos\Gamma + \frac{\eta_{\mathrm{m}} - x}{\sin\varphi}\sin(\Gamma - \varphi) \tag{2.79}$$

$$\zeta_{\mathrm{s}} = \zeta_{\mathrm{s}} \tag{2.80}$$

or in vector format

$$\mathbf{r}_{\mathrm{s}} = (\xi_{\mathrm{s}}, \eta_{\mathrm{s}}, \zeta_{\mathrm{s}}) \tag{2.81}$$

The vector $\mathbf{r}_{\mathrm{s}}$ describes the flank from the gap. Description of the flank from the symmetry line of the tooth is found from the rotation

$$\mathbf{r} = \mathbf{R}(-\frac{\pi}{z})\mathbf{r}_{\mathrm{s}} \tag{2.82}$$

where

$$\mathbf{R}(\theta) = \begin{pmatrix} \cos\theta & -\sin\theta & 0 \\ \sin\theta & \cos\theta & 0 \\ 0 & 0 & -1 \end{pmatrix} \tag{2.83}$$

Consequently,

$$\mathbf{r} = \begin{pmatrix} \cos\frac{\pi}{z} & \sin\frac{\pi}{z} & 0 \\ -\sin\frac{\pi}{z} & \cos\frac{\pi}{z} & 0 \\ 0 & 0 & -1 \end{pmatrix} \begin{pmatrix} \xi_\mathrm{s} \\ \eta_\mathrm{s} \\ \zeta_\mathrm{s} \end{pmatrix} = \begin{pmatrix} \xi_\mathrm{s}\cos\frac{\pi}{z} + \eta_\mathrm{s}\sin\frac{\pi}{z} \\ -\xi_\mathrm{s}\sin\frac{\pi}{z} + \eta_\mathrm{s}\cos\frac{\pi}{z} \\ -\zeta_\mathrm{s} \end{pmatrix} = \begin{pmatrix} \xi \\ \eta \\ \zeta \end{pmatrix} \tag{2.84}$$

The normal $\mathbf{n} = (n_\xi, n_\eta, n_\zeta)$ is given by

$$\mathbf{n} = \frac{\partial \mathbf{r}}{\partial \xi_\mathrm{n}} \times \frac{\partial \mathbf{r}}{\partial \zeta} = \begin{vmatrix} \hat{\xi} & \hat{\eta} & \hat{\zeta} \\ \frac{\partial \xi}{\partial \xi_\mathrm{n}} & \frac{\partial \eta}{\partial \xi_\mathrm{n}} & 0 \\ \frac{\partial \xi}{\partial \zeta} & \frac{\partial \eta}{\partial \zeta} & 1 \end{vmatrix} = \left(\frac{\partial \eta}{\partial \xi_\mathrm{n}}, -\frac{\partial \xi}{\partial \xi_\mathrm{n}}, \frac{\partial \xi}{\partial \xi_\mathrm{n}}\frac{\partial \eta}{\partial \zeta} - \frac{\partial \xi}{\partial \zeta}\frac{\partial \eta}{\partial \xi_\mathrm{n}} \right) \tag{2.85}$$

where the derivatives are given by

$$\frac{\partial \xi}{\partial \xi_\mathrm{n}} = \frac{\partial \xi}{\partial \xi_\mathrm{m}}\frac{\partial \xi_\mathrm{m}}{\partial \xi_\mathrm{n}} = \left(\frac{\partial \xi_\mathrm{s}}{\partial \xi_\mathrm{n}} \cos\frac{\pi}{z} + \frac{\partial \eta_\mathrm{s}}{\partial \xi_\mathrm{n}} \sin\frac{\pi}{z} \right) \cos\Delta\alpha \tag{2.86}$$

$$\frac{\partial \eta}{\partial \xi_\mathrm{n}} = \left(-\frac{\partial \xi_\mathrm{s}}{\partial \xi_\mathrm{n}} \sin\frac{\pi}{z} + \frac{\partial \eta_\mathrm{s}}{\partial \xi_\mathrm{n}} \cos\frac{\pi}{z} \right) \cos\Delta\alpha \tag{2.87}$$

$$\frac{\partial \xi}{\partial \zeta} = \frac{\partial \xi}{\partial \zeta_\mathrm{s}}\frac{\partial \zeta_\mathrm{s}}{\partial \zeta} = \left(\frac{\partial \xi_\mathrm{s}}{\partial \zeta_\mathrm{s}} \cos\frac{\pi}{z} + \frac{\partial \eta_\mathrm{s}}{\partial \zeta_\mathrm{s}} \sin\frac{\pi}{z} \right) (-1) \tag{2.88}$$

$$\frac{\partial \eta}{\partial \zeta} = \left(-\frac{\partial \xi_\mathrm{s}}{\partial \zeta_\mathrm{s}} \sin\frac{\pi}{z} + \frac{\partial \eta_\mathrm{s}}{\partial \zeta_\mathrm{s}} \cos\frac{\pi}{z} \right) (-1) \tag{2.89}$$

where in turn

$$\begin{aligned}\frac{\partial \xi_\mathrm{s}}{\partial \xi_\mathrm{m}} &= R_{0,\mathrm{t}} \cos\Gamma \frac{\partial \Gamma}{\partial \xi_\mathrm{m}} - \frac{\mathrm{d}\eta_\mathrm{m}}{\mathrm{d}\xi_\mathrm{m}} \frac{\cos(\Gamma-\varphi)}{\sin\varphi} \\ &\quad + (\eta_\mathrm{m} - x) \frac{\cos\varphi}{\sin^2\varphi} \frac{\mathrm{d}\varphi}{\mathrm{d}\xi_\mathrm{m}} \cos(\Gamma-\varphi) \\ &\quad + \frac{\eta_\mathrm{m} - x}{\sin\varphi} \sin(\Gamma-\varphi) \left(\frac{\partial \Gamma}{\partial \xi_\mathrm{m}} - \frac{\mathrm{d}\varphi}{\mathrm{d}\xi_\mathrm{m}} \right)\end{aligned} \tag{2.90}$$

$$\begin{aligned}\frac{\partial \eta_\mathrm{s}}{\partial \xi_\mathrm{m}} &= -R_{0,\mathrm{t}} \sin\Gamma \frac{\partial \Gamma}{\partial \xi_\mathrm{m}} + \frac{\mathrm{d}\eta_\mathrm{m}}{\mathrm{d}\xi_\mathrm{m}} \frac{\sin(\Gamma-\varphi)}{\sin\varphi} \\ &\quad - (\eta_\mathrm{m} - x) \frac{\cos\varphi}{\sin^2\varphi} \frac{\mathrm{d}\varphi}{\mathrm{d}\xi_\mathrm{m}} \sin(\Gamma-\varphi) \\ &\quad + \frac{\eta_\mathrm{m} - x}{\sin\varphi} \cos(\Gamma-\varphi) \left(\frac{\partial \Gamma}{\partial \xi_\mathrm{m}} - \frac{\mathrm{d}\varphi}{\mathrm{d}\xi_\mathrm{m}} \right)\end{aligned} \tag{2.91}$$

$$\begin{aligned}\frac{\partial \xi_\mathrm{s}}{\partial \zeta_\mathrm{s}} &= \left(R_{0,\mathrm{t}} \cos\Gamma + \frac{\eta_\mathrm{m} - x}{\sin\varphi} \sin(\Gamma-\varphi) \right) \frac{\partial \Gamma}{\partial \zeta_\mathrm{s}} \\ &= \left(R_{0,\mathrm{t}} \cos\Gamma + \frac{\eta_\mathrm{m} - x}{\sin\varphi} \sin(\Gamma-\varphi) \right) \frac{\tan\beta}{R_{0,\mathrm{t}}}\end{aligned} \tag{2.92}$$

$$\frac{\partial \eta_\mathrm{s}}{\partial \zeta_\mathrm{s}} = \left(-R_{0,\mathrm{t}} \sin\Gamma + \frac{\eta_\mathrm{m} - x}{\sin\varphi} \cos(\Gamma-\varphi) \right) \frac{\tan\beta}{R_{0,\mathrm{t}}} \tag{2.93}$$

From

$$\cot\varphi = -\frac{\mathrm{d}\eta_\mathrm{m}}{\mathrm{d}\xi_\mathrm{m}} \cos\beta \tag{2.94}$$

it follows that

$$\frac{\mathrm{d}}{\mathrm{d}\xi_\mathrm{m}}(\cot\varphi) = -\frac{\mathrm{d}^2\eta_\mathrm{m}}{\mathrm{d}\xi_\mathrm{m}^2} \cos\beta \tag{2.95}$$

Simultaneously,

$$\frac{\mathrm{d}}{\mathrm{d}\xi_\mathrm{m}}(\cot\varphi) = -\frac{1}{\sin^2\varphi} \frac{\mathrm{d}\varphi}{\mathrm{d}\xi_\mathrm{m}} \tag{2.96}$$

Thus

$$\frac{\mathrm{d}\varphi}{\mathrm{d}\xi_{\mathrm{m}}} = \frac{\mathrm{d}^2\eta_{\mathrm{m}}}{\mathrm{d}\xi_{\mathrm{m}}^2}\sin^2\varphi\cos\beta \tag{2.97}$$

Furthermore,

$$\Gamma = \frac{1}{R_{0,\mathrm{t}}}\left[-\frac{\xi_{\mathrm{m}}}{\cos\beta} + (\eta_{\mathrm{m}} - x)\cot\varphi + \zeta_{\mathrm{s}}\tan\beta\right] \tag{2.98}$$

which gives

$$\frac{\partial\Gamma}{\partial\xi_{\mathrm{m}}} = \frac{1}{R_{0,\mathrm{t}}}\left[-\frac{1}{\cos\beta} + \frac{\mathrm{d}\eta_{\mathrm{m}}}{\mathrm{d}\xi_{\mathrm{m}}}\cot\varphi - \frac{\eta_{\mathrm{m}} - x}{\sin^2\varphi}\frac{\mathrm{d}\varphi}{\mathrm{d}\xi_{\mathrm{m}}}\right] \tag{2.99}$$

2.2.3 Contact conditions

The position of tooth i, $i = 1, 2, ..., z_p$ or z_g are denoted by $\phi_{p,i}$ and $\phi_{g,i}$ for the pinion and the gear, respectively, where

$$\begin{cases}\phi_{p,i} = \phi_{p,0} + i\frac{2\pi}{z_p} + \Delta\phi_{p,i} \\ \phi_{g,i} = \phi_{g,0} + i\frac{2\pi}{z_g} + \Delta\phi_{g,i}\end{cases} \tag{2.100}$$

Thus, $\Delta\phi_{p,i} \neq 0$ and $\Delta\phi_{g,i} \neq 0$ correspond to pitch errors on the pinion and gear, respectively.

Assume

$$s_p + s_g + \delta/2 = a\sin\alpha \tag{2.101}$$

where

$$\tan\varphi_p = \frac{s_p}{r_{b,p}} \implies s_p = r_{b,p}\tan\varphi_p; \quad s_g = r_{b,g}\tan\varphi_g \tag{2.102}$$

From the definition of the involute function,

$$\mathrm{inv}\varphi = \tan\varphi - \varphi \tag{2.103}$$

it follows that

$$\tan\varphi_p = \alpha + \phi_{p,0} + \frac{\pi + 4x_p \tan\alpha_\mathrm{t}}{2z_p}\mathrm{inv}\alpha_\mathrm{t} \tag{2.104}$$

and

$$\tan\varphi_g = \alpha - \phi_{g,0} + \frac{\pi + 4x_g \tan\alpha_\mathrm{t}}{2z_g} + \mathrm{inv}\alpha_\mathrm{t} \tag{2.105}$$

Thus it follows that

$$\begin{aligned} &r_{b,p}\left(\alpha + \phi_{p,0} + \frac{\pi + 4x_p \tan\alpha_\mathrm{t}}{2z_p} + \mathrm{inv}\alpha_\mathrm{t}\right) + \\ &r_{b,g}\left(\alpha - \phi_{g,0} + \frac{\pi + 4x_g \tan\alpha_\mathrm{t}}{2z_g} + \mathrm{inv}\alpha_\mathrm{t}\right) = a\sin\alpha - \delta/2 \end{aligned} \tag{2.106}$$

or

$$\begin{aligned} \phi_{p,0} = &\frac{a\sin\alpha - \delta/2}{r_{b,p}} - \frac{r_{b,g}}{r_{b,p}}\left(\alpha - \phi_{g,0} + \frac{\pi + 4x_g \tan\alpha_\mathrm{t}}{2z_g} + \mathrm{inv}\alpha_\mathrm{t}\right) \\ &- \alpha - \frac{\pi + 4x_p \tan\alpha_\mathrm{t}}{2z_p} - \mathrm{inv}\alpha_\mathrm{t} \end{aligned} \tag{2.107}$$

i.e. $\phi_{p,0} = \phi_{p,0}(\phi_{g,0})$.

In the same coordinate system, the contact positions are given by

$$\begin{aligned} \mathbf{R}_p = (&-\xi_p \cos(\phi_{p,i} + \phi) - \eta_p \sin(\phi_{p,i} + \phi), \\ &a + \xi_p \sin(\phi_{p,i} + \phi) - \eta_p \cos(\phi_{p,i} + \phi), \zeta_p) \end{aligned} \tag{2.108}$$

and

$$\mathbf{R}_g = (\xi_g \cos\phi_{g,i} - \eta_g \sin\phi_{g,i}, \xi_g \sin\phi_{g,i} + \eta_g \cos\phi_{g,i}, \zeta_g) \tag{2.109}$$

and the normals are given by

$$\begin{aligned}\mathbf{N}_p = (&-n_{p,\xi}\cos(\phi_{p,i}+\phi) - n_{p,\eta}\sin(\phi_{p,i}+\phi),\\ &n_{p,\xi}\sin(\phi_{p,i}+\phi) - n_{p,\eta}\cos(\phi_{p,i}+\phi), n_{p,\zeta})\end{aligned} \tag{2.110}$$

and

$$\mathbf{N}_g = (n_{g,\xi}\cos\phi_{g,i} - n_{g,\eta}\sin\phi_{g,i}, n_{g,\xi}\sin\phi_{g,i} + n_{g,\eta}\cos\phi_{g,i}, n_{g,\zeta}) \tag{2.111}$$

Common normal in the contact yields

$$\tan\psi_i = \frac{N_{g,y}}{N_{g,x}} = \frac{N_{p,y}}{N_{p,x}} = \frac{R_{p,y} - R_{g,y}}{R_{p,x} - R_{g,x}} \tag{2.112}$$

This equation contains $\mathbf{N}_p$, $\mathbf{N}_g$, $\mathbf{R}_p$, and $\mathbf{R}_g$. These are in turn functions of $\mathbf{n}_p$, $\mathbf{n}_g$, $\mathbf{r}_p$, and $\mathbf{r}_g$ where

$$\mathbf{r} = \mathbf{r}(\xi_\mathrm{n}, \zeta, \Delta\alpha_\mathrm{n}), \quad \mathbf{n} = \mathbf{n}(\xi_\mathrm{n}, \zeta, \Delta\alpha_\mathrm{n}) \tag{2.113}$$

These conditions can be written as

$$\begin{cases} N_{p,x}N_{g,y} - N_{g,x}N_{p,y} = f_1 = 0 \\ (R_{p,y} - R_{g,y})N_{p,x} - (R_{p,x} - R_{g,x})N_{p,y} = f_2 = 0 \end{cases} \tag{2.114}$$

or

$$\begin{cases} f_1(\xi_{\mathrm{n},p}, \xi_{\mathrm{n},g}) = 0 \\ f_2(\xi_{\mathrm{n},p}, \xi_{\mathrm{n},g}) = 0 \end{cases} \tag{2.115}$$

where the equations include the following terms.

$$N_{p,x} = -n_{p,\xi}\cos(\phi_{p,i}+\phi) - n_{p,\eta}\sin(\phi_{p,i}+\phi) \tag{2.116}$$

$$N_{p,y} = n_{p,\xi} \sin(\phi_{p,i} + \phi) - n_{p,\eta} \cos(\phi_{p,i} + \phi) \tag{2.117}$$

$$N_{g,x} = n_{g,\xi} \cos \phi_{g,i} - n_{g,\eta} \sin \phi_{g,i} \tag{2.118}$$

$$N_{g,y} = n_{g,\xi} \sin \phi_{g,i} + n_{g,\eta} \cos \phi_{g,i} \tag{2.119}$$

$$R_{p,x} = -\xi_p \cos(\phi_{p,i} + \phi) - \eta_p \sin(\phi_{p,i} + \phi) \tag{2.120}$$

$$R_{p,y} = a + \xi_p \sin(\phi_{p,i} + \phi) - \eta_p \cos(\phi_{p,i} + \phi) \tag{2.121}$$

$$R_{g,x} = \xi_g \cos \phi_{g,i} - \eta_g \sin \phi_{g,i} \tag{2.122}$$

$$R_{g,y} = \xi_g \sin \phi_{g,i} + \eta_g \cos \phi_{g,i} \tag{2.123}$$

where

$$n_{p,\xi} = -\left.\frac{\partial \eta}{\partial \xi_{\mathrm{n}}}\right|_p \tag{2.124}$$

$$n_{p,\eta} = \left.\frac{\partial \xi}{\partial \xi_{\mathrm{n}}}\right|_p \tag{2.125}$$

$$n_{g,\xi} = -\left.\frac{\partial \eta}{\partial \xi_{\mathrm{n}}}\right|_g \tag{2.126}$$

$$n_{g,\eta} = \left.\frac{\partial \xi}{\partial \xi_{\mathrm{n}}}\right|_p \tag{2.127}$$

The equations

$$\begin{cases} f_1(\xi_{\mathrm{n},p}, \xi_{\mathrm{n},g}) = 0 \\ f_2(\xi_{\mathrm{n},p}, \xi_{\mathrm{n},g}) = 0 \end{cases} \tag{2.128}$$

are solved by Newton-Raphson. Generally, the equations

$$\begin{cases} f_1(x_1, x_2) = 0 \\ f_2(x_1, x_2) = 0 \end{cases} \tag{2.129}$$

are solved by introducing

$$\mathbf{x} = \begin{pmatrix} x_1 \\ x_2 \end{pmatrix} \tag{2.130}$$

and

$$\mathbf{f} = \begin{pmatrix} f_1 \\ f_2 \end{pmatrix} \tag{2.131}$$

Approximate

$$\mathbf{f}(\mathbf{x}) = \mathbf{f}(\mathbf{x}_0) + D\mathbf{f}(\mathbf{x}_0)(\mathbf{x} - \mathbf{x}_0) \tag{2.132}$$

where

$$\mathbf{f}(\mathbf{x}) = \mathbf{0} \implies D\mathbf{f}(\mathbf{x}_0)\Delta\mathbf{x} = -\mathbf{f}(\mathbf{x}_0) \tag{2.133}$$

with solution

$$\Delta\mathbf{x} = -\left(D\mathbf{f}(\mathbf{x}_0)\right)^{-1}\mathbf{f}(\mathbf{x}_0) \tag{2.134}$$

where

$$D\mathbf{f}(\mathbf{x}) = \begin{pmatrix} \frac{\partial f_1}{\partial x_1}(\mathbf{x}) & \frac{\partial f_1}{\partial x_2}(\mathbf{x}) \\ \frac{\partial f_2}{\partial x_1}(\mathbf{x}) & \frac{\partial f_2}{\partial x_2}(\mathbf{x}) \end{pmatrix} \tag{2.135}$$

The elements of the functional matrix are given by

$$\begin{aligned}\frac{\partial f_1}{\partial \xi_{\mathrm{n},p}} =& \frac{\partial N_{p,x}}{\partial \xi_{\mathrm{n},p}} N_{g,y} + N_{p,x} \underbrace{\frac{\partial N_{g,y}}{\partial \xi_{\mathrm{n},p}}}_{=0} - \underbrace{\frac{\partial N_{g,x}}{\partial \xi_{\mathrm{n},p}}}_{=0} N_{p,y} \\ -N_{g,x} \frac{\partial N_{p,y}}{\partial \xi_{\mathrm{n},p}} =& \frac{\partial N_{p,x}}{\partial \xi_{\mathrm{n},p}} N_{g,y} - N_{g,x} \frac{\partial N_{p,y}}{\partial \xi_{\mathrm{n},p}}\end{aligned} \tag{2.136}$$

$$\frac{\partial f_1}{\partial \xi_{\mathrm{n},g}} = N_{p,x} \frac{\partial N_{g,y}}{\partial \xi_{\mathrm{n},g}} - \frac{\partial N_{g,x}}{\partial \xi_{\mathrm{n},g}} N_{p,y} \tag{2.137}$$

$$\begin{aligned}\frac{\partial f_2}{\partial \xi_{\mathrm{n},p}} =& \frac{\partial R_{p,y}}{\partial \xi_{\mathrm{n},p}} N_{p,x} + (R_{p,y} - R_{g,y}) \frac{\partial N_{p,x}}{\partial \xi_{\mathrm{n},p}} \\ & - \frac{\partial R_{p,x}}{\partial \xi_{\mathrm{n},p}} N_{p,y} - (R_{p,x} - R_{g,x}) \frac{\partial N_{p,y}}{\partial \xi_{\mathrm{n},p}}\end{aligned} \tag{2.138}$$

and

$$\frac{\partial f_2}{\partial \xi_{\mathrm{n},g}} = -\frac{\partial R_{g,y}}{\partial \xi_{\mathrm{n},g}} N_{p,x} + \frac{\partial R_{g,x}}{\partial \xi_{\mathrm{n},g}} N_{p,y} \tag{2.139}$$

These expressions contain the following derivatives.

$$\frac{\partial N_{p,x}}{\partial \xi_{\mathrm{n},p}} = \left.\frac{\partial^2 \eta}{\partial \xi_{\mathrm{n}}^2}\right|_p \cos(\phi_{p,i} + \phi) - \left.\frac{\partial^2 \xi}{\partial \xi_{\mathrm{n}}^2}\right|_p \sin(\phi_{p,i} + \phi) \tag{2.140}$$

$$\frac{\partial N_{p,y}}{\partial \xi_{\mathrm{n},p}} = -\left.\frac{\partial^2 \eta}{\partial \xi_{\mathrm{n}}^2}\right|_p \sin(\phi_{p,i} + \phi) - \left.\frac{\partial^2 \xi}{\partial \xi_{\mathrm{n}}^2}\right|_p \cos(\phi_{p,i} + \phi) \tag{2.141}$$

$$\frac{\partial N_{g,x}}{\partial \xi_{\mathrm{n},g}} = -\left.\frac{\partial^2 \eta}{\partial \xi_{\mathrm{n}}^2}\right|_g \cos \phi_{g,i} - \left.\frac{\partial^2 \xi}{\partial \xi_{\mathrm{n}}^2}\right|_g \sin \phi_{g,i} \tag{2.142}$$

$$\frac{\partial N_{g,y}}{\partial \xi_{\mathrm{n},g}} = -\left.\frac{\partial^2 \eta}{\partial \xi_{\mathrm{n}}^2}\right|_g \sin \phi_{g,i} + \left.\frac{\partial^2 \xi}{\partial \xi_{\mathrm{n}}^2}\right|_g \cos \phi_{g,i} \tag{2.143}$$

$$\frac{\partial R_{p,x}}{\partial \xi_{\mathrm{n},p}} = -\left.\frac{\partial \xi}{\partial \xi_{\mathrm{n}}}\right|_p \cos(\phi_{p,i} + \phi) - \left.\frac{\partial \eta}{\partial \xi_{\mathrm{n}}}\right|_p \sin(\phi_{p,i} + \phi) \tag{2.144}$$

$$\frac{\partial R_{p,y}}{\partial \xi_{\mathrm{n},p}} = \left.\frac{\partial \xi}{\partial \xi_{\mathrm{n}}}\right|_p \sin(\phi_{p,i} + \phi) - \left.\frac{\partial \eta}{\partial \xi_{\mathrm{n}}}\right|_p \cos(\phi_{p,i} + \phi) \tag{2.145}$$

$$\frac{\partial R_{g,x}}{\partial \xi_{\mathrm{n},g}} = \left.\frac{\partial \xi}{\partial \xi_{\mathrm{n}}}\right|_g \cos\phi_{g,i} - \left.\frac{\partial \eta}{\partial \xi_{\mathrm{n}}}\right|_g \sin\phi_{g,i} \tag{2.146}$$

$$\frac{\partial R_{g,y}}{\partial \xi_{\mathrm{n},g}} = \left.\frac{\partial \xi}{\partial \xi_{\mathrm{n}}}\right|_g \sin\phi_{g,i} + \left.\frac{\partial \eta}{\partial \xi_{\mathrm{n}}}\right|_g \cos\phi_{g,i} \tag{2.147}$$

The deformation is then calculated as

$$\delta_i = \frac{R_{p,x} - R_{g,x}}{\cos\psi_i} \tag{2.148}$$

where

$$\tan\psi_i = \frac{N_{p,y}}{N_{p,x}} \tag{2.149}$$

2.2.4 Contact geometry

R_{gx} denotes both the point and the radius to it. Generally,

$$\xi_{\mathrm{n}} \to \begin{cases} \xi = \xi(\xi_{\mathrm{n}}) \\ \eta = \eta(\xi_{\mathrm{n}}) \end{cases} \tag{2.150}$$

which implies

$$\xi_{\mathrm{n}} = \xi_{\mathrm{n}g,x} \to \begin{cases} \xi = \xi_{gx} \\ \eta = \eta_{gx} \end{cases} \tag{2.151}$$

The vector $\mathbf{R}_{gx}$ is then given by

$$\mathbf{R}_{gx} = \begin{pmatrix} R_{gx,x} \\ R_{gx,y} \\ R_{gx,z} \end{pmatrix} = \begin{pmatrix} \xi_{gx}\cos\phi_{g,i} - \eta_{gx}\sin\phi_{g,i} \\ \xi_{gx}\sin\phi_{g,i} + \eta_{gx}\cos\phi_{g,i} \\ \zeta_{gx} \end{pmatrix} \tag{2.152}$$

From the geometry it follows that

$$\begin{cases} R_{g,x} - x\sin\psi_i - h_g\cos\psi_i = R_{gx,x}(\xi_{\mathrm{n}g,x}) \\ R_{g,y} + x\cos\psi_i - h_g\sin\psi_i = R_{gx,y}(\xi_{\mathrm{n}g,x}) \end{cases} \iff \tag{2.153}$$

$$\begin{cases} (R_{g,x} - x\sin\psi_i - R_{gx,x})\sin\psi_i = h_g\cos\psi_i\sin\psi_i \\ (R_{g,y} + x\cos\psi_i - R_{gx,y})\cos\psi_i = h_g\sin\psi_i\cos\psi_i \end{cases} \iff \tag{2.154}$$

$$\begin{aligned} &-(R_{g,x} - x\sin\psi_i - R_{gx,x})\sin\psi_i \\ &+(R_{g,y} + x\cos\psi_i - R_{gx,y})\cos\psi_i = 0 \iff \end{aligned} \tag{2.155}$$

$$\begin{aligned} R_{gx,x}(\xi_{\mathrm{n}g,x})\sin\psi_i - R_{gx,y}(\xi_{\mathrm{n}g,x})\cos\psi_i \\ -R_{g,x}\sin\psi_i + R_{g,y}\cos\psi_i + x = 0 \end{aligned} \tag{2.156}$$

or

$$\begin{aligned} f(\xi_{\mathrm{n}g,x}) = (R_{gx,x}(\xi_{\mathrm{n}g,x}) - R_{g,x})\sin\psi_i \\ +(R_{g,y} - R_{gx,y}(\xi_{\mathrm{n}g,x}))\cos\psi_i + x = 0 \end{aligned} \tag{2.157}$$

This equation is solved by Newton-Raphson. The derivative is given by

$$f'(\xi_{\mathrm{n}g,x}) = \frac{\mathrm{d}R_{gx,x}}{\mathrm{d}\xi_{\mathrm{n}g,x}}\sin\psi_i - \frac{\mathrm{d}R_{gx,y}}{\mathrm{d}\xi_{\mathrm{n}g,x}}\cos\psi_i \tag{2.158}$$

where

$$\frac{\mathrm{d}R_{gx,x}}{\mathrm{d}\xi_{\mathrm{n}g,x}} = \left.\frac{\partial\xi}{\partial\xi_{\mathrm{n}}}\right|_{g,x}\cos\phi_{g,i} - \left.\frac{\partial\eta}{\partial\xi_{\mathrm{n}}}\right|_{g,x}\sin\phi_{g,i} \tag{2.159}$$

and

$$\frac{\mathrm{d}R_{gx,y}}{\mathrm{d}\xi_{\mathrm{n}g,x}} = \left.\frac{\partial\xi}{\partial\xi_{\mathrm{n}}}\right|_{g,x}\sin\phi_{g,i} + \left.\frac{\partial\eta}{\partial\xi_{\mathrm{n}}}\right|_{g,x}\cos\phi_{g,i} \tag{2.160}$$

Similarly, R_{px} denotes both the point and the radius to it. Generally,

$$\xi_{\mathrm{n}} \to \begin{cases} \xi = \xi(\xi_{\mathrm{n}}) \\ \eta = \eta(\xi_{\mathrm{n}}) \end{cases} \tag{2.161}$$

which implies

$$\xi_{\mathrm{n}} = \xi_{\mathrm{n}p,x} \to \begin{cases} \xi = \xi_{px} \\ \eta = \eta_{px} \end{cases} \tag{2.162}$$

The vector $\mathbf{R}_{px}$ is then given by

$$\mathbf{R}_{px} = \begin{pmatrix} R_{px,x} \\ R_{px,y} \\ R_{px,z} \end{pmatrix} = \begin{pmatrix} -\xi_{px}\cos(\phi_{p,i}+\phi) - \eta_{px}\sin(\phi_{p,i}+\phi) \\ a + \xi_{px}\sin(\phi_{p,i}+\phi) - \eta_{px}\cos(\phi_{p,i}+\phi) \\ \zeta_{px} \end{pmatrix} \tag{2.163}$$

From the geometry it follows that

$$\begin{cases} R_{p,x} - x\sin\psi_i - h_p\cos\psi_i = R_{px,x}(\xi_{\mathrm{n}p,x}) \\ R_{p,y} + x\cos\psi_i - h_p\sin\psi_i = R_{px,y}(\xi_{\mathrm{n}p,x}) \end{cases} \iff \tag{2.164}$$

$$\begin{cases} (R_{p,x} - x\sin\psi_i - R_{px,x})\sin\psi_i = h_p\cos\psi_i\sin\psi_i \\ (R_{p,y} + x\cos\psi_i - R_{px,y})\cos\psi_i = h_p\sin\psi_i\cos\psi_i \end{cases} \iff \tag{2.165}$$

$$\begin{aligned} &-(R_{p,x} - x\sin\psi_i - R_{px,x})\sin\psi_i \\ &+(R_{p,y} + x\cos\psi_i - R_{px,y})\cos\psi_i = 0 \iff \end{aligned} \tag{2.166}$$

$$\begin{aligned} &R_{px,x}(\xi_{\mathrm{n}p,x})\sin\psi_i - R_{px,y}(\xi_{\mathrm{n}p,x})\cos\psi_i \\ &-R_{p,x}\sin\psi_i + R_{p,y}\cos\psi_i + x = 0 \end{aligned} \tag{2.167}$$

or

$$\begin{aligned} f(\xi_{\mathrm{n}p,x}) = &(R_{px,x}(\xi_{\mathrm{n}p,x}) - R_{p,x})\sin\psi_i \\ &+(R_{p,y} - R_{px,y}(\xi_{\mathrm{n}p,x}))\cos\psi_i + x = 0 \end{aligned} \tag{2.168}$$

This equation is solved by Newton-Raphson. The derivative is given by

$$f'(\xi_{\mathrm{n}p,x}) = \frac{\mathrm{d}R_{px,x}}{\mathrm{d}\xi_{\mathrm{n}p,x}} \sin\psi_i - \frac{\mathrm{d}R_{px,y}}{\mathrm{d}\xi_{\mathrm{n}p,x}} \cos\psi_i \tag{2.169}$$

where

$$\frac{\mathrm{d}R_{px,x}}{\mathrm{d}\xi_{\mathrm{n}p,x}} = -\frac{\partial\xi}{\partial\xi_{\mathrm{n}}}\bigg|_{p,x} \cos(\phi_{p,i}+\phi) - \frac{\partial\eta}{\partial\xi_{\mathrm{n}}}\bigg|_{p,x} \sin(\phi_{p,i}+\phi) \tag{2.170}$$

and

$$\frac{\mathrm{d}R_{px,y}}{\mathrm{d}\xi_{\mathrm{n}p,x}} = \frac{\partial\xi}{\partial\xi_{\mathrm{n}}}\bigg|_{p,x} \sin(\phi_{p,i}+\phi) - \frac{\partial\eta}{\partial\xi_{\mathrm{n}}}\bigg|_{p,x} \cos(\phi_{p,i}+\phi) \tag{2.171}$$

With $\xi_{\mathrm{n}p,x}$ and $\xi_{\mathrm{n}g,x}$ known, $R_{px,x}$ and $R_{gx,x}$ can be calculated. Then,

$$\delta_x = \frac{R_{px,x} - R_{gx,x}}{\cos\psi_i} \tag{2.172}$$

i.e., the overlap is known at all positions in the contact.

2.2.5 Deformation

The deformation is comprised of a contact deformation and a bending deformation. These are modeled analytically and numerically using FEM, respectively. This division, the so-called hybrid model, can be seen in Figure 2.4.

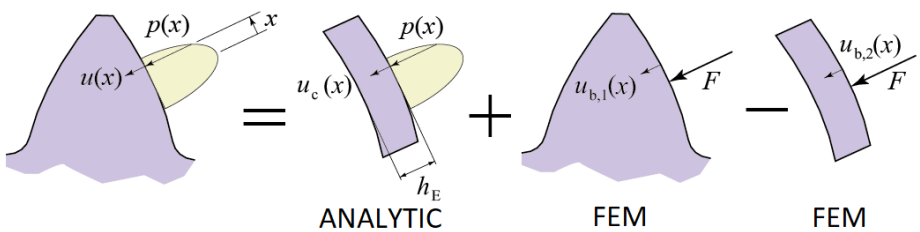

Figure 2.4: Schematic representation of the hybrid model. Total deformation is divided into contact deformation (analytic) and bending deformation (FEM). Since the finite element method also gives a contact deformation (but with low accuracy), this is subtracted. Reproduced with permission from Paper I.

The displacement w at the distance r in the plane and the depth z from a force F is given [171] as

$$w = \frac{F}{2\pi E}\left[(1+\nu)z^2(r^2+z^2)^{-3/2} + 2(1-\nu^2)(r^2+z^2)^{-1/2}\right] \tag{2.173}$$

which gives

$$w_{z=0} - w_{z=h_\mathrm{E}} = \frac{F}{2\pi E}\left[\frac{2(1-\nu^2)}{r} - \frac{2(1-\nu^2)}{(r^2+h_\mathrm{E}^2)^{1/2}} - \frac{(1+\nu)h_\mathrm{E}^2}{(r^2+h_\mathrm{E}^2)^{3/2}}\right] \tag{2.174}$$

With the coordinates ξ and η in the surface it follows that $r^2 = \xi^2 + \eta^2$. Replace the force with a pressure distribution. At point (x, y) the contact deformation becomes

$$\begin{aligned} u_c(x,y) = \frac{1}{2\pi E}\int_{x_{min}}^{x_{max}}\int_{-b/2}^{b/2} p(\xi,\eta)\Bigg[&\frac{2(1-\nu^2)}{\left((\xi-x)^2+(\eta-y)^2\right)^{1/2}} \\ &- \frac{2(1-\nu^2)}{\left((\xi-x)^2+(\eta-y)^2+h_\mathrm{E}^2\right)^{1/2}} \\ &- \frac{(1+\nu)h_\mathrm{E}^2}{\left((\xi-x)^2+(\eta-y)^2+h_\mathrm{E}^2\right)^{3/2}}\Bigg]\mathrm{d}\xi\mathrm{d}\eta \end{aligned} \tag{2.175}$$

With no variation over the width,

$$\begin{aligned} u_c(x) = \frac{1}{2\pi E}\int_{x_{min}}^{x_{max}}\int_{-b/2}^{b/2} p(\xi)\Bigg[&\frac{2(1-\nu^2)}{\left((\xi-x)^2+\eta^2\right)^{1/2}} \\ &- \frac{2(1-\nu^2)}{\left((\xi-x)^2+\eta^2+h_\mathrm{E}^2\right)^{1/2}} \\ &- \frac{(1+\nu)h_\mathrm{E}^2}{\left((\xi-x)^2+\eta^2+h_\mathrm{E}^2\right)^{3/2}}\Bigg]\mathrm{d}\xi\mathrm{d}\eta \end{aligned} \tag{2.176}$$

With a sufficiently fine discretization,

$$u_c(x) = \frac{1}{2\pi E}\sum_j p(x_j)\int_{x_j^-}^{x_j^+}\int_{-b/2}^{b/2}\left[\frac{2(1-\nu^2)}{\left((\xi-x)^2+\eta^2\right)^{1/2}}\right.$$
$$\left.-\frac{2(1-\nu^2)}{\left((\xi-x)^2+\eta^2+h_{\mathrm{E}}^2\right)^{1/2}}-\frac{(1+\nu)h_{\mathrm{E}}^2}{\left((\xi-x)^2+\eta^2+h_{\mathrm{E}}^2\right)^{3/2}}\right]\mathrm{d}\xi\mathrm{d}\eta \tag{2.177}$$

where

$$x_j^{\pm} = \frac{1}{2}(x_j + x_{j\pm1}) \tag{2.178}$$

The three integrals are calculated separately. With respect to η we have

$$\int_{-b/2}^{b/2}\frac{2(1-\nu^2)}{\left((\xi-x)^2+\eta^2\right)^{1/2}}\mathrm{d}\eta =$$
$$2(1-\nu^2)\ln\left(\sqrt{(\xi-x_i)^2+b^2/4}+\frac{b}{2}\right) \tag{2.179}$$
$$-2(1-\nu^2)\ln\left(\sqrt{(\xi-x_i)^2+b^2/4}-\frac{b}{2}\right)$$

and

$$\int_{-b/2}^{b/2}\frac{2(1-\nu^2)}{\left((\xi-x)^2+\eta^2+h_{\mathrm{E}}^2\right)^{1/2}}\mathrm{d}\eta =$$
$$2(1-\nu^2)\ln\left(\sqrt{(\xi-x_i)^2+b^2/4+h_{\mathrm{E}}^2}+\frac{b}{2}\right) \tag{2.180}$$
$$-2(1-\nu^2)\ln\left(\sqrt{(\xi-x_i)^2+b^2/4+h_{\mathrm{E}}^2}-\frac{b}{2}\right)$$

and

$$\int_{-b/2}^{b/2}\frac{(1+\nu)h_{\mathrm{E}}^2}{\left((\xi-x)^2+\eta^2+h_{\mathrm{E}}^2\right)^{3/2}}\mathrm{d}\eta =$$
$$\frac{(1+\nu)h_{\mathrm{E}}^2}{(\xi-x_i)^2+h_{\mathrm{E}}^2}\frac{b}{\sqrt{(\xi-x_i)^2+b^2/4+h_{\mathrm{E}}^2}} \tag{2.181}$$

These functions are then integrated with respect to ξ, rendering

$$\begin{aligned}
&\int_{x_j^-}^{x_j^+} 2(1-\nu^2)\ln\left(\sqrt{(\xi-x_i)^2+b^2/4}\pm\frac{b}{2}\right)\mathrm{d}\xi = \\
&2(1-\nu^2)\Bigg[(\xi-x_i)\ln\left(\sqrt{(\xi-x_i)^2+b^2/4}\pm\frac{b}{2}\right) \\
&\pm\frac{b}{2}\ln\left(\sqrt{(\xi-x_i)^2+b^2/4}+(\xi-x_i)\right)-(\xi-x_i)\Bigg]_{x_j^-}^{x_j^+}
\end{aligned} \tag{2.182}$$

and

$$\begin{aligned}
&\int_{x_j^-}^{x_j^+} 2(1-\nu^2)\ln\left(\sqrt{(\xi-x_i)^2+b^2/4+h_{\mathrm{E}}^2}\pm\frac{b}{2}\right)\mathrm{d}\xi = \\
&2(1-\nu^2)\Bigg[(\xi-x_i)\ln\left(\sqrt{(\xi-x_i)^2+b^2/4+h_{\mathrm{E}}^2}\pm\frac{b}{2}\right) \\
&\pm\frac{b}{2}\ln\left(\sqrt{(\xi-x_i)^2+b^2/4+h_{\mathrm{E}}^2}+(\xi-x_i)\right) \\
&-(\xi-x_i)-h_{\mathrm{E}}\arctan\left(\frac{\pm b(\xi-x_i)}{2h_{\mathrm{E}}\sqrt{(\xi-x_i)^2+b^2/4+h_{\mathrm{E}}^2}}\right) \\
&h_{\mathrm{E}}\arctan\left(\frac{\xi-x_i}{h_{\mathrm{E}}}\right)\Bigg]_{x_j^-}^{x_j^+}
\end{aligned} \tag{2.183}$$

and finally

$$\begin{aligned}
&\int_{x_j^-}^{x_j^+}\frac{(1+\nu)h_{\mathrm{E}}^2}{(\xi-x_i)^2+h_{\mathrm{E}}^2}\frac{b}{\sqrt{(\xi-x_i)^2+b^2/4+h_{\mathrm{E}}^2}}\mathrm{d}\xi = \\
&2(1+\nu)h_{\mathrm{E}}\Bigg[\arctan\left(\frac{b(\xi-x_i)}{2h_{\mathrm{E}}\sqrt{(\xi-x_i)^2+b^2/4+h_{\mathrm{E}}^2}}\right)\Bigg]_{x_j^-}^{x_j^+}
\end{aligned} \tag{2.184}$$

The bending deformation u_b at point x_i is given by

$$u_b(x_i) = \frac{u_{0,b}}{E} \sum_j \int_{x_j^-}^{x_j^+} p(x_j) \mathrm{d}x \tag{2.185}$$

where

$$u_{0,b} = u_{0,b,p}(s_p, -x) + u_{0,b,g}(s_g, x) \tag{2.186}$$

The nominal dimensionless bending deformation is given by

$$\begin{aligned} u_{0,b,k}^{\mathrm{nom}}(s,x) = \left(a_0 + a_1 \left(\frac{s-s_1}{m_\mathrm{t}} \right)^p + a_2 \left(\frac{s-s_1}{m_\mathrm{t}} \right)^q \right) \\ \cdot \left(1 + b_1 \left(\frac{x}{m_\mathrm{t}} \right)^p + b_2 \left(\frac{x}{m_\mathrm{t}} \right)^q \right) \end{aligned} \tag{2.187}$$

$k = p,\ g$, where the coefficients are given by curve fitting deformations given by FEM calculations. Moreover,

$$\sum_j \int_{x_j^-}^{x_j^+} p(x_j) \mathrm{d}x = \Delta x \sum_j p(x_j) \tag{2.188}$$

To account for the change of normal direction of the flank, and thus the direction of the contact force, in the tip relief and tip rounding regions without having to perform new FEM calculations, a correction factor is introduced. The factor is based on elastic beam theory. For a cantilever beam, it holds that

$$\delta_{FEM} = \frac{F_{FEM} \cos\psi_0 L^3}{3EI} \cos\psi_0; \quad \alpha_{FEM} = \frac{\delta_{FEM}}{F_{FEM}} = \frac{L^3}{3EI} \cos^2\psi_0 \tag{2.189}$$

and

$$\delta = \frac{FL^3}{3EI} \cos^2\psi; \quad \alpha = \frac{\delta}{F} = \frac{L^3}{3EI} \cos^2\psi \tag{2.190}$$

It follows that

$$\frac{L^3}{3EI} = \frac{\alpha_{FEM}}{\cos^2\psi_0} = \frac{\alpha}{\cos^2\psi} \iff \alpha = \alpha_{FEM}\frac{\cos^2\psi}{\cos^2\psi_0} \tag{2.191}$$

Therefore,

$$u_{0,b} = u_{0,b}^{\text{nom}}\frac{\cos^2\psi}{\cos^2\psi_0} \tag{2.192}$$

The total deformation u is the sum of bending and contact deformation,

$$u = u_b + u_c \tag{2.193}$$

The bending deformation

$$\begin{aligned} u_b(x_i) &= \frac{u_{0,b}}{E}\sum_j \int_{x_j^-}^{x_j^+} p(x_j)\mathrm{d}x \\ &= u_{0,b}\frac{\Delta x}{E}\sum_j p(x_j) = K_b(x_i)\sum_j p(x_j) \end{aligned} \tag{2.194}$$

which in matrix format becomes

$$\begin{bmatrix} u_b(x_1) \\ u_b(x_2) \\ \vdots \\ u_b(x_n) \end{bmatrix} = \begin{bmatrix} K_b(x_1) & K_b(x_1) & \cdots & K_b(x_1) \\ K_b(x_2) & \ddots & & \vdots \\ \vdots & & & \\ K_b(x_n) & \cdots & & K_b(k_n) \end{bmatrix} = \begin{bmatrix} p(x_1) \\ p(x_2) \\ \vdots \\ p(x_n) \end{bmatrix} \tag{2.195}$$

or

$$\mathbf{u}_b = \mathbf{K}_b\mathbf{p} \tag{2.196}$$

For the contact deformation,

$$
\begin{aligned}
u_c(x_i) &= 2\frac{1}{2\pi E}\sum_j p(x_j)\int_{x_j^-}^{x_j^+}\int_{-b/2}^{b/2}\left[\frac{2(1-\nu^2)}{((\xi-x)^2+\eta^2)^{1/2}}\right. \\
&\quad \left. - \frac{2(1-\nu^2)}{\left((\xi-x)^2+\eta^2+h_{\mathrm{E}}^2\right)^{1/2}} - \frac{(1+\nu)h_{\mathrm{E}}^2}{\left((\xi-x)^2+\eta^2+h_{\mathrm{E}}^2\right)^{3/2}}\right]\mathrm{d}\xi\mathrm{d}\eta \\
&= \sum_j K_c(|x_i-x_j|)p_j
\end{aligned}
\tag{2.197}
$$

which in matrix format becomes

$$
\begin{bmatrix} u_c(x_1) \\ u_c(x_2) \\ \vdots \\ u_c(x_n) \end{bmatrix} = \begin{bmatrix} K_c(|x_1-x_1|) & \cdots & K_c(|x_1-x_n|) \\ K_c(|x_2-x_1|) & \ddots & \vdots \\ \vdots & & \\ K_c(|x_n-x_1|) & \cdots & K_c(|x_n-x_n|) \end{bmatrix} \begin{bmatrix} p(x_1) \\ p(x_2) \\ \vdots \\ p(x_n) \end{bmatrix} \tag{2.198}
$$

or

$$
\mathbf{u}_c = \mathbf{K}_c\mathbf{p} \tag{2.199}
$$

Altogether,

$$
\mathbf{u} = \mathbf{u}_b + \mathbf{u}_c = (\mathbf{K}_b + \mathbf{K}_c)\mathbf{p} = \mathbf{K}\mathbf{p} \tag{2.200}
$$

Simultaneously, the total deformation must equal the overlap, i.e.,

$$
\mathbf{u} = \boldsymbol{\delta} \tag{2.201}
$$

where

$$
\boldsymbol{\delta} = \begin{pmatrix} \delta_1 & \delta_2 & \cdots & \delta_n \end{pmatrix}^T \tag{2.202}
$$

thus giving the equation system

$$
\mathbf{K}\mathbf{p} = \boldsymbol{\delta} \tag{2.203}
$$

with the constraint

$$\forall k : p(x_k) \geq 0 \tag{2.204}$$

i.e., all pressure values must be positive.

All simultaneous contacts contribute to the transmitted torque. Once the pressure distribution from tooth pair i is found, along with its position, the corresponding torque contribution is calculated as

$$\begin{aligned} M_i = &\int p(x)(r_g + x)b\mathrm{d}x \\ &+ \mu \int p(x)b\mathrm{d}x\sqrt{R_g^2 - r_g^2}\mathrm{sign}\left(r_g\sqrt{R_g^2 - r_g^2} - r_p\sqrt{R_p^2 - r_p^2}\right) \end{aligned} \tag{2.205}$$

Here it is seen how friction contributes to the torque as well. When all torque contributions are summarized, the total torque is compared to the user-defined output torque. The overlap angle ϕ is then adjusted until the torque is equal to the desired torque within a certain tolerance. A solution is then found. This method and some example results are shown in Paper I.

A variety of parameters can then be changed. Paper II describes the results of the contact analysis for gearsets with manufacturing error combinations, relating tolerances to contact pressure.

2.2.6 Transmission error

The overlap angle corresponds to the deformation, since it is the angle that the pinion is rotated while torque is applied and the gear is kept in a fixed angular position. This gives the angular positions

$$\varphi_p = \phi_p + \phi \tag{2.206}$$

for the pinion, and

$$\varphi_g = \phi_g \tag{2.207}$$

for the gear. The static transmission error is then defines as

$$\mathrm{STE} = r_{b,p}\varphi_p - r_{b,g}\varphi_g \tag{2.208}$$

i.e., a distance along the line of action. For prefect and rigid involute gears, this distance should be zero. Due to the varying stiffness along the LOA, together with modifications and manufacturing errors, it takes non-zero values.

When STE is computed for all positions along the LOA, the evolution of the STE is found. If instead, due to e.g. simplicity, a single value is desired, the peak-to-peak transmission error, or $PPTE$, can be used. It is defined as

$$\mathrm{PPTE} = \max(\mathrm{STE}) - \min(\mathrm{STE}) \tag{2.209}$$

Since contact pressure and transmission error do not have coinciding minima, a simultaneous optimization can be performed. This is done in Paper III.

2.2.7 Tip contact threshold torque

Tip contact occurs when the tip of one tooth comes in contact with the mating tooth, resulting in excessive contact pressure. The tip relief is chosen to prevent tip contact, but is typically kept fairly low as it imposes a deviation from the involute profile.

As deformation is load-dependent, so is tip contact. When the deflection at the tip becomes larger than the tip relief, tip contact occurs. Since the radius of curvature of the tip is several magnitudes smaller than that of the flank, the contact pressure becomes immense even for a low contact force, i.e., a pressure spike behavior. Thus, tip contact exhibits a binary type of behavior. The novel concept of tip contact threshold torque is thus introduced, and is defined as the torque below which tip contact does not occur, and above which it does. It is found by incrementally increasing the torque until a pressure spike is detected, or by using the bisection method.

The method of assessing the severity of manufacturing error by their corresponding tip contact threshold torque is proposed in Paper IV.

2.3 Implementation

The theoretical framework derived above was implemented in Java. In this section, the implementation is described.

The *Main* class takes all inputs, and prints all output. It contains the following classes.

Reference profile, with a description of the reference profile. Two reference profiles are created, one for the pinion and one for the gear. The respective reference profiles contain properties such as pressure angle, as well as the coordinates and derivatives described in Section 2.2.1. Profile slope error is introduced here, by a rotation of the flank.

Gear, with all properties pertaining to the gears that cannot be described by the reference profile, such as number of teeth. Again, one is created for the pinion and one for the gear. Pitch error is introduced here, by a displacement of teeth.

Gearset, with all geometric properties that cannot be described by the reference profiles and gears, such as center distance.

Mesh, that describes the gear meshing. This class contains all routines for finding the common normal, calculate overlap, and find the contact pressure from the deformation and stiffness.

The simulation approach can be seen in Figure 2.5.

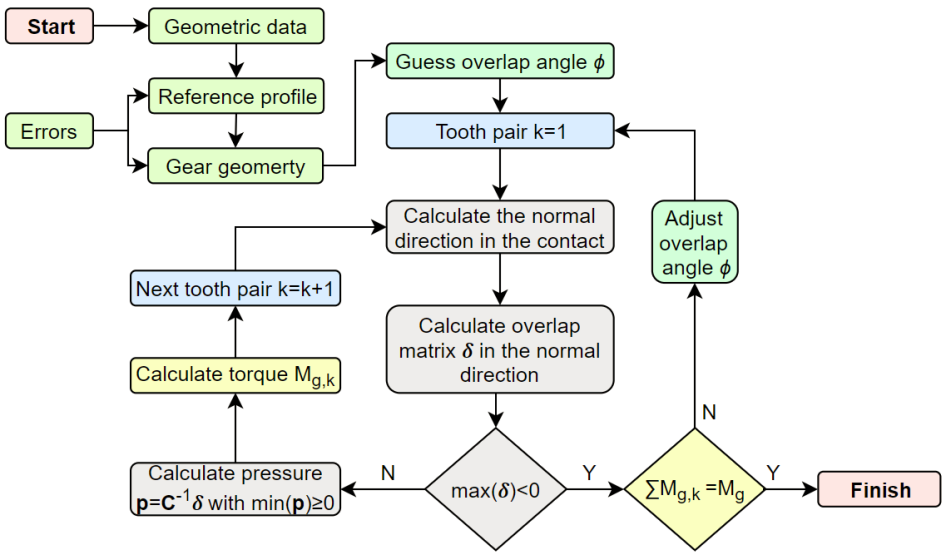

Figure 2.5: Flowchart of the LTCA algorithm. The flowchart utilizes the following color coding. Light pink: start and finish. Light green: input and pre-processing. Dark green: overlap angle iteration. Blue: tooth pair iteration. Grey: contact analysis. Yellow: torque convergence routine. Reproduced with permission from Paper I.

The simulation approach described above is explained in greater detail in Paper I.

2.4 Numerical Example

To demonstrate the feasibility of the simulation tool, a numerical example is needed. The gearset taken as input is the FZG[1] C gear pair, with data according to Table 2.1.

Table 2.1: Data for the gear set used for the simulations.

Property	**Value** (pinion/gear)
Module, m_{n} [mm]	4.5
Pressure angle, α_{n} [°]	20
Helix angle, β [°]	0
Number of teeth, z [-]	16 / 24
Addendum modification, x_{n} [-]	0.1657 / 0.1546
Tip radius, R_{tip} [mm]	41.23 / 59.18
Tip relief start radius, R_{tr} [mm]	40.18 / 57.96
Face width, b [mm]	14
Center distance, a [mm]	91.5
Normal backlash, δ_0 [-]	0.02249
Modulus of elasticity, E [GPa]	206
Poisson ratio, ν [-]	0.3
Coefficient of friction, μ [-]	0.07

The gearset is subjected to manufacturing errors. Classes 1-12 are shown in Table 2.2 together with their corresponding values of pitch error tolerance, f_{pT}, and profile slope error tolerance, $f_{\mathrm{H}\alpha\mathrm{T}}$, according to ISO standard [37].

Table 2.2: Tolerance classes and error magnitudes and typical applications. Tolerances typically used in the automotive industry are shown in boldface.

Class	1	2	3	4	
f_{pT} [μm]	1.7	2.4	3.4	4.9	precision
$f_{\mathrm{H}\alpha\mathrm{T}}$ [μm]	1.5	2.1	2.9	4.2	
Class	**5**	**6**	7	**8**	
f_{pT} [μm]	**7.0**	**10.0**	**14**	**19**	**automotive**
$f_{\mathrm{H}\alpha\mathrm{T}}$ [μm]	**6.0**	**8.5**	**12**	**17**	
Class	9	10	11	12	
f_{pT} [μm]	27	39	55	78	course
$f_{\mathrm{H}\alpha\mathrm{T}}$ [μm]	23	33	47	66	

[1] Forschungsstelle für Zahnräder und Getriebebau

2.5 Results

This section contains numerical results, but it also shows the work flow, ties together the papers, and adds some commentary.

The most rudimentary result of the LTCA is the contact pressure distribution at a single position. By varying the position, in terms of angular position or the equivalent position along the line of action, the maximum contact pressure along the entire tooth flank can be found. An example of this is shown in Figure 2.6.

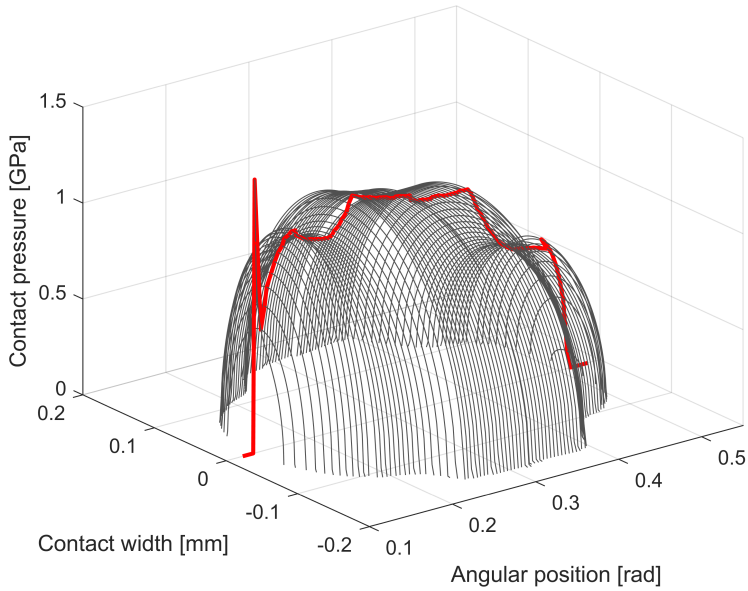

Figure 2.6: Contact pressure distribution for different mesh positions (grey curves). The maximum pressure values for each position are highlighted (solid red curve). The pinion is subjected to profile slope error. The pressure spike is caused by tip contact. Reproduced with permission from Paper IV.

Typically the maximum pressure value is of the most interest. The maximum pressure at each position is marked in red. This creates a new curve which can be extracted, see Figure 2.7.

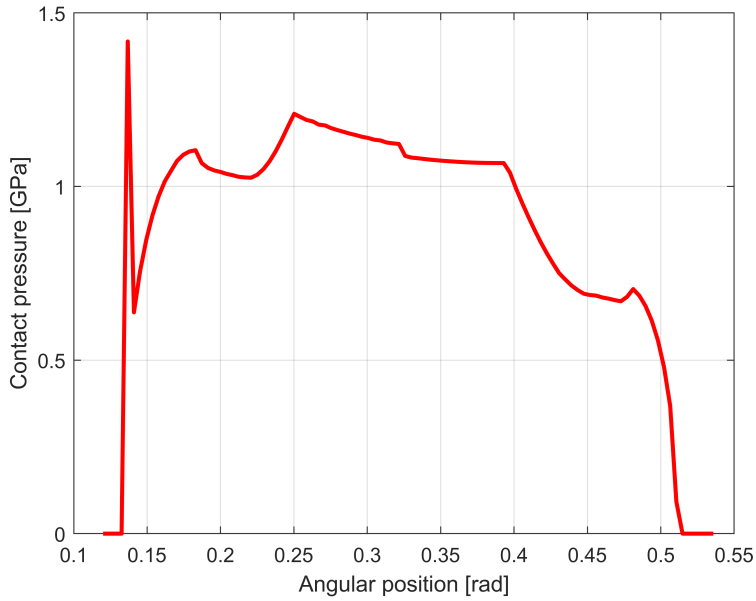

Figure 2.7: Maximum contact pressure values for each position extracted from Figure 2.6. Note the pressure spike and the friction effect at the pitch point. Reproduced with permission from Paper IV.

Here it can be noted that a pressure spike appears due to tip contact. Note also the friction effect at the pitch point as previously discussed, see Section 2.1.1.

It can also be seen that the curve is somewhat distorted or tilted. This is due to the pinion being subjected to manufacturing errors. This case is referenced here for completeness of the methodology, and discussed in greater detail in Paper IV.

Figure 2.7 shows the maximum contact pressure for different positions along a certain tooth. However, other tooth pairs may simultaneously be in mesh. To get the full picture, the curves corresponding to the one in Figure 2.7 are shown in Figure 2.8 for a certain tooth pair, denoted by current, together with the previous and the next. The positions where the curves overlap correspond to dual engagement.

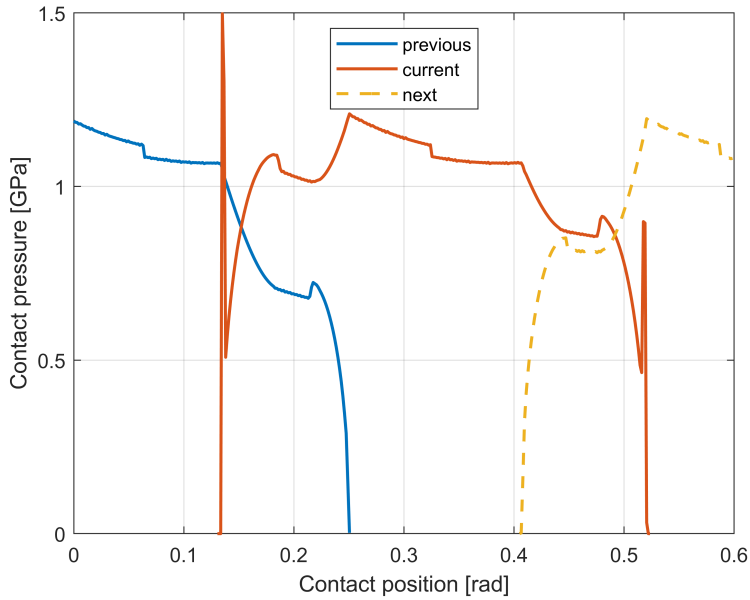

Figure 2.8: Maximum pressure for each mesh position for a specific tooth pair (current), together with the previous and next tooth pairs. Note the pressure spikes when the current pair goes into and out of mesh. Reproduced with permission from Paper I.

This is the same case as that presented in Paper I, where the pinion is subjected to pitch error. Also for this case, tip contact is present. To see this more clearly, three cases of dual engagement are extracted in Figure 2.9. When the current pair first comes into mesh, only the tip rounding region is in contact, resulting in the spike seen in Figure 2.9 case A. The contact then moves partially to the tip relief region, where the radius of curvature is much larger. This corresponds to case B, where non-symmetric behavior is exhibited. Finally, in case C, tip contact has vanished and the spike is no longer present.

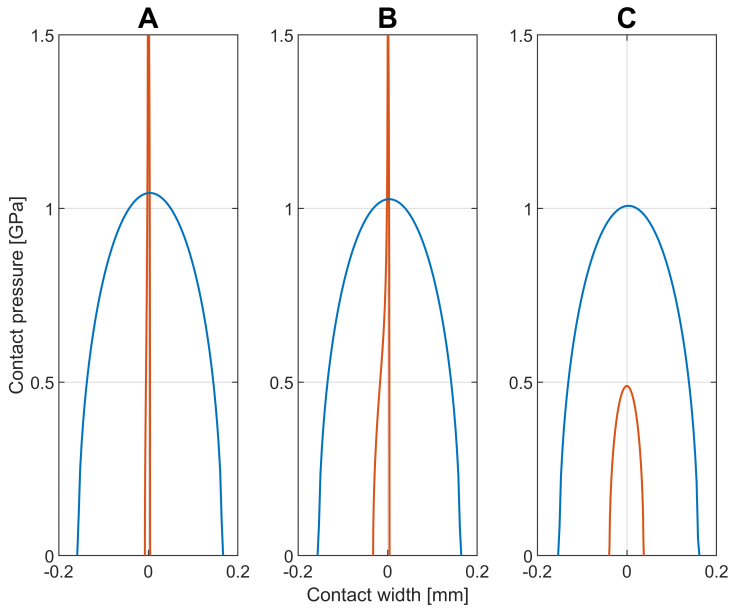

Figure 2.9: Three different types of dual engagement. A: pressure spike due to tip contact of the current tooth pair coming into mesh. B: asymmetric pressure distribution due to the contact moving from tip rounding to tip relief region. C: contact fully in tip relief region. As the current tooth pair just came into mesh, its equivalent load is yet fairly light which corresponds to a low maximum contact pressure value. Reproduced with permission from Paper I.

The tip contact demonstrated in Figures 2.6 to 2.9 can occur even for gears with no manufacturing errors. A way to study the influence of manufacturing errors on contact pressure in the gearset is to use a tip relief that is large enough to prevent tip contact for a certain torque in the case of no manufacturing errors, and then applying the manufacturing errors of interest. This is done in Figure 2.10.

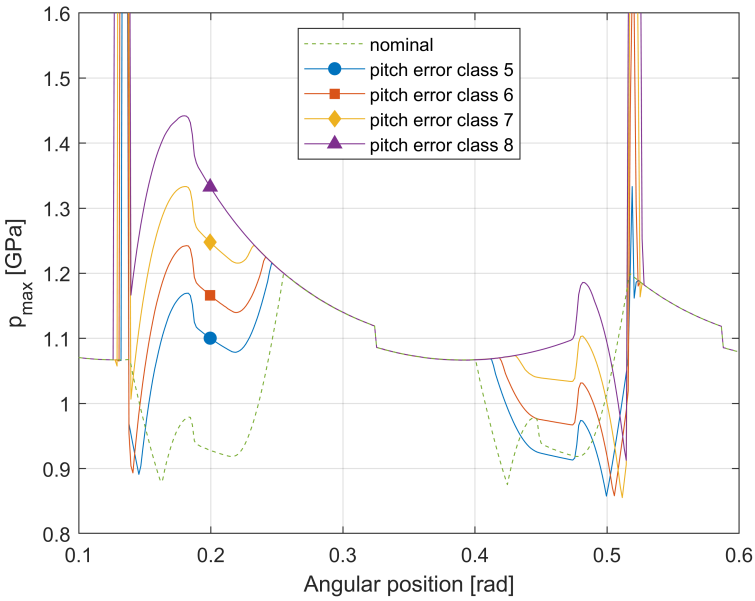

Figure 2.10: Maximum contact pressure for different positions. The gearset either has no errors (nominal) or pitch error of different tolerance classes. Here it can be noted that pressure spike are cause, but even without pressure spikes there is a considerable increase in contact pressure. Reproduced with permission from Paper II.

Figure 2.10 displays pressure curves for cases with pitch error of class 5 - 8, together with a nominal case for reference. Two phenomena can be observed, namely that tip contact appears in form of spikes, and that the pressure curve is altered even outside of the spikes. This means that even if tip contact is prevented, e.g. by using a larger tip relief or if sharp edges get worn down, there will still be a remaining contact pressure increase. This is due to factors such as prolonged contact caused by the altered geometry.

Curves similar to those of Figure 2.10 can also be constructed for profile slope error, and combinations of pitch error and profile slope error, of different tolerances. Other parameters, such as tip relief, can also be varied. This is done in detail in Paper II. Especially, it is shown that manufacturing errors tend to amplify each other, and thus need to be considered simultaneously.

Transmission error, as previously discussed, is caused by varying stiffness, which in turn is affected by geometric deviations, both intentional such as tip relief and unintentional such as manufacturing errors. The transmission error during slightly more than two pitches is shown in Figure 2.11.

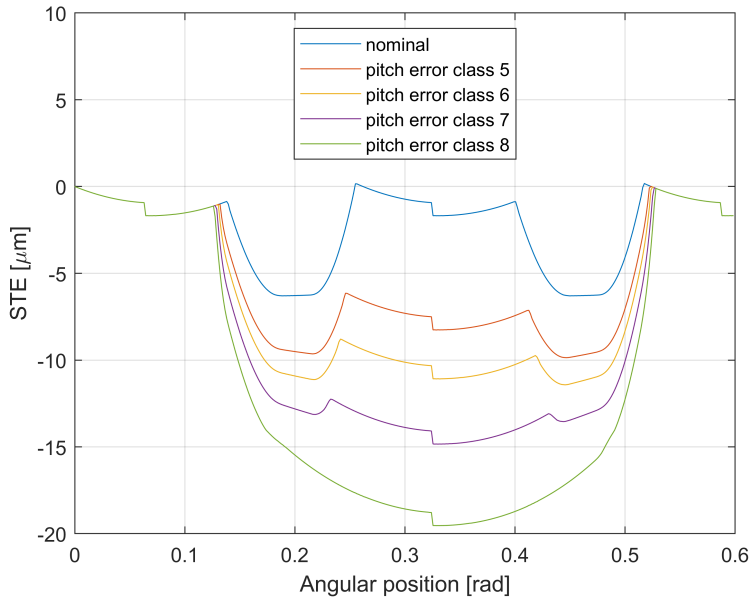

Figure 2.11: STE evolution curves, i.e., STE for different positions. The gearset either has no errors (nominal) or pitch error of different tolerance classes. Larger pitch error corresponds to larger STE. Again, the friction effect at the pitch point can be seen. Reproduced with permission from Paper III.

Here, a few conclusions can be drawn. Just like for pressure, a jump at the pitch point is occurs. The friction changing direction at the pitch point corresponds to a change in stiffness. This is also demonstrated by Fernandez del Rincon et al. [172].

The most noteworthy conclusion from Figure 2.11 is the more and more severe effect of increasing pitch error in terms of the size of the transmission error. For this reason, the peak-to-peak transmission error (PPTE) can be used. Using a single numeric value makes it easy to assess the severity of different manufacturing error tolerances, just like the maximum contact pressure. Thus, it also becomes possible to compare PPTE and maximum pressure. This is demonstrated in Figure 2.12.

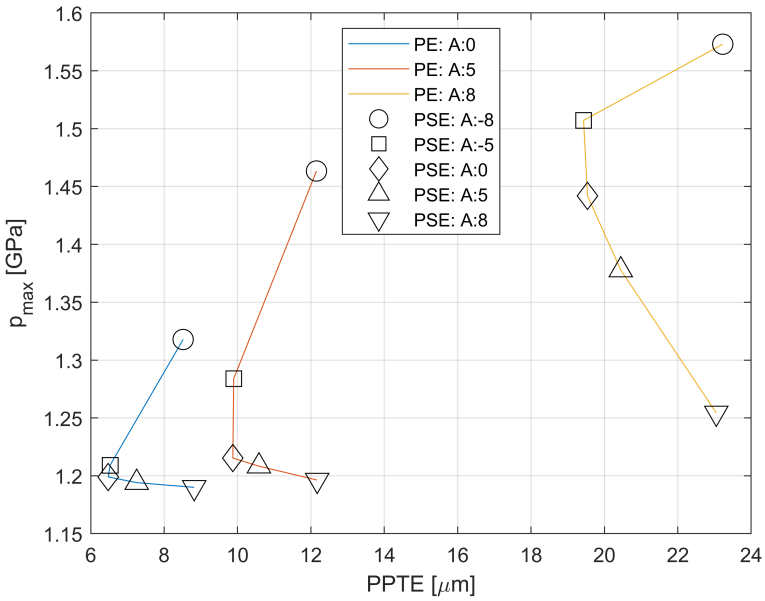

Figure 2.12: Design curves for comparison of maximum contact pressure and peak-to-peak STE. Curves correspond to pitch error (PE) classes, and markers correspond to profile slope error (PSE) classes. Reproduced with permission from Paper III.

As it is desirable to keep both contact pressure and transmission error at low levels, the design curves in Figure 2.12 can be used when choosing tolerances. It can be seen that certain changes in the allowed tolerances simultaneously decrease both transmission error and contact pressure, while other changes have little or no effect on one of the properties.

In Figure 2.12, only a few values are plotted. More detailed design curves are displayed in Figure 2.13.

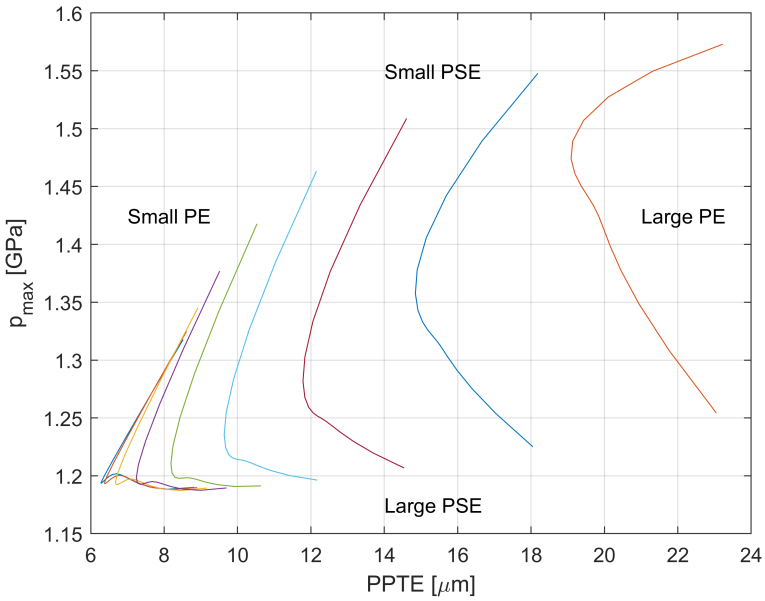

Figure 2.13: Extended design curves for a gearset with pitch error (PE) and profile slope error (PSE). Here simulated values are augmented by predicted values using polynomial fits and interpolation. Reproduced with permission from Paper III.

Thus, using the LTCA, it is possible to construct design curves and then choose manufacturing error tolerances such that transmission error and contact pressure are simultaneously optimized. This methodology is proposed in Paper III, where it is also explained in greater detail.

As previously mentioned, tip contact may occur even in absence of manufacturing errors. This happens when the deformation, caused by the applied load, overcomes the tip relief. Thus, tip contact is torque dependent. To quantify this, different levels of torque are applied to gearsets without manufacturing errors, but with different magnitudes of tip relief. The result can be seen in Figure 2.14.

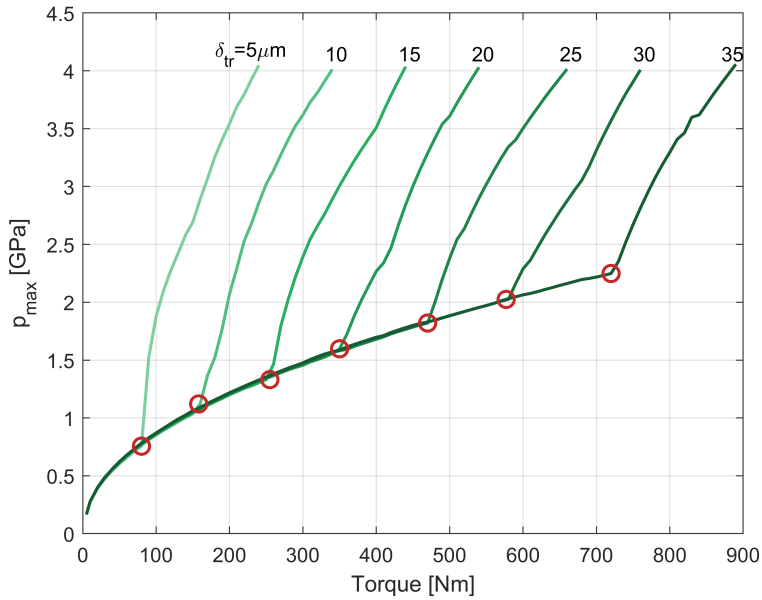

Figure 2.14: Tip contact threshold torque for a gearset with different magnitudes of tip relief. Red circles mark the threshold for each tip relief. Reproduced with permission from Paper IV.

The relation between torque and pressure behaves as expected. It closely resembles a square root curve, which is the relation suggested by Hertzian contact theory. This is however only true as long as tip contact does not occur.

The onset of tip contact is marked by circles in Figure 2.14. The notation of tip contact threshold torque, or just threshold torque when there is no ambiguity, for the corresponding torque is suggested. Below the threshold torque, no tip contact occurs, and above the threshold it does. Since tip contact should never occur, and might severely damage the gears as previously discussed, the threshold torque acts as binary switch for whether the gearset would work properly or not.

Before moving on, the regular behavior of the curves in Figure 2.14 is noted. While simulations save time compared to experiments, they may still be cumbersome and time consuming. Therefore, it is investigated whether threshold torque can be predicted using interpolation based on polynomial fits to a low number of simulated values. The results are displayed in Figure 2.15.

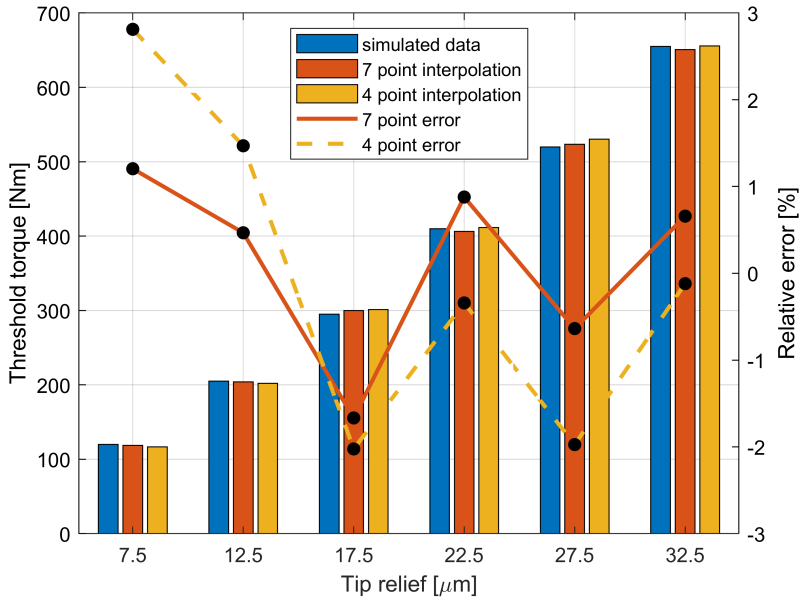

Figure 2.15: Bar plots of simulated data (blue) and interpolated data (orange and yellow) using polynomial fits. Left scale (bars) shows tip contact threshold torque. Right scale (solid or dashed lines) shows relative error of interpolated values compared to simulated values. Both seven and four simulations are used as a basis for the interpolations. Reproduced with permission from Paper IV.

From Figure 2.15 it can be seen that predictions are accurate within a few percent even when only four values are simulated. This result turns out to be useful as it reduces the number of necessary simulations, and thereby also the time consumption and complexity.

To investigate how tip contact is affected by manufacturing errors, curves similar to those in Figure 2.14 are constructed and, and predictions based on interpolation according to the described method are performed. This presents a way to assess the severity of different manufacturing errors: if two manufacturing errors or error combinations yield the same threshold torque, the are equally severe. This is true for all manufacturing error combinations on the same threshold torque iso-line.

The proposed assessment method can be used to evaluate whether gears should be kept or scrapped depending on manufacturing outcome. To show this, a case study is made. After manufacturing, the gears are control measured. The result of the measurement is shown in Figure 2.16, where each dot represents a manufactured gear, placed according to its pitch error and profile slope error. In total, the batch consists of 30 gears.

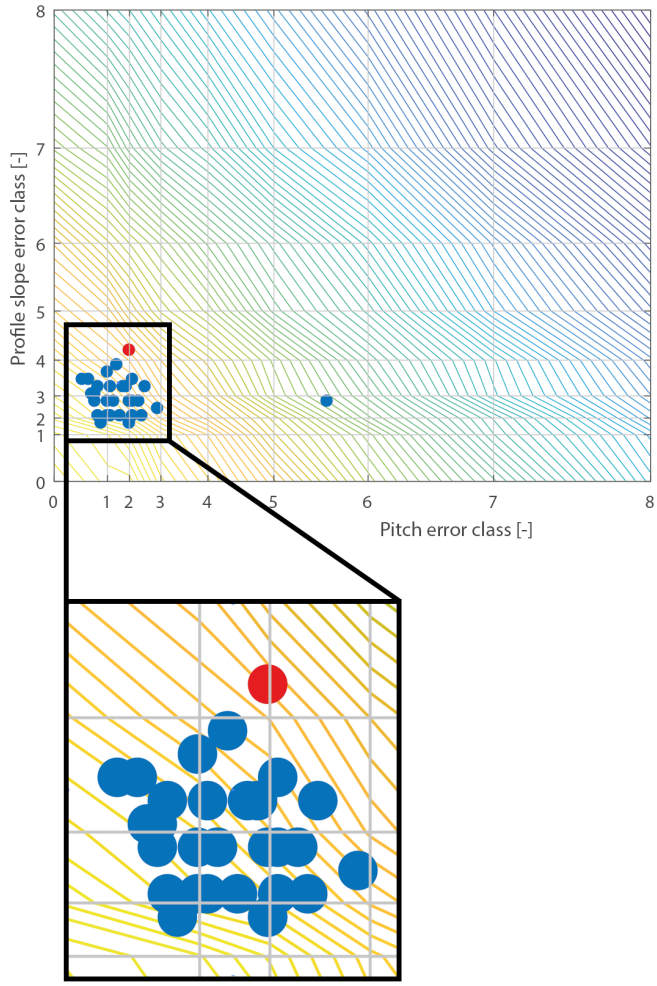

Figure 2.16: Control measurement outcome of a batch of manufactured gears. Each dot represents a gear. Note that some dots overlap partially or fully. Curves are threshold torque iso-lines. The gear marked in red is suggested to be kept instead of scrapped by assessment of its threshold torque. Reproduced with permission from Paper IV.

Figure 2.16 also shows the threshold torque iso-lines. Dots above a certain iso-line means that tip contact will occur if the gear is used in a gearset subjected to that torque. Conversely, if the dot is below the line, tip contact will not occur. This assessment method is therefore of Monte Carlo type.

If tolerance class 4 is desired, the gear corresponding to the red dot would be scrapped based on geometry. However, it sits below iso-lines that pass through the permissible region, and would therefore not experience tip contact. This is because the large profile slope error value is compensated by a small pitch error value. Scrapping this

specimen would therefore be unjustified. The gear corresponding to the lone dot to the right of the rest of the dots should however be scrapped, as it would cause tip contact.

To avoid unjustified scrapping, the iso-lines are used to extend the permissible region. This is done in Paper IV, where the method and case study are explained in greater detail, and scrapping is discussed in relation to the Sustainable Development Goals [173].

The method on predictions based on interpolation using polynomial fits is also used and discussed in Paper III.

2.6 Discussion

When the radius of curvature of the contact is fairly constant, the contact pressure distribution produced by the LTCA is in good accordance with Hertzian contact pressure distribution. This can be seen in Figure 2.6 and Figure 2.9. Thus, the LTCA yields the correct result in a known case. While this does not necessarily mean that it always gives a correct result, it decreases the risk of errors.

Many studies neglect friction in the equilibrium, and thereby use a constant contact force throughout the single engagement zone. In the LTCA, the equilibrium includes friction, which results in a jump or step at the pitch point. This can be seen in Figures 2.6 - 2.8 and Figure 2.10. Studies that do include friction, see Reimann et al. [166] and Marques et al. [167], display the same phenomenon.

The LTCA produces a non-symmetric contact pressure distribution when the radius of curvature varies considerably in the contact, i.e., visual accordance between contact region and contact pressure distribution prevails; cf. Paper I. Similar results for non-symmetric pressure were obtained by Ye and Tsai [51] and Bruzzone et al. [59].

Figure 2.10 shows how contact pressure and thereby load is increased even in regions without pressure spikes. This is confirmed experimentally for gears subjected to pitch errors, see Handschuh et al. [9], who measured root stress. Increased root stress is caused by the increased load, which also corresponds to increased contact pressure. Root stress therefore serves as confirmation even though it is not a direct measurement of contact pressure.

In the LTCA, the gears are assumed to be fully elastic, i.e., no plastic deformation or wear is modeled. It is possible that a sharp tip quickly gets worn down and/or plasticises during run-in. However, it still likely makes a dent during the few cycles where it is present, see Errichello et al. [52], which is enough to cause onset of pitting.

In the LTCA, elasticity couplings between the teeth are neglected. Elasticity couplings are important when considering transmission error as it relates to deformation. However, it has greater impact on transmission error offset than variation, i.e., peak-to-peak transmission error is not affected much by elasticity couplings, as concluded by Rigaud and Barday [174].

In Paper III, transmission error is defined as a distance along the line of action which is obtained by multiplying rotation angle of the gears with the respective base circle radius. Only perfect involutes have a base circle, so the definition is slightly unphysical. However, the geometric deviation from the perfect involute is small, and the definition used allows for a good comparison with magnitudes of manufacturing errors and tip relief.

Thermal expansion is neglected. This is mostly a problem in lack of proper backlash. In fact, some thermal expansion may be beneficial to transmission error, see Arana et al. [131]. However, thermal expansion, and contact temperature in general, is an important topic. A thermal treatment requires a description of the lubricant, see Chapter 3.

In conclusion, the trends shown by the LTCA seem reasonable. All specific results, i.e., certain numerical values, in the numerical examples pertain to the gearset in Table 2.1. Thus, exact values cannot be used in other cases. The important conclusions, however, are the more general ones about the presented and suggested methodologies.

Still, validation against experiments is an important part of developing numerical methods. To accomplish this, a description of the lubrication is also needed. Therefore, see Section 3.7.

Performing experiments also gives a more realistic variation between different gears with the same error. Different flanks may well have different geometry but yield the same error measurement, which is an effect that appears when a single error value is used to describe the complex flank. The drawback, on the other hand, is that many new error sources are introduced, and the effect of single parameters is difficult or impossible to isolate.

Paper IV suggests the method of assessing manufacturing errors of different types, tolerances, and combinations, by their tip contact threshold torque. This method is quite general, and does in principle not need an LTCA. Another method, such as a finite element analysis, could be used instead. Furthermore, it would be possible to make an equivalent experimental study. A brief outline of an experimental procedure is staked out in paper IV. While experiments tend to be expensive and time consuming, a statistical analysis of already measured data could be used. For example, Lin et al. [175] and Bergstedt et al. [176] have made measurements of that kind. Using a

statistical approach to relate fatigue life and manufacturing errors to threshold torque remains as future work.

If a manufactured and control measured gear is below an iso-line passing through the permissible region, it should be kept even though the gear itself is outside the permissible region. This is one of the major findings of the LTCA simulations. This method can be expanded to include more errors, such as helix of form deviations, and/or other criteria such as temperature or transmission error.

The method of using interpolations is shown to be useful. When a few cases have been simulated, they can be used as a basis for polynomial fits. The polynomials can then be used to interpolate intermediary values, which reduces the time consumption.

2.6.1 Conclusions and reflections

The performed analyses show that manufacturing errors have a large impact on meshing and behavior of gearsets, and thus need to be included in contact analyses for results to be accurate. Finding, e.g., the optimal tip relief for gears without manufacturing errors may have low significance in a real application, where manufacturing errors always are present to some extent.

The LTCA is believed to work well to study the effect of manufacturing errors on contact pressure of gearsets. However, to move on another method is needed. Such a method is presented in Chapter 3. For a more detailed discussion about future work, see Chapter 6.

Mainly Paper I, but also Papers II-IV, answer RQ1. Conversely, Papers II-IV but also, to some extent, Paper I, answer RQ2. As new demands on NVH are imposed by electrification, P3 to some extent answers RQ3. Papers I-IV are also linked to RQ3 by tolerances, since electrification imposes new demands via the tolerances.

Again, it should be noted that 'answer' does not mean 'fully exhausts the field', but rather 'provides some answers and insights', and also highlights the need for further development.

Chapter 3

Lubricated contacts - TEHL

This chapter describes the Thermal Elasto- Hydrodynamic Lubrication (TEHL) tool, i.e., model and simulation method of lubricated contacts. It was concluded from the literature review of the introduction that the model should include a full description of temperature, and include dependence on temperature and pressure in lubricant viscosity and density descriptions. Cavitation of the lubricant should also be considered. Furthermore, it is desirable to include manufacturing errors in the lubricated contact analysis as well.

3.1 The TEHL Model

In the previous chapter, dry contacts were studied. While gearsets in real applications are lubricated, dry contact modeling is sufficient to study some phenomena. However, dry contact models fall short in some cases:

- When properties related to the lubricant are of interest, such as temperature
- When properties related to the surfaces are of interest, such as roughness

For this reason, a TEHL model is created. Focus lies heavily on the first point, lubricant behavior, whereas surface roughness is briefly discussed at the end of this chapter.

The first step is to create a model that treats smooth surfaces, i.e., surface roughness is neglected. This is a good assumption for full film lubrication, and reduces the complexity of the model. However, as discussed in the Implementation section, Section 3.4, the model is constructed with further development in mind.

3.1.1 Load distribution

The TEHL model is constructed such that it can take any load distribution model as input. This allows for a connection between the TEHL and the LTCA, such that manufacturing errors can be included in the TEHL. Alternatively, any relation between contact position and load can be used, such as the standard assumption of equal load in the simultaneous contacts during dual engagement.

3.1.2 Singularity

Due to the Boussinesq formulation of deformation caused by a point load, a singularity appears in the deformation formula. This makes deformation mesh-dependent, which is undesirable. Special consideration is taken to this in the discretization of the deformation, where the deformation kernel is evaluated between grid points.

This problem is seldom addressed even though it has a large impact on results. The singularity can be avoided by combining the Boussinesq–Cerruti solution with a constant solution (i.e., introducing a limit to Boussineq's solution) or using the more complicated Love's solution [177]. Thorough treatments of singularities, the Boussinesq solution, and contact problems are presented by Lubarda [178] and Marmo and Rosati [179].

3.2 TED and Effigears

The idea to continue the research by studying lubricated contacts coincided with the following two Vinnova projects. Drafts of the TEHL methodology were made, and the corresponding parts of the funding applications were written. As the applications were approved, this part of the research was financed by Vinnova. Here, the projects are briefly decribed.

Driveline components for electrified powertrains [180] (Swedish: TED - Transmissionskomponenter för Elektrifierade Drivlinor). This is a Swedish project with a broad perspective of electrification, including un-synchronized meshing, material fatigue, and selection of materials including powder metals. It involves many industrial project parts, as well as universities and institutes. One part of the project concerns gears, both simulation and testing. In ongoing work, a test rig is being built.

E!115140 Effigears [181]. This is a European project that treats efficiency of gearsets in general applications. It includes novel surface treatments and measuring techniques.

While focus lies on testing, using an FZG test rig, of gears subjected to surface treatments, the project also includes simulations.

It is a goal in both these projects to obtain experimental results that can be compared to simulation results, such that the simulation models can be improved until satisfactory agreement is reached, as shown in Figure 3.1.

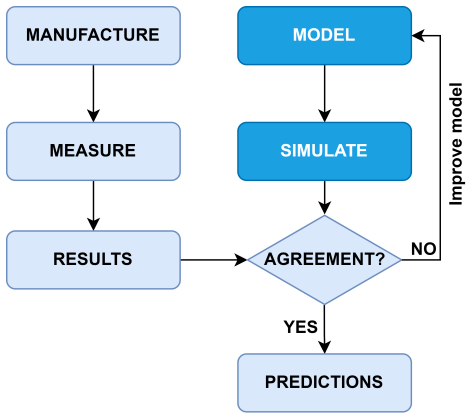

Figure 3.1: The relation between experimental and modeling work. Paper V, summarized in this chapter, models and simulates gear meshing under lubricated conditions (corresponding to dark blue boxes). Further work is dictated by the level of agreement with experimental results. Reproduced with permission from Paper V.

3.3 Theory

The theoretical framework of the TEHL model, with extensive derivations and definitions of all parameters and constants, is presented in Paper V. Here it is summarized for the sake of completeness. See also Tables 3.1 - 3.3 for explanations.

The lubricant pressure in a thin film is governed by the Reynolds equation,

$$\frac{\mathrm{d}}{\mathrm{d}x}\left(\frac{\rho h^3}{12\eta}\frac{\mathrm{d}p}{\mathrm{d}x}\right) = U_m \frac{\mathrm{d}}{\mathrm{d}x}\left(\rho h\right) \tag{3.1}$$

This equation relates pressure p, lubricant film height h, viscosity η, density ρ, and mean surface velocity U_m. The temperature T is governed by the heat equation,

$$\underbrace{\beta T u \frac{\mathrm{d}p}{\mathrm{d}x}}_{\text{compression}} + \underbrace{\tau \frac{\mathrm{d}u}{\mathrm{d}z}}_{\text{shearing}} = \underbrace{c\rho u \frac{\mathrm{d}T}{\mathrm{d}x}}_{\text{convection}} - \underbrace{\lambda \frac{\mathrm{d}^2 T}{\mathrm{d}x^2}}_{\text{conduction}} \tag{3.2}$$

This equation is comprised of a compression part (where β is the volume expansion coefficient and u is the velocity of a point in lubricant film), a shearing part (where τ is the shear stress), a convection part (where c is the specific heat), and a conduction part (where λ is the thermal conductivity).

These equations are used to find pressure p and temperature T. Both pressure and temperature affect viscosity and density. Here, the Rodermund [122] viscosity model is used, i.e.,

$$\eta(p,T) = A_\eta \exp\left(\frac{B_\eta}{T + C_\eta - 273}\left(\frac{p}{2\cdot 10^8}+1\right)^{D_\eta + E_\eta \frac{B_\eta}{T+C_\eta-273}}\right) \tag{3.3}$$

where $A_\eta - E_\eta$ are viscosity parameters, cf. Table 3.3. The density model is that of Dowson–Higginson [123],

$$\rho(p,T) = \rho_0\left(1+\frac{\beta_{\rho 1}p}{\beta_{\rho 2}p+1}\right)(1-\alpha_\rho(T-T_0)) \tag{3.4}$$

The density parameters are also presented in Table 3.3.

These equations are coupled since, for example, pressure depends on viscosity according to the Reynolds equation, but viscosity simultaneously depends on pressure according to the Rodermund equation. Furthermore, for pressure of the magnitude typically found in gearsets, deformation is not negligible. The relation between pressure and deformation is given by Johnson [101]:

$$\upsilon = \int_{x_s}^{x_e} C(x-x')p(x')\mathrm{d}x' \tag{3.5}$$

where the kernel C is given by

$$C(x) = -\frac{4}{\pi E'}\ln|x| \tag{3.6}$$

E' is the equivalent modulus of elasticity, given by

$$E' = \frac{E}{1-\nu^2} \tag{3.7}$$

assuming that both pinion and gear are made from the same material.

The deformation thus alters the height, which again affects the Reynolds equation, and so on.

The above equations are solved under some boundary conditions. Inlet temperature is specified, i.e., a Dirichlet boundary condition, whereas outlet temperature is assumed to have a zero derivative, i.e., a Neumann boundary condition.

Pressure distribution is found under the condition that all pressure values must be positive. The cavitation border is moved iteratively until this condition is satisfied. In the cavitation zone, the pressure is zero, and the pressure derivative (with respect to the coordinate in the contact) is zero at the cavitation border. The fill factor θ describes the proportion of lubricant in the cavitation zone.

The equations are also subjected to the load balance equation, which states that the surface integral of the pressure distribution should be equal to the applied load.

Before implementation, the equations are discretized. A Forward Euler method is used. The detailed discretization is appended in Paper V.

3.4 Implementation

The LTCA is quite straightforward, where start values used in the Newton–Raphson schemes are guessed fairly easily and the remaining behavior of the solver is predictable. The TEHL, on the other hand, is less straightforward due to its couplings as well as sensitivity. This section describes the implementation of the TEHL solver as a Matlab program. The description in this section is more heuristic; for a detailed description, see Paper V.

3.4.1 Initial guesses

As the program is started, all necessary data is taken as input. The coupled nature of the TEHL problem means that either all quantities are known (at least within a certain residual), or all are unknown. Therefore, the algorithm is constructed such that there are a few options for the initial guess of the unknown quantities.

- If the chosen contact position is the first of the simulation, and no similar cases have been simulated before, a pressure distribution is assumed. This is close to Hertzian, but with a smoothing factor to avoid sharp gradients where the Hertzian contact zone ends. This is guaranteed to give the correct equivalent load, and should therefore be reasonably close to the true pressure distribution.

The temperature is guessed to start at the inlet temperature, increase with the pressure, and then drop to a value at the outlet somewhere between the inlet temperature and the maximum temperature. With pressure and temperature guessed, viscosity and density are calculated. Deformation is calculated according to the guessed pressure and added to the height. The height is then adjusted until the Reynolds equation yields a pressure distribution with a correct equivalent load. Thus, values of pressure, temperature, viscosity, density, and height are found in the first iteration. These values are then fed into the solver. The method resembles that of Sivayogan et al. [182], who feed their solver with initial values found from a Lubricated Loaded Tooth Contact Analysis (LLTCA).

- If instead the problem was solved at a previous position, the solution at the previous position is used as an initial guess for the current position. For positions fairly close along the line of action, the solutions are similar and the previous solution is thus a good guess.

- If the contact position is the first in the simulation, but simulations have been made previously under similar conditions, the solution from the previous simulation can be used by taking a file as input.

3.4.2 Convergence routine

Once an initial guess has been made according to one of the methods above, it is fed into the main solver. This solver then uses the intrinsic feedback mechanism of the TEHL problem. For example, an updated pressure (i.e., next iteration) gives an updated deformation, and thereby an updated height. This height is again used in the Reynolds equation. When height increases (all other values kept unchanged), the pressure decreases. Consequently, deformation decreases, height decreases, and pressure increases. A too large pressure in one iteration thus yields a too low pressure in the next. This principle holds for all quantities.

The intrinsic feedback mechanism thus seeks the true solution. However, it is possible that the difference in values between two iterations becomes too large, such that the solution in one iteration falls outside the convergence radius. To avoid this, it is assumed that the step suggested by the solver is in the right direction, but with a too large step size. The pressure is therefore updated with a fraction of the suggested update, dictated by a damping factor. Larger damping means increased numeric stability but decreased computational speed, and vice versa.

Convergence is reached when the pressure residual, essentially the difference in pressure between two consecutive iterations, is sufficiently small.

3.4.3 Load distribution – relation to LTCA

One of the inputs in the program is a load distribution model. The simplest method is to neglect friction, and assume that the load is shared equally between the tooth pairs during dual engagement. Here, this load distribution model is referred to as standard. While the standard approach requires no computational effort, it is not always accurate and fails to include some phenomena, such as the fact that the dual engagement region increases with load.

An alternative is to used the load distribution found from the previously described LTCA method. The major gain from this is that manufacturing errors can be included through their alteration of the load distribution.

3.5 Numerical Example

The same gearset as in Chapter 2 is used, cf. Table 2.1. In addition, the following conditions are used.

Table 3.1: Input data for the gear set operation parameters.

Property	Value	Unit
Output torque, M_g	200	Nm
Input speed, n_p	6000	rpm
Lubricant inlet temperature, T_0	80	$^\circ$C

Additionally, the lubricant heat parameters, see Equation 3.2, are given the following values.

Table 3.2: Input data for the lubricant parameters.

Property	Value	Unit
Specific heat, c	2000	$\mathrm{J \cdot kg^{-1} \cdot K^{-1}}$
Thermal conductivity, λ	0.135	$\mathrm{W \cdot m^{-1} \cdot K^{-1}}$
Volume expansion coefficient, β	0.0007	$\mathrm{K^{-1}}$

The density and viscosity data are based on based on FVA[1] reference oil no. 3 [107] and have the following values.

[1] Forschungsvereinigung Antriebstechnik

Table 3.3: Input data for density (top half of the table) and viscosity (bottom half of the table) parameters.

Symbol	Value	Unit
ρ_0	889.4	$\mathrm{kg/m^2}$
$\beta_{\rho 1}$	$0.6 \cdot 10^{-9}$	$\mathrm{Pa^{-1}}$
$\beta_{\rho 2}$	$1.7 \cdot 10^{-9}$	$\mathrm{Pa^{-1}}$
α_ρ	$6.4347 \cdot 10^{-4}$	$\mathrm{K^{-1}}$
A_η	$3.18 \cdot 10^{-5}$	Pas
B_η	1165.51	°C
C_η	108.804	°C
D_η	0.6458	-
E_η	$-6.23 \cdot 10^{-3}$	-

3.6 Results

This section summarizes results from the TEHL simulation tool together with some commentary.

The result of a TEHL simulation at a certain contact position is shown in Figure 3.2.

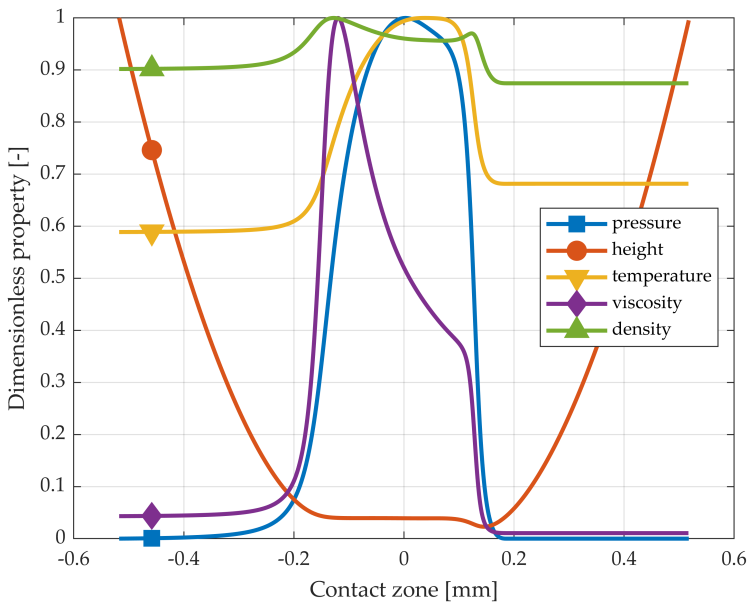

Figure 3.2: TEHL simulation results at a position in the single engagement zone. All properties (pressure, film height, temperature, viscosity, and density) are made dimensionless by division of their respective maximum values. Reproduced with permission from Paper V.

Here a few conclusions can be drawn from visual inspection. The pressure distribution exhibits the typical fluid pressure behavior, with a gradual build-up rather than the very steep build-up of e.g. Hertzian pressure. In the cavitation zone, it goes down to zero, with a zero derivative. The lubricant film height becomes almost flat, and shows a dent near the cavitation boundary. The temperature starts at the inlet temperature, rises with the pressure, and then drops with a zero derivative at the outlet, thus satisfying both its boundary conditions. Viscosity increases with increasing pressure, and then decreases with increasing temperature. Finally, density does not change very much, only about 10 % throughout the contact.

The contact in Figure 3.2 is in the single engagement zone, where all load distribution models predict the same load (apart from friction contributions). In the dual engagement zone, however, there might be a large difference. This is seen in Figure 3.3.

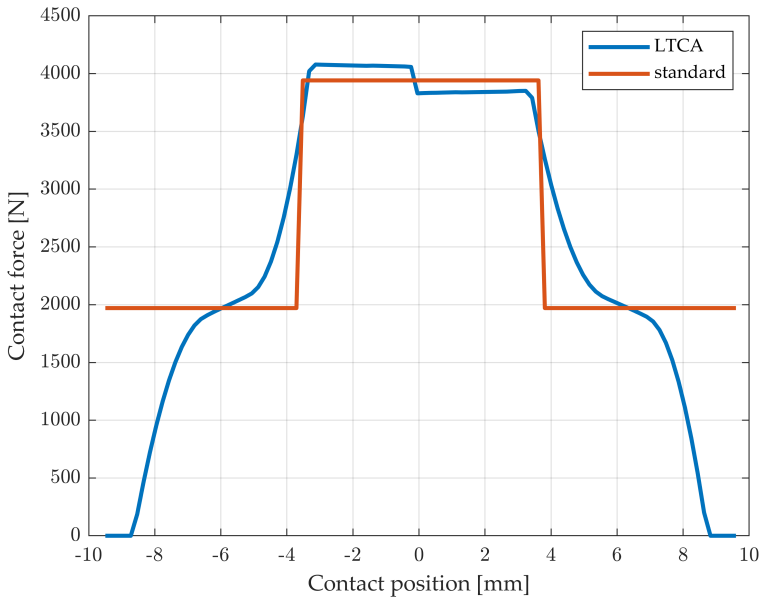

Figure 3.3: Load distribution, i.e., equivalent load as a function of position. LTCA: load distribution found from LTCA simulations. Standard: load distribution found from the standard assumption of equal load between tooth pairs in the dual engagement zone. Reproduced with permission from Paper V.

The standard load distribution model both over- and underestimates load in the dual engagement zone compared to the LTCA. This is reflected in the TEHL solution at a point just outside of the nominal single engagement zone, where pressure from the TEHL method is considerable higher using load from the LTCA than from the standard.

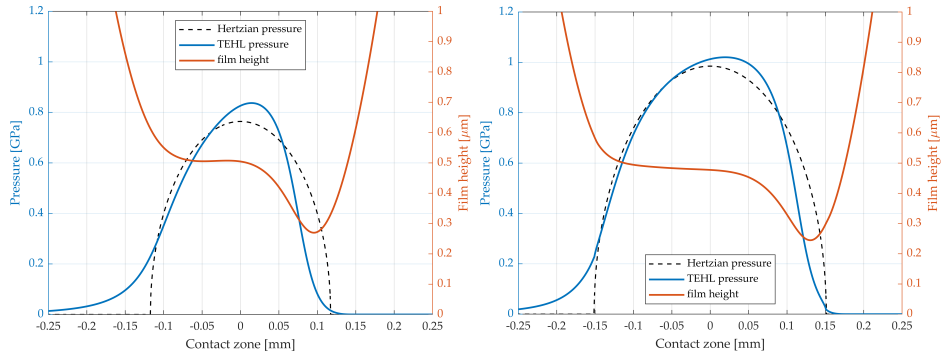

Figure 3.4: Lubricant pressure and lubricant film height from TEHL simulations. Hertzian pressure is shown as a reference. Left: load found from the standard load distribution model. Right: load found from LTCA simulations. Reproduced with permission from Paper V.

Since manufacturing errors alter the meshing and thereby the load distribution, the phenomenon seen in Figure 3.4 can also be expected in the presence of manufacturing errors. Paper V displays the load distribution for different cases of manufacturing error combinations. Here, the result of the corresponding TEHL simulations are shown.

Figure 3.5 show the lubricant pressure for three cases, nominal (no error), pitch error class 8, profile slope error class 8, and pitch error class 8, profile slope error class 5.

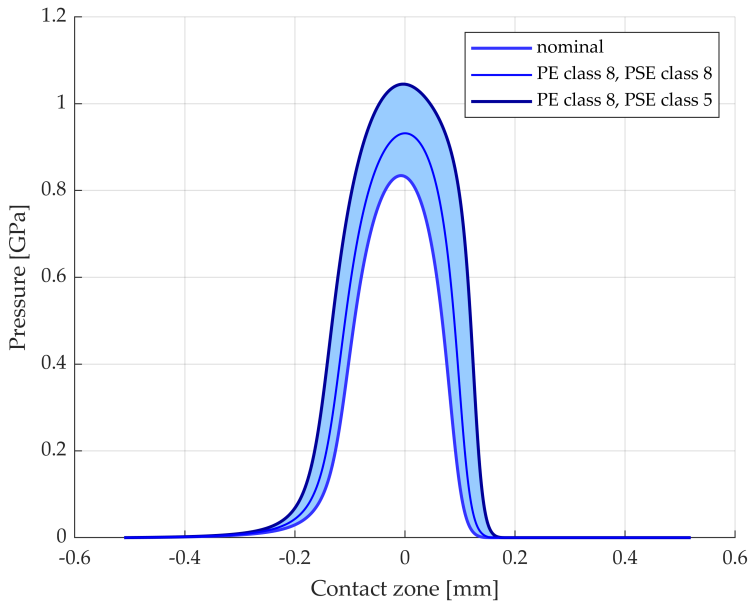

Figure 3.5: Lubricant pressure for one error free case, together with two cases of manufacturing error combinations. Reproduced with permission from Paper V.

While it is seen that both manufacturing error cases cause an increase in pressure, profile slope error of class 5 actually constitutes a worse case (at this position) than profile slope error of class 8, since it counteracts the load increase caused by the pitch error.

Similar behavior can be observed in Figure 3.6 for lubricant temperature. Increased load results in a greater heat generation.

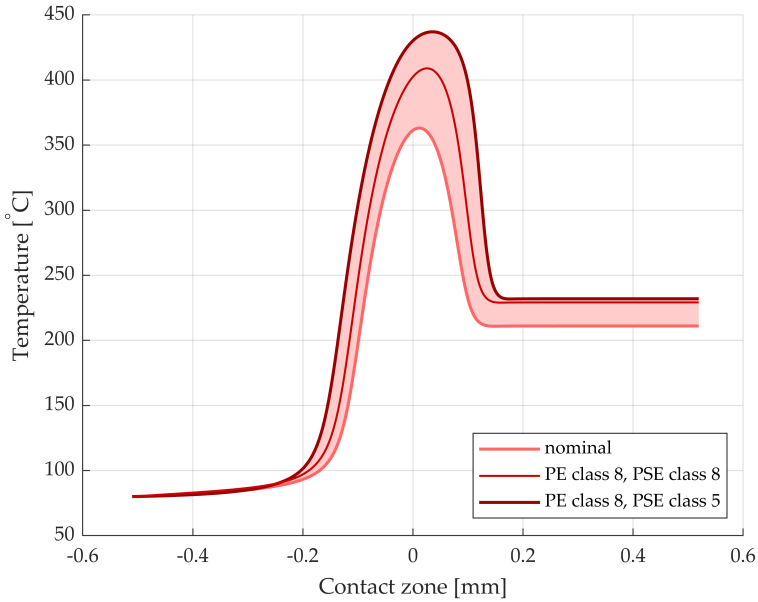

Figure 3.6: Lubricant temperature for one error free case, together with two cases of manufacturing error combinations. Reproduced with permission from Paper V.

The effect on film height is a bit less pronounced, but still clearly visible.

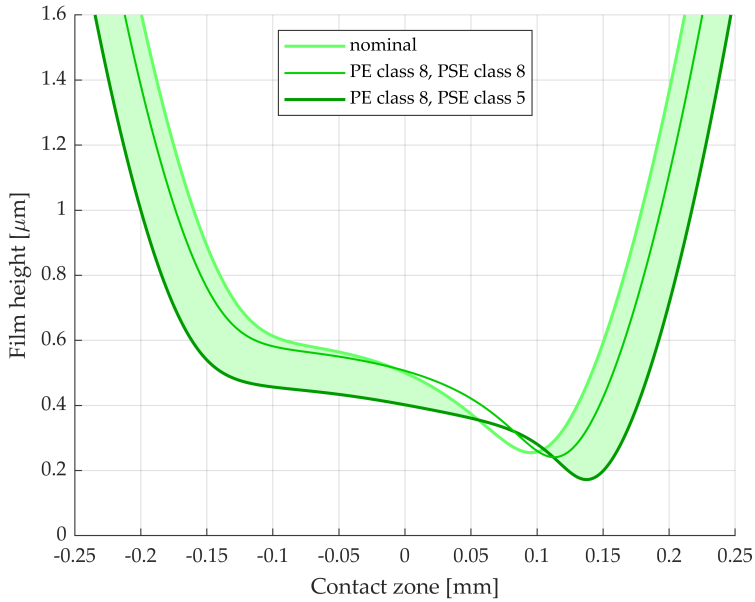

Figure 3.7: Lubricant film height for one error free case, together with two cases of manufacturing error combinations. Reproduced with permission from Paper V.

3.7 Discussion

As previously discussed, the lubricant pressure distribution resulting from the TEHL simulations, see Figure 3.2, exhibits the typical lubricant pressure features, such as gradual pressure build-up and cavitation. Simultaneously, it is also fairly close to Hertzian pressure distribution. Pressure, film height, temperature, viscosity, and density all seem reasonable from visual inspection, as well as comparison with the literature, see for example Chu et al. [106] or Bobach et al. [102].

Furthermore, the imposed boundary conditions are shown to be satisfied. While this does not guarantee that the TEHL model equations are suitable, it does show that the solutions fulfill the equations, eliminating some possible implementation errors.

Implementation of a damping factor applied to the new pressure in each iteration is typical for numerical EHL solvers. This is often known as relaxation, as described early by Ai et al. [183] and employed by other authors [182, 184, 185].

The impact of manufacturing errors is shown to be adverse, with increased pressure and temperature. The decreased film height is also an adverse effect, since it makes the gearset more sensitive to contamination of debris [186]. It also makes the gearset

more susceptible to asperity contact.

The start and end of mesh are found by assuming a layer of lubricant on the surface of each gear tooth. This is the supply thickness, as discussed in Paper V. The contact zone starts when these no-load lubricant films first meet. A sensitivity analysis shows that the supply thickness itself has little or no influence on the solution as long as it is large enough. If the contact zone increases following an increased supply thickness, there will be a larger region with very low pressure at the inlet. The outlet is determined in the same way, but due to cavitation, the pressure is zero everywhere after the cavitation boundary.

The reason behind establishing the contact zone this way is to avoid enforcing Hertzian pressure distribution. Many authors base the contact zone on Hertzian contact width. If there is no temperature dependence in the viscosity expression, the viscosity becomes immensely large, like that of a solid. If, in addition, Hertzian pressure is used as an initial value, there is a risk that the resulting pressure accidentally becomes very close to Hertzian. By not assuming values related to Hertzian contact theory, this risk is reduced.

Non-Newtonian fluid descriptions are omitted. The corresponding effects are believed to be small, see Liu et al. [121]. However, if a discrepancy between simulated and measure values exists, this is a possible point to improve. It also depends on which description will be available for the lubricants used in the experiments, see Chapter 6.

Another possibility of improvement is to make a more advanced temperature analysis. For example, heat parameters could be allowed to vary, cf. Mihailidis et al. [107]. It would also be possible to include heat transport in the gear bodies, shafts, and so on.

In the present TEHL model, no variation over the width of the tooth is assumed. This is motivated computationally by decreased complexity and time consumption, and physically by the fact that this direction is perpendicular to the flow direction. It is also several magnitudes larger than the contact region in the flow direction, making the 'infinite width' approximation reasonable.

Dynamics are neglected in accordance with Yang et al. [130]. Combining TEHL analysis, dynamics, manufacturing errors, and a system perspective could be meaningful, see Chapter 6.

Surface roughness is also neglected at this stage, i.e., in this first iteration of the model development. This assumption is supported by preliminary results obtained in the Effigears project, where lubricants seem to have a larger effect on gearset behavior, such as efficiency, than surface roughness. Still, it remains as future work to establish

and implement a mixed TEHL solver.

Using results from the LTCA as input in the TEHL simulations is one of the major contributions of this work. The fact that dry contacts are used as input to lubricated contacts is motivated by the fact that the treated manufacturing errors are much larger than the changes in lubricant film thickness they impose, which makes the influence of film height difference negligible in the contact positions.

3.7.1 Conclusions and reflections

Manufacturing errors have a large effect on lubricant properties, as summarized in Figures 3.5 to 3.7 and shown in more detail in Paper V. Large effects are also reported by Liu et al. [127]. It seems that very few authors include manufacturing errors like pitch error and profile slope error in their studies, but those who do report large impact. This conclusion is in line with that of Clarke et al. [139].

The manufacturing errors cause an alteration of the contact geometry, but this alteration is quite small. If manufacturing errors are included only by altering contact geometry, their effect will be small. The great effect comes from the difference in load as shown in Paper V.

There is evidently a need of further investigation of the subject.

Paper V answers RQ1 and RQ2. Continued TEHL work will look at RQ3 through the high-speed TED rig, see Chapter 6.

Chapter 4

System perspective

This section describes the system perspective, where not only a single gear pair is treated, but instead the perspective is lifted to the whole system, including more gear stages, bearings, and housing.

4.1 Introduction to Systems

Describing a whole complex system, such as an electric vehicle (EV) is of course a very tedious task. Even if a subsystem, such as the gearbox, is considered, a vast amount of parameters and degrees of freedom exist. Therefore, one often goes further, and typically describes either a single contact thoroughly, ignoring all other elements of the gearbox, or describes the whole system, using a simplified contact model.

In Paper I-V, the former approach is used, see Chapters 2 and 3. There, the only influence of the surroundings are input data and boundary conditions. In the current chapter, the latter approach is used. Here, not only gear meshing is of interest, but also gearset layout, bearing life rating, and housing mass.

Due to the complexity of the system, many new possibilities of optimization arise. An overview of these optimizations is given in Chapter 1. This chapter shows how to optimize the dog-leg angle of a two stage reducer, minimizing bearing forces and housing mass. It is assumed that other parameters, such as gear ratio in each stage, geometric data, and so on, already have been optimized.

4.2 Theory

In the transition from internal combustion engine (ICE) to electric motor (EM) of a passenger vehicle, the typical vehicle speed and wheel size are left unchanged. This imposes new demands on the transmission, which has to compensate the higher rotational of the EM compared to the ICE by an increased gear ratio. It is advantageous to divide this larger gear ratio into two or more stages. A two stage reduction is shown in Figure 4.1.

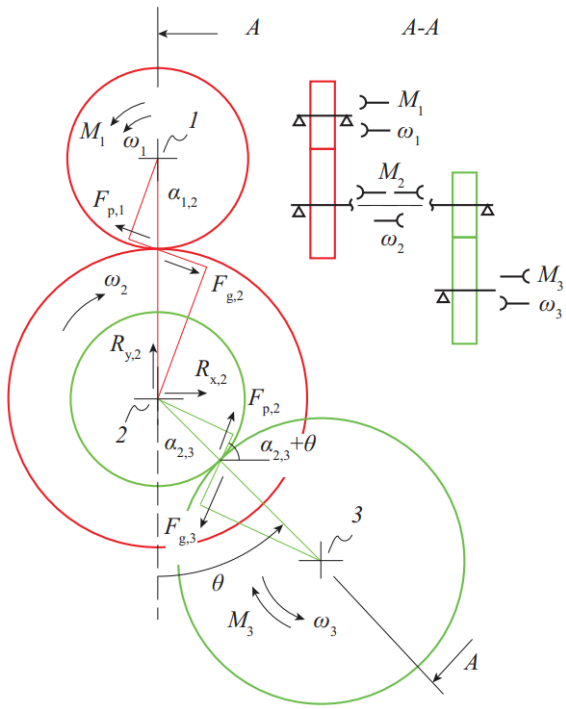

Figure 4.1: Schematic overview and free body diagram of a two stage reducer. All gears in this case are spur gears. Note that the position of shaft 3 is dictated by the dog-leg angle θ. Reproduced with permission from Paper VI.

In Figure 4.1, the dog-leg angle θ, sometimes denoted by diversion angle, is introduced. $\theta = 0$ corresponds to the center point of each shaft being placed on a straight line, and $\theta = 90°$ corresponds to an L shape.

Each shaft is supported by two bearings, one on either side of the gear. The bearings on each shaft together accommodate the reaction force of the gear. For the first and last shaft, shafts 1 and 3 in Figure 4.1, the reaction forces cannot be decreased without interfering with parameter choice, loads or similar, which were assumed to be fixed.

However, by varying θ, reaction forces on the intermediary shaft, shaft 2, can be redirected. This means the reaction forces can counteract each other and cancel out to some degree, thus decreasing the total reaction force on the shaft, and thereby the bearing forces.

From force equilibrium of the intermediary shaft, the dimensionless reaction force R_0 is found as

$$R_0 = \sqrt{1 + u^2 + 2u\cos(\alpha_{1,2} + \alpha_{2,3} + \theta)} \tag{4.1}$$

where $\alpha_{1,2}$ and $\alpha_{2,3}$ are the working pressure angles of each stage. u is the ratio between the number of teeth of the gears on the intermediary shaft. This is, however, not a gear ratio, since the gears on the same shaft never go into mesh with each other.

By differentiating the R_0 force with respect to θ, it is found that extreme values occur when

$$\sin(\alpha_{1,2} + \alpha_{2,3} + \theta) = 0 \tag{4.2}$$

i.e., the smallest possible reaction force can be found.

Once the reaction forces are found, the corresponding bearing forces can be calculated. Bearing rating life is then found according to standard calculations such as ISO 281 [187].

The same methodology is then applied to a case with helical gears; see Figure 4.2 where also the housing is included. As helical gears introduce non-zero axial forces, the bearing reaction forces also depend on distances acting a levers in the moment equilibrium. The expressions thus get more involved, and a neat expression such as Equation 4.2 is not attainable.

An example is shown in Section 4.3.

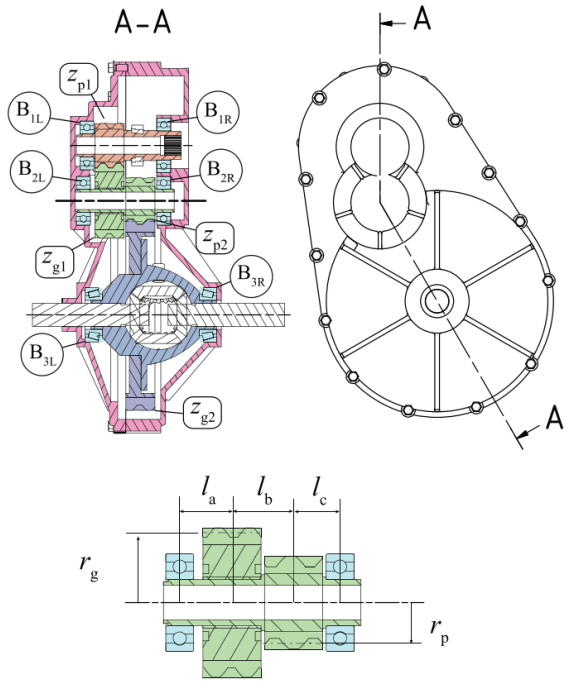

Figure 4.2: Two stage reducer with housing and intermediary shaft. Top left: Section view of CAD model of the reducer. Top right: Top view of the housing. Bottom: intermediary shaft with its gears and bearings. Reproduced with permission from Paper VI.

While driving the vehicle, a variety of speed and torque values are applied. To model this, a duty cycle is applied. Contrary to ICE vehicles, electric vehicles also use regenerative braking [188], which means reversing the torque direction. This has the same effect as mirroring the dog-leg angle, i.e., changing θ to $-\theta$. This gives the ability to include regenerative braking in the cycle.

An estimation of housing mass is made by studying the enclosed volume of the gearset. With a certain wall thickness and material selection, this corresponds to a mass.

4.3 Numerical example

The reducer used in the numerical example can be seen in Table 4.1.

Table 4.1: Numerical example. Tooth numbers from Nissan Leaf gearbox, model year 2011-2013.

Property	Symbol	Value
1st stage		
tooth number pinion	$z_{p,1}$	17
tooth number gear	$z_{g,1}$	31
normal module, [mm]	m_n	1.75
normal pressure angle, [°]	α_n	20
helix angle, [°]	β	28
gear width, [mm]	b	25
2nd stage		
tooth number pinion	$z_{p,2}$	17
tooth number gear	$z_{g,2}$	73
normal module, [mm]	m_n	2.03
normal pressure angle, [°]	α_n	20
helix angle, [°]	β	20
gear width, [mm]	b	25
intermediate shaft		
distance, [mm]	l_a	22.5
distance, [mm]	l_b	26.5
distance, [mm]	l_c	22.5
pitch radius 1st gear, [mm]	R_c	30.78
pitch radius 2nd pinion, [mm]	R_c	18.34
Total ratio	U_{tot}	7.94
Ratio step intermediate shaft	u_2	$\frac{31}{17} \approx 1.8$

4.4 Results

This section contains some results from the dog-leg optimization performed in Paper VI, together with some remarks.

The dimensionless reaction force can be seen in Figure 4.3, where it it normalized by the dimensionless reaction force at $\theta = 0$. This is done for different values of u.

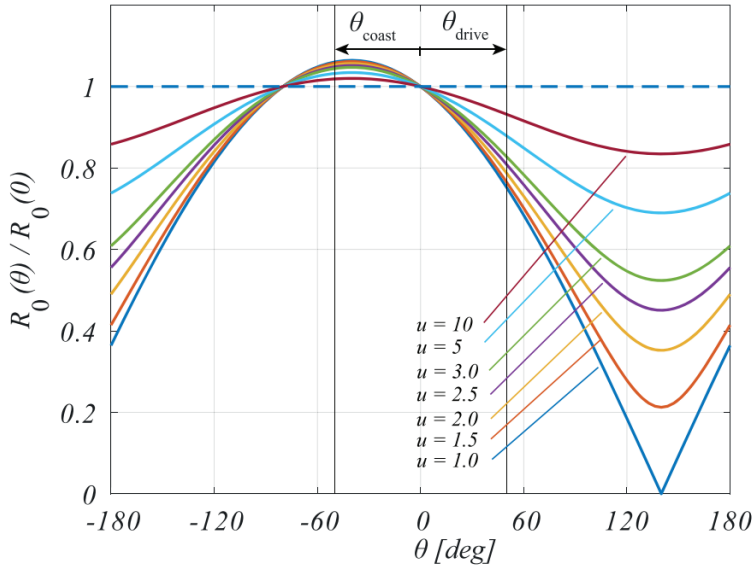

Figure 4.3: Normalized dimensionless reaction force for different u values. Note that coasting corresponds to changing sign of θ. Reproduced with permission from Paper VI.

It can be observed in Figure 4.3 that for $u = 1$, the reaction force becomes zero. This result is slightly artificial, since $u = 1$ would hardly be used in practice as this would mean that both gears on the intermediary shaft would have the same number of teeth, thus, there would be no use in it for gearing purposes. However, it serves a a control of the method. Mathematically, Equation 4.1 yields $R_0 = 0$ when the cosine takes the value -1. Physically, two equal gears would give reaction forces of equal size but opposed direction.

For more reasonable u values, a large decrease is still seen. The decrease during driving may however come at the expense of increased reaction force when coasting, as torque is reversed. For large u values, not much happens with the reaction force. This is because the contact force of the larger gear become too small to have any significant impact on the total reaction force, no matter how it is directed.

For helical gears, the equations get less neat, but the same principle is used. Apart from lowering reaction forces, and thus allowing smaller and lighter bearings, the enclosed volume also decreases. This can be seen in Figure 4.4.

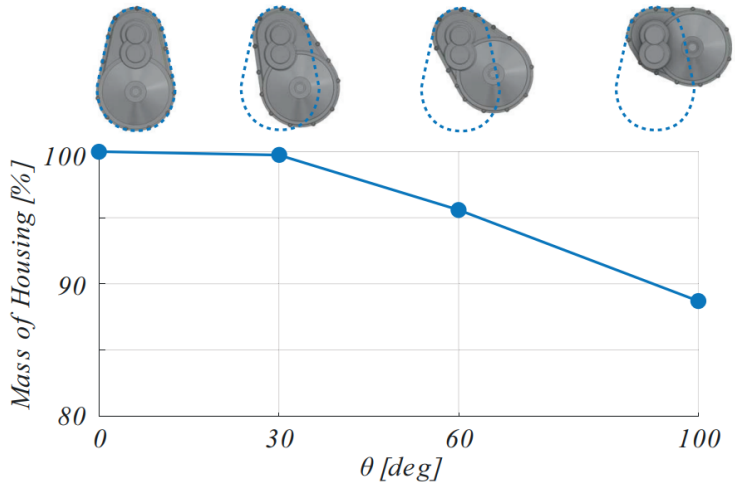

Figure 4.4: Housing mass for dog-leg angle θ relative to housing mass for $\theta = 0$. Reproduced with permission from Paper VI.

Figure 4.4 displays a fairly large decrease in housing mass due to optimizing the dog-leg angle. Here, the optimization is made under the implicit constraint that gears and shafts must not interfere.

4.5 Discussion

Paper VI treats a method to perform an optimization of a gearset with two or more stages, without changing gear data, such as pressure angle, or loads or similar - these are assumed to already be chosen based on optimization or due to other favorable reasons.

The dog-leg angle optimization provides several advantages. Decreased reaction forces imply decreased equivalent load for the bearings, see Figure 4.3, which can then be smaller and lighter. The decrease in enclosed volume renders a decreased housing mass, as shown in Figure 4.4.

In practice, the advantages are more pronounced. By considering housing stiffness, the housing mass can be decreased even further since the more compact design requires less material. Decreased bearing loads also imply decreased load-dependent power loss.

The suggested method is intended for design of electric vehicle transmissions. While the method of opposing reaction forces is not limited to EVs, it requires at least one

intermediary shaft. The layshaft of a manual transmission, for example, does not benefit from a reposition. Other applications, such as industrial machinery, could however see an advantage of using the proposed method.

In addition to the proposed method, other constraints may apply. These are, however, not general but rather specific to the case at hand, such as limits in housing size. The analysis should be made with these in mind. Furthermore, interference between gears and shafts should be avoided.

4.5.1 Conclusions and reflections

The study in paper VI served the purpose of increasing knowledge about systems, as opposed to the contact analysis that constitutes the majority of this thesis. It gives a broader view and better understanding of the whole field of gearing.

Contact analysis, including manufacturing errors, is omitted from paper VI. The reason for this is that while manufacturing errors greatly alter the load distribution, i.e., the proportion of load carried by each simultaneous contact, they do not alter the total load. Therefore, manufacturing errors do not influence bearing forces.

Thus, there is no need, at this stage, for a more complicated contact model. There are, however, a few possible connections between contact and system perspectives:

- The analysis of transmission error in Paper III only considers deflection of the gears. While this is an effective way of isolating the effect of manufacturing errors, it would be of interest to incorporate the transmission error analysis in a larger system, with more stages, and bending and torsion of shafts. Varying the dog-leg angle redirects forces, which contributes to bending and torsion. This links the LTCA to the system perspective.
- The difference in lubricant film height for different loads in the TEHL method corresponds to viscous damping. Film height is, in turn, affected by manufacturing errors. Therefore, manufacturing errors could be related to the system model by means of dynamics together with a TEHL analysis. The earlier claim that manufacturing errors have no effect on system level is therefore augmented by ”under static conditions”. This links the TEHL to the system perspective.

Furthermore, contact analysis and system analysis are connected since they provide input to each other. A system optimization may suggest stages that are optimal from, e.g., a mass perspective. A subsequent contact analysis may however show that this solution would result in tip contact.

Contact analysis and system perspective will inevitably be intertwined when performing experiments with the high-speed TED rig, see Chapter 6.

In addition to the points above, the system perspective contributes with important insights that are useful in the design of the test rig in the TED project.

Paper VI answers RQ3, due to the strong connection to electrified drivelines.

Chapter 5

Conclusions

This chapter summarizes Chapter 2 - 4, concludes the discussions, and returns to the research questions and their answers.

5.1 Summary

This thesis summarizes the research work disseminated in the appended papers. It has been shown that contact pressure is an important part of gearset behavior, closely related to fatigue. Since contact pressure cannot be directly measured, an LTCA simulation tool was created by modeling and simulation. The tool accounts for manufacturing errors of different types and tolerance classes.

Simulation results show that gear meshing is adversely affected by tip contact, which then can be used for assessment of manufactured gears. Even without tip contact, manufacturing errors have a large impact on load distribution. To investigate this effect further, a TEHL simulation tool was developed, and further results showed a negative impact of manufacturing errors on lubricant properties such as temperature and film height.

Manufacturing error tolerances are chosen based on several criteria. Due to electrification, new demands are imposed on low gearset noise. Therefore, tolerances are chosen to decrease transmission error. Electrification also impose new demands on gearset layout, such as large gear ratios split into several stages. It is shown how careful layout design can minimize bearing forces and housing mass.

5.2 Research questions

From the literature review presented in Section 1.1, the following research questions were formulated, and the answers obtained thus far read as follows.

5.2.1 Research Question 1

RQ1: *How could gear contacts be modeled, in a physically reasonable way, to account for modifications and manufacturing errors?*

In this case, just like in general, the model should be as simple as possible. If only forces are needed, as in the system study of Paper VI, there is no need for a contact analysis.

If no lubricant properties are of interest, a dry contact model is shown to work well. Such a model is developed in Paper I. Even though real gearsets are lubricated, deformations and manufacturing errors (i.e., flank errors such as pitch error and profile slope error) are several orders of magnitude larger than the change in lubricant film thickness they impose, which means that the impact of the lubricant is overshadowed and a dry model suffices. The model should include a treatment of tip contact, and calculate load distribution based on deformation and a compliance condition, rather than assuming it *a priori*, which erases the effect of manufacturing errors.

If, on the other hand, lubricant properties are of interest, a TEHL model is needed. Such a model is developed in Paper V. It is here necessary for an accurate simulation to include temperature to properly account for varying viscosity. An accurate load distribution model is shown to be of high importance.

All models are shown to be physically reasonable by preliminary evaluation, such as comparison with existing literature.

5.2.2 Research Question 2

RQ2: *How do manufacturing errors and their tolerances influence gearset behavior?*

Manufacturing errors of different tolerances are shown to have large impact on the running gearset. Typically, the effect is adverse, with increasing pressure, as shown in Paper II, increasing transmission error, as shown in Paper III, and decreased tip contact threshold torque as shown in Paper IV. Lubricant properties are also negatively correlated with manufacturing errors, typically by increased temperature, as shown in

Paper V. The adverse effects are particularly pronounced when the errors appear in combination, amplifying the individual effects.

Contrarily, some cases of manufacturing errors do not cause much difference in meshing. In such a case, a fairly large error is permissible. It is shown that some gears that would be scrapped due to control measurement would work properly in running gearsets, i.e., scrapping is unjustified, as demonstrated in Paper IV.

Contact pressure and transmission error are shown in Paper III to both co-vary and counter-vary for different manufacturing error combinations.

5.2.3 Research Question 3

RQ3: *How could new challenges, imposed by electrification, be addressed at the gearbox design phase?*

A new demand stemming from electrification is lower noise acceptance in electric vehicles. Noise is typically translated into transmission error. It is shown in Paper III how tolerances are related to transmission error, and how they can be chosen to minimize transmission error.

Electrification also imposes new demands on gearbox layout, due to the larger gear ratio needed to account for the high rotational speed of the electric motor. It is shown in Paper VI how the layout can be optimized, such that bearing forces and enclosed volume can be decreased. Thus, both bearing and housing mass can be considerably decreased, which is of particular interest in already heavy electric vehicles.

Chapter 6

Future work

This chapter describes future work, including ongoing, planned, and potential or possible future work, connected to the topics of this thesis. It provides some ideas on how to continue answering the research questions. It is slightly less rigorous and provides some more personal reflections.

It is difficult to make predictions, especially about the future. The path the forthcoming research will take depends to large extent on what funding it will receive, which in turn depends on possible applications, potential partners, and so on. Collaboration with companies, other departments and/or universities, and so on, plays a major role.

6.1 Ongoing work

This section discusses work that is ongoing as of early 2023. This work mainly focuses on the TEHL method, used in the projects TED and Effigears.

6.1.1 TED

In the TED project, a test rig is currently under construction. This rig is similar in design to an FZG rig, but will run at higher speed to replicate conditions of a gearset driven by an electric motor, for example in an electric car. While not yet disseminated, parts of the rig design have been included in this part of the PhD project.

The gears intended for testing in the TED rig will be of high contact ratio (HCR) type [51, 189], i.e., the contact ratio will be larger than 2. Thus, both dual and triple

engagement will prevail. For the TEHL method, this just means changing the load distribution model. An overview of load distribution models is presented by Ravivarman and Prabhu Sekar [190].

EHL analyses of HCR spur gears have been performed by Huang et al. [191], but they did not solve the Reynolds equation. Furthermore, temperature and manufacturing errors were not considered. Hussein and Abdullah [192] also studied lubricated HCR spur gears, but they too used EHL formulas rather than solving the Reynolds equation.

A convenient parameter to measure in a test rig is the power loss. HCR gears are associated with greater power loss according to Thirumurugan and Muthuveerappan [193]. It remains to establish a model for the lubricant. Furthermore, lubrication type influences efficiency [16].

This work will mainly provide more answer to RQ1 and RQ3.

In conclusion, a joint publication within the TED project is at the planning stage. In Figure 6.1, this paper is denoted by 'TED'.

6.1.2 Effigears

In the Effigears project, work has started towards a joint paper. Some results from testing have been obtained, in terms of efficiency and fatigue testing. Also here, a lubricant model remains to be established. However, a comparative analysis can be made irrespective of lubricant, under the assumption that errors introduced by assuming a lubricant model are the same for all cases, where 'case' refers to load stage, manufacturing error combinations, and so on.

In the preliminary testing, some scuffing issues were experienced. This can be investigated by comparing test results to simulations, where tip contact may cause scuffing. Even outside of the tip contact region, scuffing may occur as a result of the lubricant film collapsing due to unfavorable conditions, i.e., combinations of speed, load, geometry, and lubricant properties.

By using the measurement protocols, manufacturing error combinations can be related to scuffing or fatigue resistance in a stochastic approach, i.e., as a continuation of the method proposed in Paper IV. This may, however, fall outside of the scope of the Effigears project. Instead, it will possibly be a separate study.

This work will mainly provide more answer to RQ1 and RQ2.

In conclusion, a joint publication within the Effigears project is at its initial stage. In

Figure 6.1, this paper is denoted by 'Effigears'. Possibly, another publication based on these or similar measurement results can be made. This is not included in Figure 6.1.

6.1.3 Surface roughness

Apart from the project specific tasks described in Sections 6.1.1 and 6.1.2, there is a natural way to proceed with the TEHL model. In Paper V, only smooth surfaces are considered. At the current stage, rough surfaces can be included in the analysis, and some preliminary testing of this has been made. Rough surfaces can be included either directly by taking a rough profile as input, or indirectly by adding stochastic roughness to a smooth surface.

In reality, the manufactured surfaces will always be rough to some extent. The reason this is important is that roughness affects lubricant film height. In turn, film height is related to pressure and the other lubricant properties, as discussed in Paper V and Chapter 3. Furthermore, asperity contact may occur, i.e., roughness peaks of either surface may come into contact with each other.

For a better understanding, it is important to include surface roughness, as done by several authors [102, 105, 108, 111, 117, 124, 128, 130, 139, 184, 194].

Evans et al. [184] studied damage of gears with surfaces subjected to different degrees of roughness. They conclude that areas with significant asperity contact correlate well to areas that are subject to scuffing. This might explain the scuffing issues experienced in the experiments of the Effigears project.

Clarke et al. [139] used Klingelnberg measurements of surface roughness, and show the effect of using different cut-off lengths. They showed that pressure peaks are underestimated when the cut-off length is too large. Rough surfaces are often filtered, using, e.g., an Abbott–Firestone curve [195].

Lubrication where the mating surfaces are completely separated by the lubricant film, such as in Paper V, is called full film lubrication. Lubrication where asperities come into contact is known as boundary lubrication. The lubrication regime where both full film lubrication and boundary lubrication prevail is denoted by mixed lubrication. This type is studied by, e.g., Dong et al. [108] and Evans et al. [184]. Li and Kahraman [117] modeled mixed lubrication statically by a transient Reynolds equation. They also used an Eyring fluid, i.e., a non-Newtonian lubricant description. Li et al. [194] used a mixed lubrication model to calculate gear stresses with the aim of finding the onset of cracks.

During contact, asperities experience large pressure together with sliding. This causes

wear, as studied by, e.g., Walker et al. [196] or Wang et al. [197]. Since the TEHL program can tack rough surface profiles as input, the effect of wear can be included. For example, running-in [198] can be studied this way.

An insight obtained from the Effigears project is that accurate surface roughness models are needed. While stylus type profilometers are commonly used, such done by Clarke et al. [139], some criticism is brought forth against the method, and optic methods are instead suggested by Seewig et al. [199] and Brodmann et al. [200]. Zhao et al. [201] use a Weierstrass-Mandelbrot fractal roughness.

This work will mainly provide more answer to RQ1 and RQ2.

In conclusion, it is planned to include surface roughness in the TEHL method, such that mixed lubrication can be modeled. In Figure 6.1, this paper is denoted by 'Mixed'.

6.2 Possible future work

This section is a bit more speculative, but contains a few suggestions of studies that would be feasible to carry out.

6.2.1 Part matching

It was demonstrated, mainly in Paper II and IV, that while manufacturing errors may amplify each other, with respect to, e.g., tip contact threshold torque, they may also counteract each other. Here it would be of interest to further investigate meshing of gears with manufacturing errors. For example, if both pinion and gear have profile slope errors of the same sign, the situation is close to having a slightly altered pressure angle, which causes no problems. Profile slope errors of opposite signs, however, rather implies different pressure angles, which is detrimental to meshing. Could therefore some manufacturing error combinations have quite a small impact on the running gear set?

By further studying the interplay between different manufacturing errors, an investigation of possible part matching [202] could be carried out. If more gears can be kept, savings of time, material, cost, and environment could be made.

This possible work would provide some more answer to RQ2, as well as broadening the perspective to production and environment.

In Figure 6.1, this possible paper is denoted by 'Part matching'.

6.2.2 Integrating contact analysis in greater systems

As discussed in Chapter 4, there are different ways to combine contact analysis and system perspective. Mainly, transmission error of the whole gearset could be studied, or lubricated contacts could be used to model viscous damping in a dynamic analysis. In Figure 6.1, these possible papers are denoted by 'DTE' and 'Dynamics'. It is also possible to merge these possible papers into one.

This possible work, which would be both interesting and demanding, would link RQ1, RQ2, and RQ3.

6.2.3 Cost analysis

While surface treatments and other extra manufacturing steps could be used to optimize surface topography and thereby gearset performance, they also contribute to complexity. Here it would be interesting to perform a life cycle analysis (LCA) to investigate the trade-off between possible gain due to improved performance and extra consumption due to the increased complexity.

This potential study, which has seen some informal discussion, could be a possibility of cooperation with researchers from other fields.

This possible work would provide some more answer to RQ2, as well as broadening the perspective to production and economy.

In Figure 6.1, this possible paper is denoted by 'Cost analysis'.

6.3 Overview

Figure 6.1 shows an overview of the main methods and ideas.

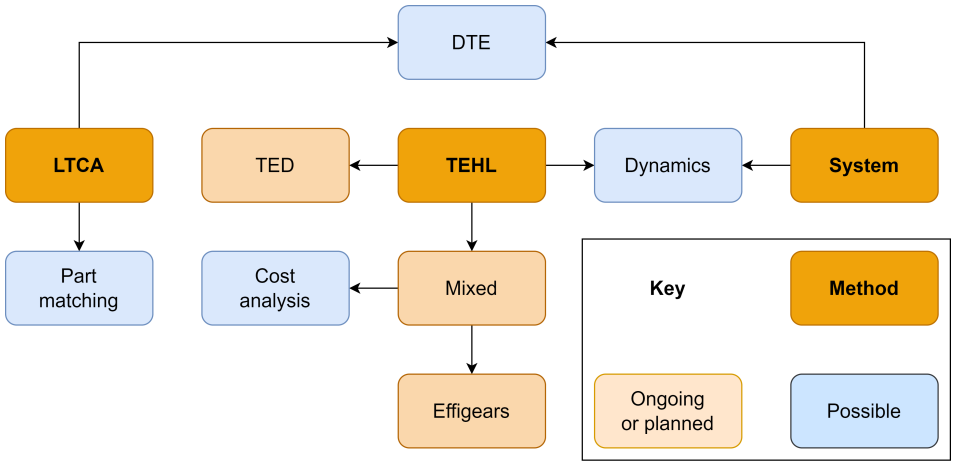

Figure 6.1: Overview of ongoing and possible future work.

While, as discussed, this work greatly depends on funding and collaboration, it serves as some structure of possible ways forward.

References

[1] M. J. T. Lewis. Gearing in the ancient world. *Endeavour, New Series*, 17:3: 110–115, 1993.

[2] John McCleary. *Geometry from a Differentiable Viewpoint*. Cambridge University Press, 2013.

[3] Stephen Radzevich. Principal accomplishments in the scientific theory of gearing. *MATEC Web of Conferences: Power Transmissions 2019*, 287:1–12, 2019. doi: 10.1051/matecconf/201928701001.

[4] Hans Christoph von Seherr-Thoss. *Die Entwicklung der Zahnrad-Technik: Zahnformen und Tragfähigkeitsberechnung*. Springer-Verlag, 1965.

[5] W. Lewis. Investigation of the strength of gear teeth. *Amer. Macht.*, 16, 1893.

[6] M. Utagawa and T. Harada. Dynamic loads of spur gear teeth having pitch errors at high speed. *Bulletin of JSME*, 5(18):374–381, 1962.

[7] D. R. Houser and A. Seireg. An experimental investigation of dynamic factors in spur and helical gears. *Journal of Engineering for Industry*, 92(2):495–503, 1970. doi: 10.1115/1.3427789.

[8] K. Ichimaru and F. Hirano. Dynamic behavior of heavy-loaded spur gears. *Journal of Engineering for Industry*, 96(2):373–381, 1974. doi: 10.1115/1.3438339.

[9] M. J. Handschuh, A. Kahraman, and M. R. Milliren. Impact of tooth spacing errors on root stresses of spur gear pairs. *Journal of Mechanical Design*, 136(6): 061010–1–061010–10, 2014. doi: 10.1115/1.4027337.

[10] Donald R. Houser and G. Wesley Blankenship. Methods for measuring gear transmission error under load and at operating speeds. *SAE Transactions: JOURNAL OF PASSENGER CARS*, 98(6):1367–1374, 1989. https://www.jstor.org/stable/44472380.

[11] M. Benatar, M. Handschuh, A. Kahraman, and D. Talbot. Static and dynamic transmission error measurements of helical gear pairs with various tooth modifications. *Journal of Mechanical Design*, 141(10):061010–1–061010–10, 2019. doi: 10.1115/1.4027337.

[12] Chanat Ratanasumawong, Shigeki Matsumura, Tetsuo Tatsuno, and Haruo Houjoh. Estimating gear tooth surface geometry by means of the vibration measurement: Distinction of the vibration characteristics of gears with tooth surface form error. *Journal of Mechanical Design*, 131(10), 2009.

[13] Mateusz Grzeszkowski, Sebastian Nowoisky, Philipp Scholzen, Gregor Kappmeyer, Clemens Gühmann, Jens Brimmers, and Christian Brecher. Classification of gear pitting damage using vibration measurements. *tm-Technisches Messen*, 88(5):282–293, 2021.

[14] Hyde JH, Tomlinson GA, and Allan GWC. An investigation of the performance of gears. *Proceedings of the Institution of Automobile Engineers*, 26(2): 416–448, 1935.

[15] R. Kasuba and E. I. Radzimovsky. A multi-purpose planetary gear testing machine for studies of gear drive dynamics, efficiency, and lubrication. *ASME. J. Eng. Ind.*, 95(4):1123–1130, 1973. doi: 10.1115/1.3438260.

[16] Martin Andersson, Mario Sosa, and Ulf Olofsson. The effect of running-in on the efficiency of superfinished gears. *Tribology International*, 93:71–77, 2016.

[17] Xinmin Li, Mario Sosa, Martin Andersson, and Ulf Olofsson. A study of the efficiency of spur gears made of powder metallurgy materials–ground versus super-finished surfaces. *Tribology International*, 95:211–220, 2016.

[18] Naresh K Raghuwanshi and Anand Parey. Experimental measurement of spur gear mesh stiffness using digital image correlation technique. *Measurement*, 111: 93–104, 2017.

[19] V. Spitas, G. A. Papadopoulos, C. Spitas, and T. Costopoulos. Experimental investigation of load sharing in multiple gear tooth contact using the stress-optical method of caustics. *Strain*, 47(1):e227–e233, 2011. doi: 10.1111/j.1475-1305.2008.00558.x.

[20] A. M. Quinn, B. W. Drinkwater, and R. S. Dwyer-Joyce. The measurement of contact pressure in machine elements using ultrasound. *Ultrasonics*, 39:495–502, 2002.

[21] M. Pau, B. Leban, A. Baldi, and F. Ginesu. Experimental contact pattern analysis for a gear-rack system. *Meccanica*, 47:51–61, 2012.

[22] B de Saint-Venant et al. Mémoire sur la torsion des prismes. *Mémoires des Savants étrangers*, 14(233):560, 1855.

[23] R v Mises. On saint venant's principle. *Bulletin of the American Mathematical Society*, 51(8):555–562, 1945.

[24] Felix Kühn, Christoph Löpenhaus, Jens Brimmers, Fritz Klocke, and Thomas Bergs. Analysis of the influence of the effective angles on the tool wear in gear hobbing. *The International Journal of Advanced Manufacturing Technology*, 108 (7):2621–2632, 2020.

[25] Ruei-Hung Hsu, Yu-Ren Wu, and Van-The Tran. Manufacturing helical gears with double-crowning and twist-free tooth flanks using a variable pressure angle shaving cutter. *Proceedings of the Institution of Mechanical Engineers, Part B: Journal of Engineering Manufacture*, 233(1):77–86, 2019.

[26] Kouji Matsuo, Yoshitomo Suzuki, Junichi Hongu, Daisuke Iba, and Ichiro Moriwaki. Method of designing gear-honing-wheel geometries (validation based on fundamental theory and honing experiments). *Journal of Advanced Mechanical Design, Systems, and Manufacturing*, 14(7):JAMDSM0098–JAMDSM0098, 2020.

[27] DT Safarov, AG Kondrashov, and KI Kozin. Determination of the parameters of adjusting the gear broaching machine, according to the measurements of the spur bevel gears. In *Journal of Physics: Conference Series*, volume 1901, page 012021. IOP Publishing, 2021.

[28] Bruno Vargas and Volker Schulze. Three-dimensional modeling of gear skiving kinematics for comprehensive process design in practical applications. *CIRP Annals*, 70(1):99–102, 2021.

[29] Duc Nam Nguyen, Hùng Anh Lý, and Cong Truyen Duong. Simulation study on polishing of gear surfaces in non-newtonian fluid. *Science & Technology Development Journal-Engineering and Technology*, 3(3):443–451, 2020.

[30] Xi Wang, Zhihui Zhang, Yuzhuo Men, Xiujuan Li, Yunhong Liang, and Luquan Ren. Fabrication of nano-tic functional gradient wear-resistant composite coating on 40cr gear steel using laser cladding under starved lubrication conditions. *Optics & Laser Technology*, 126:106136, 2020.

[31] Jiuyue Zhao, Jinyuan Tang, Weihua Zhou, Tingting Jiang, Hao Wu, Xianggui Liao, and Minzhi Guo. Surface integrity of gear shot peening considering complex geometric conditions: A sequential coupled dem-fem method. *Surface and Coatings Technology*, 449:128943, 2022.

[32] Wu Chen, Xiaofei He, Wenchao Yu, Jie Shi, Maoqiu Wang, and Kefu Yao. Characterization of the microstructure and hardness of case-carburized gear steel. *Micron*, 144:103028, 2021.

[33] Anders Flodin. Powder metal through the process steps. *Gear Technology*, 8, 2018.

[34] Mattias Svahn. A parametric analysis of the surface roughness of teeth shaped by a pinion shaper cutter and guidelines for choosing process parameters. *Proceedings of the Institution of Mechanical Engineers, Part C: Journal of Mechanical Engineering Science*, 233(21-22):7368–7377, 2019.

[35] Günther Gravel. Simulation of hobbing and generation grinding to solve quality and noise problems. *Gear Technology*, 2015.

[36] Tengjiao Lin and Zeyin He. Analytical method for coupled transmission error of helical gear system with machining errors, assembly errors and tooth modifications. *Mechanical Systems and Signal Processing*, 91:167–182, 2017.

[37] ISO 1328. Cylindrical gears - iso system of flank tolerance classification - part 1: Definitions and allowable values of deviations relevant to flanks of gear teeth, 2013.

[38] K Aslantaş and S Taşgetiren. A study of spur gear pitting formation and life prediction. *Wear*, 257(11):1167–1175, 2004.

[39] Hüseyin İmrek and Hayrettin Düzcükoğlu. Relation between wear and tooth width modification in spur gears. *Wear*, 262(3-4):390–394, 2007.

[40] Sheng Li and Ahmet Kahraman. A scuffing model for spur gear contacts. *Mechanism and Machine Theory*, 156, 2021.

[41] Shuting Li. Effects of machining errors, assembly errors and tooth modifications on loading capacity, load-sharing ratio and transmission error of a pair of spur gears. *Mechanism and Machine Theory*, 42(6):698–726, 2007.

[42] Shuting Li. Finite element analyses for contact strength and bending strength of a pair of spur gears with machining errors, assembly errors and tooth modifications. *Mechanism and machine theory*, 42(1):88–114, 2007.

[43] Tao Zhang, Jianjun Wang, Yongjun Wu, and Haiying Zhang. Effect of machining errors on the gear engagement using contact finite element method. In *Turbo Expo: Power for Land, Sea, and Air*, volume 56772, page V07BT32A016. American Society of Mechanical Engineers, 2015.

[44] Jing Wei, Wei Sun, and Licun Wang. Effects of flank deviation on load distributions for helical gear. *Journal of mechanical science and technology*, 25(7): 1781–1789, 2011.

[45] Tao Luo, Xunpeng Qin, Jinjing Huang, and Wei Guo. Effects of helix deviation on load distributions and bending stresses of continuous engaged helical gear drives. *Advances in Mechanical Engineering*, 7(6):1687814015588660, 2015.

[46] Qi-bin Wang, Hong-bo Ma, Xian-guang Kong, and Yi-min Zhang. A distributed dynamic mesh model of a helical gear pair with tooth profile errors. *Journal of Central South University*, 25(2):287–303, 2018.

[47] Raynald Guilbault, Claude Gosselin, and Louis Cloutier. Express model for load sharing and stress analysis in helical gears. *Transactions of the ASME*, 2005.

[48] Raynald Guilbault, Claude Gosselin, and Louis Cloutier. Helical gears, effects of tooth deviations and tooth modifications on load sharing and fillet stresses. *Transactions of the ASME*, 2006.

[49] Fabio Bruzzone, Tommaso Maggi, Claudio Marcellini, and Carlo Rosso. Gear teeth deflection model for spur gears: Proposal of a 3d nonlinear and non-hertzian approach. *Machines*, 9(10):223, 2021.

[50] Wennian Yu and Chris K. Mechefske. Analytical modeling of spur gear corner contact effects. *Mechanism and Machine Theory*, 96:146–164, 2016.

[51] Siang-Yu Ye and Shyi-Jeng Tsai. A computerized method for loaded tooth contact analysis of high-contact-ratio spur gears with or without flank modification considering tip corner contact and shaft misalignment. *Mechanism and Machine Theory*, 97:190–214, 2016.

[52] RL Errichello, C Hewette, and R Eckert. Point-surface-origin macropitting caused by geometric stress concentration. *Gear Technology*, 28(1):54–59, 2011.

[53] Raynald Guilbault and Sébastien Lalonde. Tip relief designed to optimize contact fatigue life of spur gears using adapted pso and firefly algorithms. *SN Applied Sciences*, 3(1):1–21, 2021.

[54] RG Munro, L Morrish, and D Palmer. Gear transmission error outside the normal path of contact due to corner and top contact. *Proceedings of the Institution of Mechanical Engineers, Part C: Journal of Mechanical Engineering Science*, 213 (4):389–400, 1999.

[55] RG Munro, Derrol Palmer, and L Morrish. An experimental method to measure gear tooth stiffness throughout and beyond the path of contact. *Proceedings*

of the Institution of Mechanical Engineers, Part C: Journal of Mechanical Engineering Science, 215(7):793–803, 2001.

[56] Łukasz Jedliński. Influence of the movement of involute profile gears along the off-line of action on the gear tooth position along the line of action direction. *Eksploatacja i Niezawodność*, 23(4), 2021.

[57] Qi Fan and Lowell Wilcox. *New developments in tooth contact analysis (TCA) and loaded TCA for spiral bevel and hypoid gear drives*. AGMA, 2005.

[58] Shadi Shweiki, Ali Rezayat, Tommaso Tamarozzi, and Domenico Mundo. Transmission error and strain analysis of lightweight gears by using a hybrid fe-analytical gear contact model. *Mechanical Systems and Signal Processing*, 123: 573–590, 2019.

[59] Fabio Bruzzone, Tommaso Maggi, Claudio Marcellini, and Carlo Rosso. 2d nonlinear and non-hertzian gear teeth deflection model for static transmission error calculation. *Mechanism and Machine Theory*, 166:104471, 2021.

[60] Jing Wei, Pan Gao, Xinglong Hu, Wei Sun, and Jing Zeng. Effects of dynamic transmission errors and vibration stability in helical gears. *Journal of mechanical science and technology*, 28(6):2253–2262, 2014.

[61] Philippe Velex and Mondher Ajmi. Dynamic tooth loads and quasi-static transmission errors in helical gears–approximate dynamic factor formulae. *Mechanism and Machine Theory*, 42(11):1512–1526, 2007.

[62] Su-chul Kim, Sang-gon Moon, Jong-hyeon Sohn, Young-jun Park, Chan-ho Choi, and Geun-ho Lee. Macro geometry optimization of a helical gear pair for mass, efficiency, and transmission error. *Mechanism and Machine Theory*, 144:103634, 2020.

[63] Miguel Pleguezuelos, Miryam B Sánchez, and José I Pedrero. Analytical model for meshing stiffness, load sharing, and transmission error for spur gears with profile modification under non-nominal load conditions. *Applied Mathematical Modelling*, 97:344–365, 2021.

[64] Fang Guo and Zongde Fang. The statistical analysis of the dynamic performance of a gear system considering random manufacturing errors under different levels of machining precision. *Proceedings of the Institution of Mechanical Engineers, Part K: Journal of Multi-body Dynamics*, 234(1):3–18, 2020.

[65] Ali Hajnayeb and Qiao Sun. Study of gear pair vibration caused by random manufacturing errors. *Archive of Applied Mechanics*, 92(5):1451–1463, 2022.

[66] Giorgio Bonori and Francesco Pellicano. Non-smooth dynamics of spur gears with manufacturing errors. *Journal of Sound and Vibration*, 306(1-2):271–283, 2007.

[67] Bing Yuan, Shan Chang, Geng Liu, and Li-Yan Wu. Quasi-static and dynamic behaviors of helical gear system with manufacturing errors. *Chinese Journal of Mechanical Engineering*, 31(1):1–9, 2018.

[68] Alfonso Fernández-del Rincón, M Iglesias, A De-Juan, Alberto Diez-Ibarbia, P García, and F Viadero. Gear transmission dynamics: Effects of index and run out errors. *Applied Acoustics*, 108:63–83, 2016.

[69] D Talbot, A Sun, and A Kahraman. Impact of tooth indexing errors on dynamic factors of spur gears: experiments and model simulations. *Journal of Mechanical Design*, 138(9), 2016.

[70] M Inalpolat, M Handschuh, and A Kahraman. Influence of indexing errors on dynamic response of spur gear pairs. *Mechanical Systems and Signal Processing*, 60:391–405, 2015.

[71] Robert White and Vikrant Palan. Measurement of transmission error using rotational laser vibrometers. In *International Design Engineering Technical Conferences and Computers and Information in Engineering Conference*, volume 48086, pages 527–545, 2007.

[72] Antonio Palermo, Laurent Britte, Karl Janssens, Domenico Mundo, and Wim Desmet. The measurement of gear transmission error as an nvh indicator: theoretical discussion and industrial application via low-cost digital encoders to an all-electric vehicle gearbox. *Mechanical Systems and Signal Processing*, 110: 368–389, 2018.

[73] Christian Brecher, Christof Gorgels, Joachim Hesse, and Martin Hellmann. Dynamic transmission error measurements of a drive train. *Production Engineering*, 5(3):321–327, 2011.

[74] Juha Hedlund and Arto Lehtovaara. Testing method for the evaluation of parametric excitation of cylindrical gears. *Nondestructive Testing and Evaluation*, 23 (4):285–299, 2008.

[75] Philippe Velex, Jérôme Bruyère, and DR Houser. Some analytical results on transmission errors in narrow-faced spur and helical gears: influence of profile modifications. *ASME. J. Mech. Des.*, 133(3), 2011.

[76] Hermann J Stadtfeld. Psychoacoustics applied to edrive noise reduction. *Gear Technol.*, pages 48–54, 2021.

[77] Gerd Kotthoff. Nvh potential of pm gears for electrified drivetrains. *Ratio*, 12: 5, 2018.

[78] Mehdi Mehrgou, Inigo Garcia de Madinabeitia, Bernhard Graf, Franz Zieher, and Christoph Priestner. Nvh aspects of electric drives-integration of electric machine, gearbox and inverter. Technical report, SAE Technical Paper, 2018.

[79] Philipp Scholzen, Michael Andersson, Christoph Löpenhaus, and Christian Brecher. Improved nvh behavior of transmission gears by the use of pm. 2019. URL `https://www.scopus.com/inward/record.uri?eid=2-s2.0-85102012797&partnerID=40&md5=1ed80ae0e9e1d42b8e89f93463f66018`.

[80] A Carbonelli, E Rigaud, J Perret-Liaudet, E Pelloli, and D Barday. Low noise design of a truck timing multi-stage gear: robust optimization of tooth surface modifications. In *International Gear Conference 2014*, pages 200–207, 2014.

[81] Jacek Pacana and Andrzej Pacana. The impact of geometry errors on the motion transmission of dual path gearing. *Advances in Science and Technology. Research Journal*, 10(32), 2016.

[82] Selman Karagoz, Nezir Aydin, and Vladimir Simic. End-of-life vehicle management: A comprehensive review. *Journal of Material Cycles and Waste Management*, 22(2):416–442, 2020.

[83] Vincent Cline, L Winkelmann, and J Michaud. Gear repair for helicopters and wind turbines via isotropic superfinishing. In *AHS International 73rd Annual Forum & Technology Display, Fort Worth, Texas, USA*, volume 73, pages 1–22, 2017.

[84] Derek L Diener and Anne-Marie Tillman. Scrapping steel components for recycling—isn't that good enough? seeking improvements in automotive component end-of-life. *Resources, Conservation and Recycling*, 110:48–60, 2016.

[85] Derek L Diener, Duncan Kushnir, and Anne-Marie Tillman. Scrap happens: A case of industrial end-users, maintenance and component remanufacturing outcome. *Journal of Cleaner Production*, 213:863–871, 2019.

[86] Zuomin Dong. Tolerance synthesis by manufacturing cost modeling and design optimization. *Advanced Tolerancing Techniques*, pages 233–260, 1997.

[87] Edward Morse, Jean-Yves Dantan, Nabil Anwer, Rikard Söderberg, Giovanni Moroni, Ahmed Qureshi, Xiangqian Jiang, and Luc Mathieu. Tolerancing: Managing uncertainty from conceptual design to final product. *CIRP Annals*, 67(2):695–717, 2018.

[88] Min Zhang, ZhaoYao Shi, Luc Mathieu, Anwer Nabil, and Jianxin Yang. Geometric product specification of gears: The geospelling perspective. *Procedia Cirp*, 27:90–96, 2015.

[89] Chu Zhang, Huimin Dong, Delun Wang, and Yi Cheng. Tolerance synthesis for lost motion requirement of planetary gear train based on a mechanism model. *Mechanism and Machine Theory*, 164:104405, 2021.

[90] Antonio Armillotta. Tolerance analysis of gear trains by static analogy. *Mechanism and Machine Theory*, 135:65–80, 2019.

[91] Ken-Shin Lin, Kuei-Yuan Chan, and Jyh-Jone Lee. Kinematic error analysis and tolerance allocation of cycloidal gear reducers. *Mechanism and Machine Theory*, 124:73–91, 2018.

[92] Martin Hallmann, Benjamin Schleich, and Sandro Wartzack. From tolerance allocation to tolerance-cost optimization: a comprehensive literature review. *The International Journal of Advanced Manufacturing Technology*, 107(11):4859–4912, 2020.

[93] Hua Chen and Xin Li. Tolerance analysis of involute spur gear from the perspective of design. *Mechanics & Industry*, 23:16, 2022.

[94] Jèrôme Bruyère, Jean-Yves Dantan, Régis Bigot, and Patrick Martin. Statistical tolerance analysis of bevel gear by tooth contact analysis and monte carlo simulation. *Mechanism and Machine Theory*, 42(10):1326–1351, 2007.

[95] Daofei Wang, Jialong Yang, Pengchong Wei, and Wei Pu. A mixed ehl model of grease lubrication considering surface roughness and the study of friction behavior. *Tribology International*, 154:106710, 2021.

[96] Phillipa Cann. Grease lubricant film distribution in rolling contacts. *NLGI spokesman*, 61(2):22–29, 1997.

[97] Osborne Reynolds. On the theory of lubrication and its application to mr. beauchamp tower's experiments, including an experimental determination of the viscosity of olive oil. *Philosophical transactions of the Royal Society of London*, 177:157–234, 1886.

[98] Torbjörn Almqvist and Roland Larsson. The navier–stokes approach for thermal ehl line contact solutions. *Tribology International*, 35(3):163–170, 2002.

[99] Torbjörn Almqvist, Andreas Almqvist, and Roland Larsson. A comparison between computational fluid dynamic and reynolds approaches for simulating transient ehl line contacts. *Tribology international*, 37(1):61–69, 2004.

[100] Wyatt Peterson, Kushagra Singh, and Farshid Sadeghi. Fluid–solid interaction modeling of elastohydrodynamic lubrication point contacts. *Journal of Tribology*, 144(11):111601, 2022.

[101] Kenneth Langstreth Johnson and Kenneth Langstreth Johnson. *Contact mechanics*. Cambridge university press, 1987.

[102] Lars Bobach, Ronny Beilicke, Dirk Bartel, and Ludger Deters. Thermal elastohydrodynamic simulation of involute spur gears incorporating mixed friction. *Tribology International*, 48:191–206, 2012.

[103] Enzo Maier, Moritz Lengmüller, and Thomas Lohner. Effect of transversely isotropic elasticity on elastohydrodynamic lubrication of point contacts. *Polymers*, 14(17):3507, 2022.

[104] Markus Hartinger and Tom Reddyhoff. Cfd modeling compared to temperature and friction measurements of an ehl line contact. *Tribology International*, 126:144–152, 2018.

[105] Ning Ren, W Wayne Chen, Dong Zhu, Yuchuan Liu, and Q Jane Wang. A three-dimensional deterministic model for rough surface line-contact ehl problems. In *International Joint Tribology Conference*, volume 48108, pages 191–192, 2007.

[106] Li-Ming Chu, Hsiang-Chen Hsu, Jaw-Ren Lin, and Yuh-Ping Chang. Inverse approach for calculating temperature in ehl of line contacts. *Tribology international*, 42(8):1154–1162, 2009.

[107] Athanassios Mihailidis, Konstantinos Agouridas, and Konstantinos Panagiotidis. Non-newtonian starved thermal-elastohydrodynamic lubrication of finite line contacts. *Tribology Transactions*, 56(1):88–100, 2013.

[108] Hui L Dong, Ji B Hu, and Xue Y Li. Temperature analysis of involute gear based on mixed elastohydrodynamic lubrication theory considering tribo-dynamic behaviors. *Journal of Tribology*, 136(2), 2014.

[109] Tao Zhang, Feng Jiang, Lan Yan, Zhengyi Jiang, and Xipeng Xu. A novel ultrahigh-speed ball-on-disc tribometer. *Tribology International*, 157:106901, 2021.

[110] Ellen Bergseth, Yi Zhu, and Anders Söderberg. Study of surface roughness on friction in rolling/sliding contacts: ball-on-disc versus twin-disc. *Tribology Letters*, 68(2):1–15, 2020.

[111] Hazim Umran Jamali, Khairi Sharif, Henry Peredur Evans, and Raymond Walter Snidle. Analysis of elastohydrodynamic lubrication of helical gear tooth contacts including the effects of crowning and the form of tip relief. In *Proc International Conference on Gears*, 2013.

[112] Alberto Diez-Ibarbia, Alfonso Fernandez-del Rincon, A De-Juan, M Iglesias, P Garcia, and F Viadero. Frictional power losses on spur gears with tip reliefs. the load sharing role. *Mechanism and Machine Theory*, 112:240–254, 2017.

[113] Alberto Diez-Ibarbia, Alfonso Fernandez-del Rincon, A De-Juan, M Iglesias, P Garcia, and F Viadero. Frictional power losses on spur gears with tip reliefs. the friction coefficient role. *Mechanism and Machine Theory*, 121:15–27, 2018.

[114] Javier Echávarri Otero, Eduardo de la Guerra Ochoa, Enrique Chacón Tanarro, Francisco Franco Martínez, and Rafael Wilmer Contreras Urgiles. An analytical approach for predicting ehl friction: Usefulness and limitations. *Lubricants*, 10 (7):141, 2022.

[115] Carl Barus. Art. x.–isothermals, isopiestics and isometrics relative to viscosity. *American Journal of Science (1880-1910)*, 45(266):87, 1893.

[116] Bo Jacobson. On the Lubrication of Heavily Loaded Cylindrical Surfaces Considering Surface Deformations and Solidification of the Lubricant. *Journal of Lubrication Technology*, 95(3):321–327, 07 1973. ISSN 0022-2305. doi: 10.1115/1.3451818. URL `https://doi.org/10.1115/1.3451818`.

[117] Sheng Li and Ahmet Kahraman. Prediction of spur gear mechanical power losses using a transient elastohydrodynamic lubrication model. *Tribology Transactions*, 53(4):554–563, 2010.

[118] P. R. Goglia, T. F. Conry, and C. Cusano. The Effects of Surface Irregularities on the Elastohydrodynamic Lubrication of Sliding Line Contacts. Part I—Single Irregularities. *Journal of Tribology*, 106(1):104–112, 01 1984. ISSN 0742-4787. doi: 10.1115/1.3260845. URL `https://doi.org/10.1115/1.3260845`.

[119] CJA Roelands. *Correlational Aspects of the Viscosity-Temperature-Pressure Relationship of Lubricating Oils*. PhD thesis, Technical University Delft, Delft, The Netherlands, 1963.

[120] L. Houpert. New Results of Traction Force Calculations in Elastohydrodynamic Contacts. *Journal of Tribology*, 107(2):241–245, 04 1985. ISSN 0742-4787. doi: 10.1115/1.3261033. URL `https://doi.org/10.1115/1.3261033`.

[121] Xiaoling Liu, Ming Jiang, Peiran Yang, and Motohiro Kaneta. Non-newtonian thermal analyses of point ehl contacts using the eyring model. *J. Trib.*, 127(1): 70–81, 2005.

[122] Heribert Rodermund. *Beitrag zur elastohydrodynamischen Schmierung von Evolventenzahnrädern*. PhD thesis, TU Clausthal, Clausthal-Zellerfeld, Germany, 1975.

[123] D Dowson and GR Higginson. Elastohydrodynamic lubrication, the fundamentals of roller and gear lubrication, 1966.

[124] Jian-hua Xue, Wei Li, and Caiyan Qin. The scuffing load capacity of involute spur gear systems based on dynamic loads and transient thermal elastohydrodynamic lubrication. *Tribology International*, 79:74–83, 2014.

[125] Huaiju Liu, Ken Mao, Caichao Zhu, Siyu Chen, Xiangyang Xu, and Mingyong Liu. Spur gear lubrication analysis with dynamic loads. *Tribology Transactions*, 56(1):41–48, 2013.

[126] Liming Wang, Chunlong Deng, Jin Xu, Lei Yin, Wennian Yu, Xiaoxi Ding, Yimin Shao, Wenbin Huang, and Xiaoqing Yang. Effects of spalling fault on dynamic responses of gear system considering three-dimensional line contact elasto-hydrodynamic lubrication. *Engineering Failure Analysis*, 132:105930, 2022.

[127] Mingyong Liu, Caichao Zhu, Huaiju Liu, and Chenhui Wu. Parametric studies of lubrication performance of a helical gear pair with non-newtonian fluids. *Journal of Mechanical Science and Technology*, 30(1):317–326, 2016.

[128] Ronny Beilicke, Lars Bobach, and Dirk Bartel. Transient thermal elastohydrodynamic simulation of a dlc coated helical gear pair considering limiting shear stress behavior of the lubricant. *Tribology International*, 97:136–150, 2016.

[129] Yanjun Peng, Ning Zhao, Mengqi Zhang, Wang Li, and Ruchuan Zhou. Non-newtonian thermal elastohydrodynamic simulation of helical gears considering modification and misalignment. *Tribology International*, 124:46–60, 2018.

[130] Yong Yang, Wenguang Li, Jiaxu Wang, and Qinghua Zhou. On the mixed ehl characteristics, friction and flash temperature in helical gears with consideration of 3d surface roughness. *Industrial Lubrication and Tribology*, 2018.

[131] A Arana, A Iñurritegui, J Larrañaga, and I Ulacia. Influence of thermal distortion on load distribution, transmission error and premature contact. In *Gears Conference 2018, Lyon, France: Conference Proceedings: Volumes 1 and 2*, page 446. Chartridge Books Oxford, 2018.

[132] A Ziegltrum, T Lohner, and Karsten Stahl. Tehl simulation on the influence of lubricants on load-dependent gear losses. *Tribology International*, 113:252–261, 2017.

[133] Marco Barbieri, Antonius A Lubrecht, and Francesco Pellicano. Behavior of lubricant fluid film in gears under dynamic conditions. *Tribology International*, 62:37–48, 2013.

[134] Leonhard Euler. Théorie plus complette des machines qui sont mises en mouvement par la réaction de l'eau. *Mémoires de l'académie des sciences de Berlin*, pages 227–295, 1756.

[135] Leif Floberg. *On hydrodynamic lubrication with special reference to cavitation in bearings*. Chalmers Tekniska Högskola (Sweden), 1961.

[136] E van Emden, Cornelis H Venner, and GE Morales-Espejel. Aspects of flow and cavitation around an ehl contact. *Tribology international*, 95:435–448, 2016.

[137] Leiming Gao, Gregory de Boer, and Rob Hewson. The role of micro-cavitation on ehl: A study using a multiscale mass conserving approach. *Tribology International*, 90:324–331, 2015.

[138] Paras Kumar and Harish Hirani. Misalignment effect on gearbox failure: An experimental study. *Measurement*, 169:108492, 2021.

[139] Alastair Clarke, HU Jamali, KJ Sharif, HP Evans, Robert Frazer, and Brian Shaw. Effects of profile errors on lubrication performance of helical gears. *Tribology International*, 111:184–191, 2017.

[140] Changjiang Zhou, Bo Hu, Xuanlv Qian, and Xu Han. A novel prediction method for gear friction coefficients based on a computational inverse technique. *Tribology International*, 127:200–208, 2018.

[141] Huaiju Liu, Heli Liu, Caichao Zhu, Peitang Wei, and Jinyuan Tang. Tribological behavior of coated spur gear pairs with tooth surface roughness. *Friction*, 7(2):117–128, 2019.

[142] MF Al-Mayali, S Hutt, KJ Sharif, A Clarke, and HP Evans. Experimental and numerical study of micropitting initiation in real rough surfaces in a micro-elastohydrodynamic lubrication regime. *Tribology letters*, 66(4):1–14, 2018.

[143] S Fricke, C Hager, S Solovyev, M Wangenheim, and J Wallaschek. Influence of surface form deviations on friction in mixed lubrication. *Tribology International*, 118:491–499, 2018.

[144] Lucian Tudose, Ovidiu Buiga, Cornel Ştefanache, and András Sóbester. Automated optimal design of a two-stage helical gear reducer. *Structural and Multidisciplinary Optimization*, 42(3):429–435, 2010.

[145] Iqbal Husain, Burak Ozpineci, Md Sariful Islam, Emre Gurpinar, Gui-Jia Su, Wensong Yu, Shajjad Chowdhury, Lincoln Xue, Dhrubo Rahman, and Raj Sahu. Electric drive technology trends, challenges, and opportunities for future electric vehicles. *Proceedings of the IEEE*, 109(6):1039–1059, 2021.

[146] William Cai, Xiaogang Wu, Minghao Zhou, Yafei Liang, and Yujin Wang. Review and development of electric motor systems and electric powertrains for new energy vehicles. *Automotive Innovation*, 4(1):3–22, 2021.

[147] Pongpun Othaganont, Francis Assadian, and Daniel J Auger. Multi-objective optimisation for battery electric vehicle powertrain topologies. *Proceedings of the Institution of Mechanical Engineers, Part D: Journal of Automobile Engineering*, 231(8):1046–1065, 2017.

[148] Cheng Wang, Shouren Wang, and Gaoqi Wang. Volume models for different structures of spur gear. *Australian Journal of Mechanical Engineering*, 2017.

[149] Jorge Laureano Moya-Rodríguez, José Roberto Marty-Delgado, and Paul Marcelo Tacle-Humanante. Optimización multiobjetivo en transmisiones por engranajes cilíndricos de dientes rectos asimétricos. *Ingeniería Mecánica*, 23(2), 2020.

[150] Maruti Patil, Penchaliah Ramkumar, and Shankar Krishnapillai. Multi-objective optimization of two stage spur gearbox using nsga-ii. Technical report, SAE Technical Paper, 2017.

[151] Maruti Patil, P Ramkumar, and K Shankar. Multi-objective optimization of the two-stage helical gearbox with tribological constraints. *Mechanism and Machine Theory*, 138:38–57, 2019.

[152] Vu Ngoc Pi, Tran Thi Hong, Tran Thi Phuong Thao, Nguyen Khac Tuan, Le Xuan Hung, and Luu Anh Tung. Calculating optimum gear ratios of a two-stage helical reducer with first stage double gear sets. In *IOP Conference Series: Materials Science and Engineering*, volume 542, page 012017. IOP Publishing, 2019.

[153] RC Sanghvi, AS Vashi, HP Patolia, and RG Jivani. Multi-objective optimization of two-stage helical gear train using nsga-ii. *Journal of Optimization*, 2014, 2014.

[154] NTH Cam, VN Pi, and TT Hong. A study on calculation of optimum gear ratios of a two-stage helical gearbox with second stage double gear sets. *a a*, 500:1, 2019.

[155] Nguyen Van Cuong, K Le Hong, T Thi Hong, et al. Splitting total gear ratio of two-stage helical reducer with first-stage double gearsets for minimal reducer length. *Int J Mech Prod Eng Res Dev*, 9(6):595–608, 2019.

[156] Xueyi Li, Shoubo Jiang, and Qingliang Zeng. Optimization of two-stage cylindrical gear reducer with adaptive boundary constraints. *J. Softw.*, 8(8):2052–2057, 2013.

[157] Sa'id Golabi, Javad Jafari Fesharaki, and Maryam Yazdipoor. Gear train optimization based on minimum volume/weight design. *Mechanism and machine theory*, 73:197–217, 2014.

[158] Jianfeng Ma, Chao Li, and Lingli Cui. Transmission error analysis and disturbance optimization of two-stage spur gear space driven mechanism with large inertia load. *Shock and Vibration*, 2018, 2018.

[159] Ajit Bodas and Ahmet Kahraman. Influence of carrier and gear manufacturing errors on the static load sharing behavior of planetary gear sets. *JSME International Journal Series C Mechanical Systems, Machine Elements and Manufacturing*, 47(3):908–915, 2004.

[160] Chao Xun, Xinhua Long, and Hongxing Hua. Effects of random tooth profile errors on the dynamic behaviors of planetary gears. *Journal of Sound and Vibration*, 415:91–110, 2018.

[161] Leonardo Israel Farfan-Cabrera. Tribology of electric vehicles: A review of critical components, current state and future improvement trends. *Tribology International*, 138:473–486, 2019.

[162] Robert Ian Taylor. Energy efficiency, emissions, tribological challenges and fluid requirements of electrified passenger car vehicles. *Lubricants*, 9(7):66, 2021.

[163] Alberto Danese, Michele Garau, Andreas Sumper, and Bendik Nybakk Torsæter. Electrical infrastructure design methodology of dynamic and static charging for heavy and light duty electric vehicles. *Energies*, 14(12):3362, 2021.

[164] Paras Kumar, Harish Hirani, and Atul Agrawal. Fatigue failure prediction in spur gear pair using agma approach. *Materials Today: Proceedings*, 4(2):2470–2477, 2017.

[165] ISO 6336. Calculation of load capacity of spur and helical gears - part 2: Calculation of surface durability (pitting), 2006.

[166] T Reimann, T Herzog, D Kadach, and K Stahl. The influence of friction on the tooth normal force of spur and helical gears. *Proceedings of the Institution of Mechanical Engineers, Part C: Journal of Mechanical Engineering Science*, 233 (21-22):7391–7400, 2019.

[167] Pedro MT Marques, Ramiro C Martins, and Jorge HO Seabra. Power loss and load distribution models including frictional effects for spur and helical gears. *Mechanism and Machine Theory*, 96:1–25, 2016.

[168] Paul Langlois, Baydu Al, and Owen Harris. Hybrid hertzian and fe-based helical gear-loaded tooth contact analysis and comparison with fe. *Gear Technology*, 6:54–57, 2016.

[169] SN Atluri and H Murakawa. On hybrid finite element models in nonlinear solid mechanics. *Finite elements in nonlinear mechanics*, 1:3–41, 1977.

[170] Lars Vedmar. *On the design of external involute helical gears*. PhD thesis, Lund University, Lund, Sweden, 1981.

[171] SP Timoshenko and JN Goodier. Theory of elasticity, international student edition. *KOGAKUSHA Co., Ltd*, page 444, 1970.

[172] A Fernandez Del Rincon, Fernando Viadero, M Iglesias, P García, A De-Juan, and R Sancibrian. A model for the study of meshing stiffness in spur gear transmissions. *Mechanism and Machine Theory*, 61:30–58, 2013.

[173] United Nations. Global Sustainable Development Goals. On the WWW, April 2021. URL `https://sdgs.un.org/goals`.

[174] Emmanuel Rigaud and Denis Barday. Modelling and analysis of static transmission error. effect of wheel body deformation and interactions between adjacent loaded teeth. In *4th World congress on gearing and power transmission*, volume 3, pages 1961–1972, 1999.

[175] Jiachun Lin, Edwin Bergstedt, Per Lindholm, Zhaoyao Shi, and Ulf Olofsson. In situ measurement of gear tooth profile during fzg gear micropitting test. *Surface Topography: Metrology and Properties*, 7(1):015018, 2019.

[176] Edwin Bergstedt, Jiachun Lin, and Ulf Olofsson. Influence of gear surface roughness on the pitting and micropitting life. *Proceedings of the Institution of Mechanical Engineers, Part C: Journal of Mechanical Engineering Science*, 234 (24):4953–4961, 2020.

[177] Wojciech Wasko, Alessandro Albini, Perla Maiolino, Fulvio Mastrogiovanni, and Giorgio Cannata. Contact modelling and tactile data processing for robot skins. *Sensors*, 19(4):814, 2019.

[178] Vlado A Lubarda. Circular loads on the surface of a half-space: displacement and stress discontinuities under the load. *International Journal of Solids and Structures*, 50(1):1–14, 2013.

[179] Francesco Marmo and Luciano Rosati. A general approach to the solution of boussinesq's problem for polynomial pressures acting over polygonal domains. *Journal of Elasticity*, 122(1):75–112, 2016.

[180] Vinnova. Driveline components for electrified powertrains. On the WWW, . URL `https://www.vinnova.se/en/p/driveline-components-for-electrified-powertrains/`.

[181] Vinnova. E!115140 effigears. On the WWW, . URL `https://www.vinnova.se/en/p/e115140-effigears-applied-nano-surfaces-sweden-ab/`.

[182] Gajarajan Sivayogan, Nader Dolatabadi, Patricia Johns-Rahnejat, Ramin Rahmani, and Homer Rahnejat. Non-newtonian thermo-elastohydrodynamics and sub-surface stress field of high-performance racing spur gears. *Lubricants*, 10(7):146, 2022.

[183] Xiaolan Ai, Herbert S Cheng, and Linqing Zheng. A transient model for micro-elastohydrodynamic lubrication with three-dimensional irregularities. *Transactions of the ASME*, 1993.

[184] Henry Peredur Evans, Raymond Walter Snidle, and KJ Sharif. Deterministic mixed lubrication modelling using roughness measurements in gear applications. *Tribology International*, 42(10):1406–1417, 2009.

[185] Yuan-zhong Hu, Hui Wang, Wen-zhong Wang, and Dong Zhu. A computer model of mixed lubrication in point contacts. *Tribology International*, 34(1): 65–73, 2001.

[186] Paras Kumar, Harish Hirani, and Atul Kumar Agrawal. Online condition monitoring of misaligned meshing gears using wear debris and oil quality sensors. *Industrial Lubrication and Tribology*, 2018.

[187] International Organization for Standardization. Rolling bearings: Dynamic load ratings and rating life, 1990.

[188] Valentin Totev, Vultchan Gueorgiev, and Plamen Rizov. Regenerative braking of electric vehicles. In *2019 11th Electrical Engineering Faculty Conference (BulEF)*, pages 1–5. IEEE, 2019.

[189] Marina Franulovic, Kristina Markovic, Zeljko Vrcan, and Matija Soban. Experimental and analytical investigation of the influence of pitch deviations on the loading capacity of hcr spur gears. *Mechanism and Machine Theory*, 117: 96–113, 2017.

[190] R Ravivarman and R Prabhu Sekar. Load share model based gear loss factor prediction in high contact ratio spur gear drive. *Proceedings of the Institution of Mechanical Engineers, Part J: Journal of Engineering Tribology*, 237(1):103–118, 2023.

[191] Kang Huang, Yangshou Xiong, Tao Wang, and Qi Chen. Research on the dynamic response of high-contact-ratio spur gears influenced by surface roughness under ehl condition. *Applied Surface Science*, 392:8–18, 2017.

[192] Ahmed W Hussein and Mohammad Q Abdullah. High-contact ratio spur gears with conformal contact and reduced sliding. *Results in Engineering*, page 100412, 2022.

[193] Rama Thirumurugan and G Muthuveerappan. Study on mesh power losses in high contact ratio (hcr) gear drives. In *1st International and 16th national conference on machines and mechanisms, iNaCoMM*, pages 169–176, 2013.

[194] S Li and A Kahraman. A tribo-dynamic model of a spur gear pair. *Journal of Sound and Vibration*, 332(20):4963–4978, 2013.

[195] Milton Coba Salcedo, Irene Buj Coral, and Guillermo Valencia Ochoa. Characterization of surface topography with abbott firestone curve. *Contemp. Eng. Sci*, 11(68):3397–3407, 2018.

[196] Jack Walker, Mahdi Mohammadpour, Stephanos Theodossiades, SR Bewsher, G Offner, H Bansal, M Leighton, M Braunstingl, and H-G Flesch. A multiphysics transient wear model for helical gear pairs. *Tribology International*, 169: 107463, 2022.

[197] Hongbing Wang, Changjiang Zhou, Yuying Lei, and Zhongming Liu. An adhesive wear model for helical gears in line-contact mixed elastohydrodynamic lubrication. *Wear*, 426:896–909, 2019.

[198] D Mallipeddi, M Norell, M Sosa, and L Nyborg. The effect of manufacturing method and running-in load on the surface integrity of efficiency tested

ground, honed and superfinished gears. *Tribology International*, 131:277–287, 2019.

[199] J Seewig, G Beichert, R Brodmann, H Bodschwinna, and M Wendel. Extraction of shape and roughness using scattering light. In *Optical Measurement Systems for Industrial Inspection VI*, volume 7389, pages 223–233. Spie, 2009.

[200] R Brodmann, B Brodmann, K Konovalenko, C Wiehr, Ching-hsien Huang, and Ya-leng Chen. Fast and precise surface measurement of back-grinding silicon wafers. *SOLID STATE TECHNOLOGY*, 60(4):18–23, 2017.

[201] Zhifang Zhao, Yang Yang, Hongzheng Han, Hui Ma, Haixu Wang, and Zhanwei Li. Meshing characteristics of spur gears considering three-dimensional fractal rough surface under elastohydrodynamic lubrication. *Machines*, 10(8): 705, 2022.

[202] Cyrus Hillsman, Yan Wang, and Dima Nazzal. A semi-automatic mold cost estimation framework based upon geometry similarity. *The international journal of advanced manufacturing technology*, 68:1387–1399, 2013.

Scientific publications

Author contributions

The following lists Hjelm's contributions to the appended papers.

Paper I: A Method for Calculating Contact Pressure and Tip Contact in Spur Gear Sets with Manufacturing Errors

Hjelm contributed to the general idea. Hjelm performed the detailed calculations. Hjelm implemented the theory in a Java program. Hjelm performed the simulations and produced the results. Hjelm made the literature review. Hjelm wrote the paper during the course Academic Writing for Publication. Hjelm made a presentation and presented the paper at a conference.

Paper II: Influence of manufacturing error tolerances on contact pressure in gears

Hjelm structured the paper. Hjelm performed the simulations. Hjelm performed the literature review. Hjelm wrote the paper.

Paper III: Gear tolerancing for simultaneous optimization of transmission error and contact pressure

Hjelm presented the idea. Hjelm performed the literature review. Hjelm performed the simulations. Hjelm wrote the paper.

Paper IV: Reducing scrapping of gears by assessment of tip contact threshold torque

Hjelm presented the idea. Hjelm performed the literature review. Hjelm performed the simulations. Hjelm wrote the paper.

Paper V: Influence of Manufacturing Error Tolerances on Thermal EHL Behavior of Gears

Hjelm presented the idea. Hjelm performed the literature review. Hjelm applied for funding. Hjelm derived the theory. Hjelm implemented the theory in a Matlab program. Hjelm performed the simulations. Hjelm wrote the paper.

Paper VI: Optimum dog-leg angle for mass and bearing force optimization of multistage gear reduction

Hjelm contributed to the concept and structure of the paper. Hjelm performed the literature review. Hjelm performed parts of the calculations. Hjelm wrote parts of the paper.